Fall 12-31-2018

# Optimizing resource allocation in eh-enabled internet of things

Ali Shahini
*New Jersey Institute of Technology*

# Copyright Warning & Restrictions

The copyright law of the United States (Title 17, United States Code) governs the making of photocopies or other reproductions of copyrighted material.

Under certain conditions specified in the law, libraries and archives are authorized to furnish a photocopy or other reproduction. One of these specified conditions is that the photocopy or reproduction is not to be "used for any purpose other than private study, scholarship, or research." If a, user makes a request for, or later uses, a photocopy or reproduction for purposes in excess of "fair use" that user may be liable for copyright infringement,

This institution reserves the right to refuse to accept a copying order if, in its judgment, fulfillment of the order would involve violation of copyright law.

Please Note: The author retains the copyright while the New Jersey Institute of Technology reserves the right to distribute this thesis or dissertation

Printing note: If you do not wish to print this page, then select "Pages from: first page # to: last page #" on the print dialog screen

## ABSTRACT

## OPTIMIZING RESOURCE ALLOCATION IN EH-ENABLED INTERNET OF THINGS

**by**
**Ali Shahini**

Internet of Things (IoT) aims to bridge everyday physical objects via the Internet. Traditional energy-constrained wireless devices are powered by fixed energy sources like batteries, but they may require frequent battery replacements or recharging. Wireless Energy Harvesting (EH), as a promising solution, can potentially eliminate the need of recharging or replacing the batteries. Unlike other types of green energy sources, wireless EH does not depend on nature and is thus a reliable source of energy for charging devices. Meanwhile, the rapid growth of IoT devices and wireless applications is likely to demand for more operating frequency bands. Although the frequency spectrum is currently scarce, owing to inefficient conventional regulatory policies, a considerable amount of the radio spectrum is greatly underutilized. Cognitive radio (CR) can be exploited to mitigate the spectrum scarcity problem of IoT applications by leveraging the spectrum holes. Therefore, transforming the IoT network into a cognitive based IoT network is essential to utilizing the available spectrum opportunistically.

To address the two aforementioned issues, a novel model is proposed to leverage wireless EH and CR for IoT. In particular, the sum rate of users is maximized for a CR-based IoT network enabled with wireless EH. Users operate in a time switching fashion, and each time slot is partitioned into three non-overlapping parts devoted for EH, spectrum sensing and data transmission. There is a trade-off among the lengths of these three operations and thus the time slot structure is to be optimized. The general problem of joint resource allocation and EH optimization is formulated as a mixed integer nonlinear programming task which is NP-hard and intractable.

Therefore, a sub-channel allocation scheme is first proposed to approximately satisfy users rate requirements and remove the integer constraints. In the second step, the general optimization problem is reduced to a convex optimization task. Another optimization framework is also designed to capture a fundamental tradeoff between energy efficiency (EE) and spectral efficiency for an EH-enabled IoT network. In particular, an EE maximization problem is formulated by taking into consideration of user buffer occupancy, data rate fairness, energy causality constraints and interference constraints. Then, a low complexity heuristic algorithm is proposed to solve the resource allocation and EE optimization problem. The proposed algorithm is shown to be capable of achieving a near optimal solution with polynomial complexity.

To support Machine Type Communications (MTC) in next generation mobile networks, NarrowBand-IoT (NB-IoT) has emerged as a promising solution to provide extended coverage and low energy consumption for low cost MTC devices. However, the existing orthogonal multiple access scheme in NB-IoT cannot provide connectivity for a massive number of MTC devices. In parallel with the development of NB-IoT, Non-Orthogonal Multiple Access (NOMA), introduced for the fifth generation wireless networks, is deemed to significantly improve the network capacity by providing massive connectivity through sharing the same spectral resources. To leverage NOMA in the context of NB-IoT, a power domain NOMA scheme is proposed with user clustering for an NB-IoT system. In particular, the MTC devices are assigned to different ranks within the NOMA clusters where they transmit over the same frequency resources. Then, an optimization problem is formulated to maximize the total throughput of the network by optimizing the resource allocation of MTC devices and NOMA clustering while satisfying the transmission power and quality of service requirements. Furthermore, an efficient heuristic algorithm is designed to solve the proposed optimization problem by jointly optimizing NOMA clustering and resource allocation of MTC devices.

# OPTIMIZING RESOURCE ALLOCATION IN EH-ENABLED INTERNET OF THINGS

by
Ali Shahini

A Dissertation
Submitted to the Faculty of
New Jersey Institute of Technology
in Partial Fulfillment of the Requirements for the Degree of
Doctor of Philosophy in Electrical Engineering

Helen and John C. Hartmann Department of
Electrical and Computer Engineering

December 2018

**APPROVAL PAGE**

**OPTIMIZING RESOURCE ALLOCATION IN EH-ENABLED INTERNET OF THINGS**

**Ali Shahini**

---

Nirwan Ansari, Dissertation Advisor — Date
Distinguished Professor, Department of Electrical and Computer Engineering, NJIT

---

Ali Abdi, Committee Member — Date
Professor, Department of Electrical and Computer Engineering, NJIT

---

Abdallah Khreishah, Committee Member — Date
Associate Professor, Department of Electrical and Computer Engineering, NJIT

---

Roberto Rojas-Cessa, Committee Member — Date
Professor, Department of Electrical and Computer Engineering, NJIT

---

Guiling Wang, Committee Member — Date
Professor, Department of Computer Science, NJIT

## BIOGRAPHICAL SKETCH

**Author:** Ali Shahini

**Degree:** Doctor of Philosophy

**Date:** December 2018

**Undergraduate and Graduate Education:**

- Doctor of Philosophy in Electrical Engineering,
  New Jersey Institute of Technology, Newark, NJ, USA.
- Master of Science in Wireless Communications,
  University of Southampton, Southampton, UK, 2013.
- Bachelor of Science in Electrical Engineering, Electronics,
  Karaj Islamic Azad University, Karaj, Tehran, Iran, 2010.

**Major:** Electrical Engineering

**Presentations and Publications:**

**A. Shahini**, A. Kiani and N. Ansari, "Energy Efficient Resource Allocation in EH-enabled CR Networks for IoT," *IEEE Internet of Things Journal,* DOI: 10.1109/JIOT.2018.2880190, early access.

**A. Shahini**, and N. Ansari, "Joint Spectrum Allocation and Energy Harvesting Optimization in Green Powered Heterogeneous Cognitive Radio Networks," *Computer Communications,* vol. 127, pp 36–49, 2018.

**A. Shahini** and N. Ansari, "NOMA Aided Narrowband IoT for Machine Type Communication with User Clustering," *IEEE Internet of Things Journal,* in review.

**A. Shahini** and N. Ansari, "Sub-channel Allocation in Green Powered Heterogeneous Cognitive Radio Networks," *2016 IEEE 37th Sarnoff Symposium*, Newark, NJ, pp. 13–18, Sep 2016.

**A. Shahini**, A. Bagheri, and A. Shahzadi, "A Unified Approach to Performance Analysis of Energy Detection With Diversity Receivers Over Nakagami-m Fading Channels," *in International Conference on Connected Vehicles and Expo (ICCVE)*, Las Vegas, NV, pp. 707–712, Dec 2013.

A. Bagheri, **A. Shahini**, and A. Shahzadi, "Analytical and Learning-Based Spectrum Sensing Over Channels With Both Fading and Shadowing," *in International Conference on Connected Vehicles and Expo (ICCVE)*, Las Vegas, NV, pp. 699–706, Dec 2013.

S. Tabatabaee, A. Bagheri, **A. Shahini**, and A. Shahzadi, "An Analytical Model for Primary User Emulation Attacks in IEEE 802.22 Networks," *in International Conference on Connected Vehicles and Expo (ICCVE)*, Las Vegas, NV, pp. 693–698, Dec 2013.

**Dedicated to my inspiring parents and loving siblings**

*For their endless love, ever-present support, and continuous encouragement throughout my life.*

## ACKNOWLEDGMENT

I would like to express my deepest gratitude to my advisor, Prof. Nirwan Ansari for the continuous support of my Ph.D study and giving me the freedom and encouragement to explore research ideas while providing excellent guidance. His persistent support and patience helped me overcome many difficult situations throughout my research. Without his continuous help, this dissertation would not have been possible.

I would also like to thank my committee members, Prof. Ali Abdi, Prof. Abdallah Khreishah, Prof. Roberto Rojas-Cessa, and Prof. Guiling Wang. I thank them for their time and advisement. I want to thank my lab-mates in Advanced Networking Laboratory: Mina Taheri, Xueqing Huang, Xiang Sun, Abbas Kiani, Xilong Liu, Qiang Fan, Liang Zhang, Di Wu, Jingjing Yao, and Shuai Zhang, who have given me support and encouragement over the last three and half years. I would like to extend my gratitude to other faculty and staff members of the Department of Electrical and Computer Engineering for their support throughout my doctoral studies.

Last but not the least, I would like to thank my family. Words cannot express how grateful I am to my mother and father for all of the sacrifices that they have made and for all of the love that they have shown me. Their prayers for me were what sustained me so far.

## TABLE OF CONTENTS

**TABLE OF CONTENTS**
**(Continued)**

**Chapter** **Page**

## TABLE OF CONTENTS
## (Continued)

**Chapter** **Page**

## LIST OF TABLES

## LIST OF FIGURES

## LIST OF FIGURES
## (Continued)

**Figure** **Page**

# CHAPTER 1

# INTRODUCTION

The available radio frequency spectrum is getting crowded by the rapid growth of wireless applications and higher data rate devices [6, 84]. Owing to inefficient conventional regulatory policies, a considerable amount of the radio spectrum is greatly underutilized. Cognitive Radio (CR), as a promising paradigm with great potential of enhancing the spectrum utilization, allows efficient spectrum sharing between Primary Users (PUs) and Secondary Users (SUs) [29]. In a CR network, SUs are allowed to sense the radio spectrum and occupy spectrum holes (i.e., spectral bands not utilized by PUs [29]) in an opportunistic manner [31]. The CR system has different functionalities in which spectrum sensing is considered to be the most challenging part of this system [8]. In practice, spectrum sensing cannot be reliably achieved by SUs due to shadowing and multipath fading. To alleviate the adverse impact of fading and achieve reliable spectrum sensing, cooperative spectrum sensing has been proposed and investigated [2, 14, 33, 64, 70]. However, this functionality of sensing the radio spectrum incurs additional energy consumption.

Recent advances in energy harvesting are empowering the green powered CR network, in which SUs are equipped with energy harvesting capabilities to capture and store ambient energy which can significantly reduce carbon footprints [28, 32, 35, 36]. In [79], the energy efficient resource allocation problem in heterogeneous CR systems is formulated and an iterative-based algorithm is proposed to solve the energy efficient resource allocation problem. Varshney [72] proposed a capacity-energy function and the idea of simultaneous data and energy transmission. Yin *et al.* [83] studied the duration of harvesting and number of sensed channels in one time slot. Their general problem is formulated as a mixed integer non-linear programming (MINLP)

problem to maximize the achievable throughput of one SU with perfect spectrum sensing and without considering interference. In practical wireless systems, there are inevitable sensing errors stemmed from estimation errors, quantization errors and feedback delays. This imperfect spectrum sensing leads to substantial interference to the PUs caused by SUs. Thus, in order to prevent performance degradation of PUs, there should be a flexible physical layer for the CR system to control the interference generated by SUs.

Orthogonal Frequency Division Multiplexing (OFDM) is commonly known as a promising air interface for CR systems due to its great flexibility of radio resource allocation [76]. In [73], sub-channel allocation and power allocation schemes have been incorporated in the OFDM based CR network with imperfect spectrum sensing. Wang *et al.* [74] proposed the sum capacity maximization for a CR system with a low complexity algorithm while satisfying SUs' rate requirements. In [25], fair resource allocation has been proposed for CR and femtocell networks. However, imperfect spectrum sensing has not been considered in [25, 74]. Since it is extremely difficult to attain perfect spectrum sensing in practical CR systems, sub-channel allocation with imperfect spectrum sensing should be considered. To the best of our knowledge, interference-aware resource allocation and structure optimization for energy harvesting enabled SUs for OFDM based heterogeneous CR networks with imperfect cooperative spectrum sensing has not been studied.

In this dissertation, we investigate the joint sub-channel allocation and structure optimization for OFDM based heterogeneous CR networks by using RF energy harvesting, with consideration of interference limitations, imperfect spectrum sensing, and various rate requirements of SUs. Since SUs are assumed to operate in a time switching fashion, each time slot is partitioned into three non-overlapping fractions devoted for energy harvesting, spectrum sensing and data transmission. The first part of each time slot is allocated for energy harvesting characterized by a metric called

harvesting ratio. Although the higher harvesting ratio implies more time allocated for energy harvesting (extracting more energy), it leads to less remaining time for data transmission. Hence, the ultimate goals are to find optimal harvesting ratios (best tradeoff between operations) of SUs and optimal sub-channel allocation to SUs in order to maximize the total throughput of the CR network. The main contributions of this dissertation can be summarized as follows.

- We formulate the joint sub-channel allocation and structure optimization as a sum rate maximization of SUs in OFDM based heterogeneous CR networks by using RF energy harvesting, where interference limits are imposed to protect the PUs, rate requirements for both real-time and non-real-time SUs are considered to guarantee fairness for SUs in each CR network, and cooperative spectrum sensing is employed to provide more reliable results of channel sensing while considering imperfect spectrum sensing.

- We analyze the general optimization problem and show that it is MINLP, computationally intractable and NP-hard. Thus, we propose to address the general problem in two steps by mathematically decomposing it into two subproblems. We thus propose a sub-channel allocation scheme based on a factor called Energy Figure of Merit to approximately satisfy SUs' rate requirements and remove the integer constraints. In the sub-channel allocation process, the real-time (RT) SUs have higher priority to receive sub-channels as compared to non-real-time (NRT) SUs.

- We prove that the general optimization problem is reduced to a nonlinear convex optimization task. Since the reduced optimization problem does not have a simple closed-form solution for optimal harvesting ratios of SUs, we thus propose a near optimal closed-form solution by utilizing Lambert-W function to obtain optimal harvesting ratios. In order to derive the closed-form solution, we prove

a lemma (Lemma 3) that can be utilized for other similar problems. We also exploit the iterative gradient method based on Lagrangian dual decomposition to achieve near optimal solutions.

- The proposed methods and algorithms are evaluated by extensive simulations. The simulation results show that the proposed sub-channel allocation scheme outperforms the existing schemes especially when the number of available sub-channels is small. The simulation and numerical results verify the effectiveness of our closed-form solution for harvesting ratios of SUs, where the performance gap from the optimal solution is less than 3.5% for various cases. Further, we analyze the performance of our system in terms of interference protection of PUs, and different SUs' required rate constraints.

# CHAPTER 2

# THE SYSTEM ARCHITECTURE

Consider an uplink OFDM-based heterogeneous CR network compromising $L$ PUs denoted by $\mathcal{L} = \{1, 2, ..., L\}$ and $K$ self-powered SUs represented by $\mathcal{K} = \{1, 2, ..., K\}$ with $N$ OFDM licensed sub-channels operating in the slotted mode. These aggregated OFDM sub-channels constitute the licensed spectrum such that parts of the spectrum are registered by PUs. The SUs harvest energy from ambient radio signals and have no other power supplies. To support diverse services, the CR network has $i_0$ NRT SUs with rate constraints $\zeta_i$, and $K - i_0$ RT SUs with minimum required rate $R_i^{req}$. In other words, the set of NRT SUs is denoted by $\mathcal{K}_N = \{1, ..., i_0\}$ and the set $\mathcal{K}_R = \{i_0+1, ..., K\}$ represents the RT SUs. The licensed sub-channels are opportunistically utilized by SUs via an Access Point (AP). We assume that the SUs have perfect knowledge of Channel State Information (CSI) between their transmitters and the AP receiver. In our work, the general system model of a heterogeneous CR network is illustrated in Figure 2.1.

## 2.1 Cooperative Spectrum Sensing

In our system model, each SU does a local spectrum sensing concerning the presence or absence of PUs. It is assumed that the sensing results of SUs are independent and SUs sense all the PUs' sub-channels appointed by the AP. In order to reduce the spectrum sensing errors arisen from fading and shadowing, Cooperative Spectrum Sensing (CSS) has been exploited. In our CSS scenario, multiple SUs sense the licensed sub-channels independently, and the PUs' activities can be predicted by the AP [48] using the collected sensing results of SUs. Figure 2.2 illustrates a CSS scenario in which $K$ SUs independently sense $N$ sub-channels and identify the absence and presence of PUs by 0 and 1, respectively. In fact, these one-bit decisions are reported

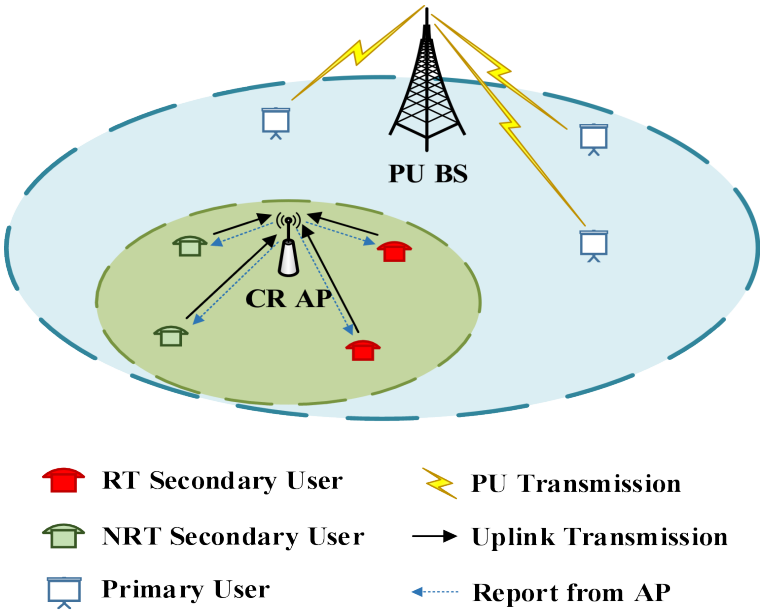


**Figure 2.1** System model of the heterogeneous CR network. Both RT SUs and NRT SUs are shown around one AP.

to a Fusion Center (FC) which is located in the AP. Then, FC applies a fusion strategy and generates final decisions regarding availability of OFDM licensed sub-channels. In this work, we assume that each SU applies the Energy Detection (ED) strategy which has low computational complexities [64], and the FC follows the Majority rule (generalized as $k$-out-of-$n$) [8]. Finally, the available sub-channels of a subset $\mathcal{M} = \{1, 2, ..., M\}$ among all the licensed sub-channels of a subset $\mathcal{N} = \{1, 2, ..., N\}$ are identified by the AP and replied to SUs at the beginning of each time slot.

## 2.2 Time Slot Model

In this work, an OFDM based CR system with SUs operating in a slotted mode is considered. Each SU in one time slot, is expected to do the following operations: (1) energy harvesting, (2) contributing in cooperative spectrum sensing, and (3) data transmission. In each time slot with duration $T$, due to the duplex-constrained hardware [34], the energy harvesting process and energy consuming process for SUs should be scheduled in a time switching fashion [35]. Thus, we assume SUs operate in

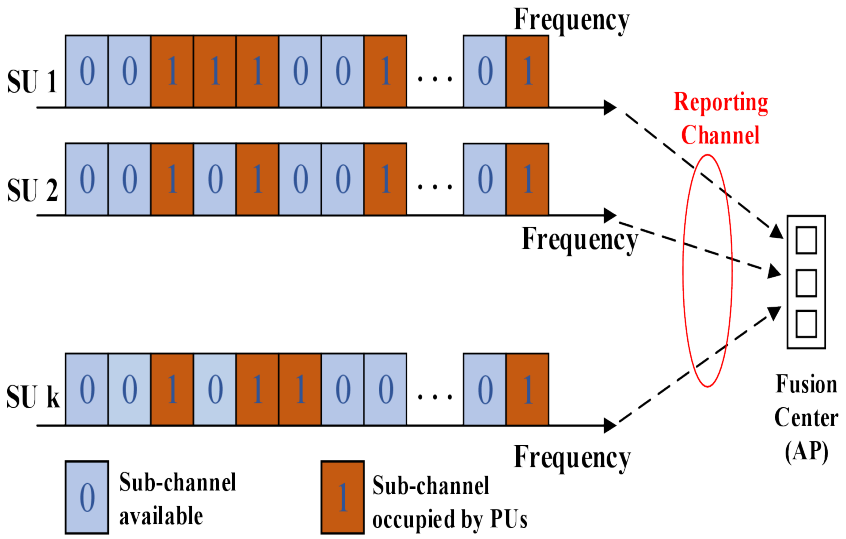


**Figure 2.2** The SUs report their spectrum sensing results to the FC for making the final decision.

a time switching fashion, and the time slot is partitioned into three non-overlapping parts devoted for energy harvesting, spectrum sensing and data transmission, respectively. Hence, the first fraction of each time slot (harvesting ratio: $\theta_i$, $\forall i \in \mathcal{K}$) is allocated for energy harvesting. Although traditional energy-constrained wireless networks are powered by fixed energy sources like batteries, it may be expensive, inconvenient[1], and even hazardous[2] [26]. Thus, the SUs are considered to have no power supplies other than harvesting energy from ambient radio signals[3]. Then, spectrum sensing, which depends on SUs' location and performance of sensing, can be accomplished in the second step of each time slot. During the sensing time ($\tau_{s_i}$, $\forall i \in \mathcal{K}$), SUs sense the licensed sub-channels and report their local sensing results to the FC, where the final decision regarding availability of sub-channels would be finalized. The third part of the time slot is utilized for data transmission. In fact, the available sub-channels are allocated to SUs by AP at the beginning of each time slot

[1]One of the dominant barriers to implementing IoT networks is providing adequate energy for operating the network in a self-sufficient manner [39].
[2]Battery replacements can be dangerous in a toxic environment [26].
[3]Energy-harvesting circuits (e.g., P2110B Powercast receiver [18]) can harvest micro-watts to milliwatts of power within the range of several meters for a transmit power of 1 W and a carrier frequency of 915MHz [18].

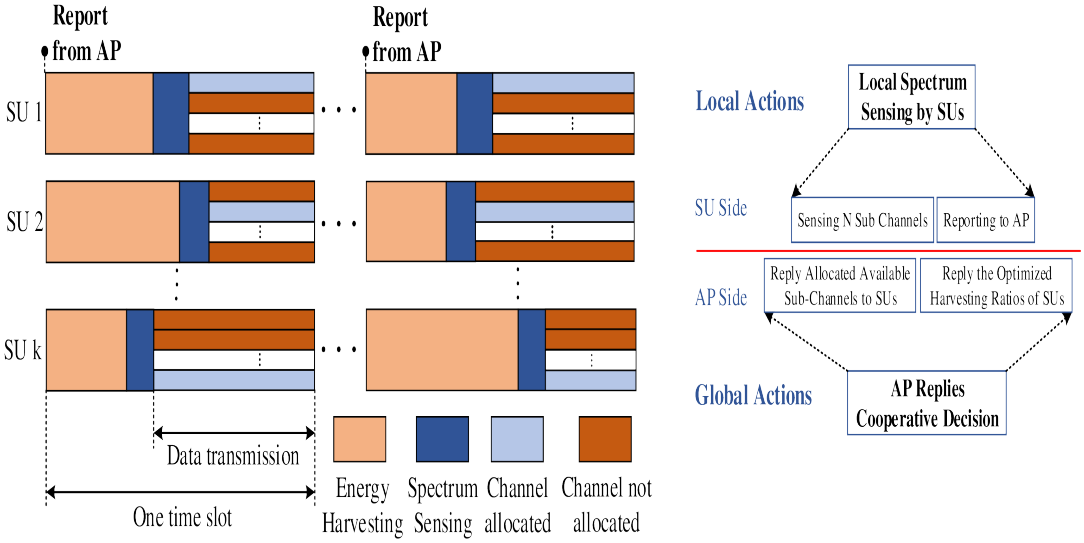


(a) Each time slot is partitioned into three non-overlapping parts.

(b) Cooperative spectrum sensing procedure.

**Figure 2.3** The time slot structure with energy harvesting for multiple SUs.

and SUs transmits data using all the remaining harvested energy after the spectrum sensing phase.

The time slot structures for $K$ SUs are illustrated in Figure 2.3(a), in which each SU has different harvesting ratio, sensing time and transmission time. At the beginning of each time slot, SUs receive reports from AP regarding the SUs' sub-channel allocations and optimized harvesting ratios. Hence, SUs start extracting energy from ambient radio signals during interval $(0, \theta_i T]$ and store it in a storage for future use within the time slot only. Then, SUs switch from harvesting to spectrum sensing during $(\theta_i T, \theta_i T+\tau_{s_i}]$. Note that, SUs have different performance of sensing, and thus various sensing time $\tau_{s_i}$. Meanwhile, AP receives the spectrum sensing results, makes the final decision, and reports it to SUs at the beginning of the next time slot. Furthermore, during the third fractions of the time slot, SUs start transmitting data using the harvested energy.

Figure 2.3(b) describes the cooperative spectrum sensing procedure, where the SUs operate and report local channel sensing to the AP during the sensing time in

**Table 2.1** Spectrum Sensing Results of SUs

| No. | Actual | Sensing | Probabilities |
|---|---|---|---|
| 1 | $\mathcal{H}_{1,\ell}$ | $\mathcal{S}_{1,\ell}$ | $P_d = P\{\mathcal{S}_{1,\ell}\|\mathcal{H}_{1,\ell}\} = 1 - Q_\ell^m$ |
| 2 | $\mathcal{H}_{1,\ell}$ | $\mathcal{S}_{0,\ell}$ | $P_m = P\{\mathcal{S}_{0,\ell}\|\mathcal{H}_{1,\ell}\} = Q_\ell^m$ |
| 3 | $\mathcal{H}_{0,\ell}$ | $\mathcal{S}_{1,\ell}$ | $P_f = P\{\mathcal{S}_{1,\ell}\|\mathcal{H}_{0,\ell}\} = Q_\ell^f$ |
| 4 | $\mathcal{H}_{0,\ell}$ | $\mathcal{S}_{0,\ell}$ | $P\{\mathcal{S}_{0,\ell}\|\mathcal{H}_{0,\ell}\} = 1 - Q_\ell^f$ |

each time slot. Hence, cooperative decision strategies are utilized at the AP side to make reliable sensing results and report them to SUs for the next time slot. However, perfect spectrum sensing in practical CR systems cannot be accomplished due to imperfect channel sensing with typical sensing errors. As a matter of fact, spectrum sensing errors are generally categorized into two groups: *miss-detections* and *false alarms*. Miss-detection happens when the CR network fails to detect the PU signals and false alarm occurs when the CR system identifies an actually vacant sub-band as being used by the PU. Clearly, co-channel interferences to the PUs arise from miss-detection errors and spectrum efficiency utilization is degraded by false alarm errors. Throughout this work, $Q_\ell^m$ and $Q_\ell^f$ denote the probabilities of miss-detection and false alarm on the $\ell^{th}$ sub-channel, respectively.

Table 2.1 illustrates possible outcomes of spectrum sensing by SUs. Presence and absence of PUs can be represented by $\mathcal{H}_{1,\ell}$ and $\mathcal{H}_{0,\ell}$, while the sensing results of the $\ell^{th}$ sub-channel for availability and unavailability of PUs are denoted by $\mathcal{S}_{1,\ell}$ and $\mathcal{S}_{0,\ell}$, respectively. Moreover, $P_d$, $P_m$, and $P_f$ are probabilities of detection, miss-detection, and false alarm, respectively. The final decision regarding availability of licensed sub-channels is made by the FC at the AP, based on the sensed information of SUs. Meanwhile, one should consider the analyzing, processing, and optimization time of the AP as well as replying time of the final decision from the AP to SUs. Hence, considering this elapsed time by the AP, the final result of cooperative spectrum

**Table 2.2** List of Symbol Notations and Description

| **Symbols** | **Descriptions** |
|---|---|
| L ($\mathcal{L}$) | The total number of PUs (the set of PUs ) |
| K ($\mathcal{K}$) | The total number of SUs (the set of SUs) |
| $\mathcal{K}_R$ ($\mathcal{K}_N$) | The set of real time SUs (the set of non real time SUs) |
| M | The number of available sub-channels determined by FC |
| $\mathcal{M}$ | The set of available sub-channel determined by FC |
| T ($f_s$ ) | The duration of time slot (the starting frequency) |
| $\omega$ ($t$) | The bandwidth of each sub-channel (the OFDM symbol duration) |
| $h_{i,j}$ | The channel gain between the $i^{th}$ SU and the AP over sub-channel $j$ |
| $\varphi(f)$ | The PSD of OFDM signal |
| $\mathcal{H}_{1,\ell}$ | The presence of the PU's signal on the $\ell^{th}$ sub-channel |
| $\mathcal{H}_{0,\ell}$ | The absence of the PU's signal on the $\ell^{th}$ sub-channel |
| $\mathcal{S}_{1,\ell}$ | The $\ell^{th}$ sub-channel is determined available by the FC |
| $\mathcal{S}_{0,\ell}$ | The $\ell^{th}$ sub-channel is determined unavailable by the FC |
| $\theta_i$ | The harvesting ratio of the $i^{th}$ SU in each time slot |
| $\tau_{s_i}$ | The sensing time of the $i^{th}$ SU |
| $\chi_i$ | The rate of energy harvesting for the $i^{th}$ SU |
| $\epsilon_{s_i}$ | The energy consumed by the $i^{th}$ SU for sensing |
| $I_m^{th}$ | The interference threshold of the $m^{th}$ PU |
| $R_i^{req}$ | The required rate of the $i^{th}$ SU for RT users |
| $\zeta_i$ | The rate constraint of the $i^{th}$ SU for NRT users |
| $f_{i,j}$ | The indicator function for assigning the $j^{th}$ sub-channel to the $i^{th}$ SU |
| $r_{i,j}$ | The transmission rate of the $i^{th}$ SU over the $j^{th}$ sub-channel |
| $\alpha_{EFM}^i$ | The energy figure of merit factor for the $i^{th}$ SU |

sensing regarding availability of sub-channels is known for SUs at the beginning of the next time slot. In fact, SUs receive reports from AP at the beginning of the time slot concerning the SUs' sub-channel allocations and optimized harvesting ratios. Note that we assume states of sub-channels do not change within a time slot and SUs have plenty of data in their buffers. The available sub-channels in the sub-band of the $m^{th}$ PU are denoted by subset $\mathcal{M}_{A,m}$, while the unavailable sub-channels are represented by subset $\mathcal{M}_{U,m}$. Some of frequently used notations and terminologies are summarized in Table 2.2.

## 2.3 Problem Formulation

In this part, an optimization framework is formulated to maximize the total throughput of a green powered OFDM based heterogeneous CR network under some practical considerations. In fact, the problem is a joint sub-channel allocation and structure optimization problem which aims at maximizing the SUs sum rate by allocating the optimal number of sub-channels to SUs and finding the optimal trade-off between fractions of the SUs' time slot.

Denote $\omega$ as the bandwidth of each OFDM sub-channel, and the range of nominal spectrum for the $\ell^{th}$ sub-channel is from $f_s+(\ell-1)\omega$ to $f_s+\ell\omega$ ($f_s$ is the starting frequency). The amount of interference introduced to the $j^{th}$ sub-channel in the sub-band of the $m^{th}$ PU caused by the $i^{th}$ SU transmission over the $\ell$ sub-channel with unit transmission power can be expressed as [9]

$$I_{i,j,m}^{\ell} = \int_{(j-1)\omega-(\ell-1/2)\omega}^{j\omega-(\ell-1/2)\omega} \varphi(f) g_{i,\ell,m} df, \tag{2.1}$$

where $\varphi(f) = t(\frac{\sin(\pi f t)}{\pi f t})^2$ represents the power spectrum density (PSD) of the OFDM signal ($t$ is the OFDM symbol duration) and $g_{i,\ell,m}$ denotes the power gain from the $i^{th}$ SU to the receiver of the $m^{th}$ PU on the $\ell$ sub-channel.

The probability of the CR system to make a correct decision that the $\ell^{th}$ sub-channel ($\ell \in \mathcal{M}$) is truly used by a PU is denoted by $P_\ell^1$:

$$\begin{aligned} P_\ell^1 =& P\{\mathcal{H}_{1,\ell}|\mathcal{S}_{1,\ell}\} \\ =& \frac{P\{\mathcal{H}_{1,\ell}\}P\{\mathcal{S}_{1,\ell}|\mathcal{H}_{1,\ell}\}}{P\{\mathcal{H}_{1,\ell}\}P\{\mathcal{S}_{1,\ell}|\mathcal{H}_{1,\ell}\} + P\{\mathcal{H}_{0,\ell}\}P\{\mathcal{S}_{1,\ell}|\mathcal{H}_{0,\ell}\}} \\ =& \frac{Q_\ell^L(1-Q_\ell^m)}{Q_\ell^L(1-Q_\ell^m) + (1-Q_\ell^L)Q_\ell^f}. \end{aligned} \tag{2.2}$$

Likewise, $P_\ell^2$ denotes the probability of the CR system in making a decision that the $\ell^{th}$ sub-channel is available but it is truly occupied:

$$\begin{aligned} P_\ell^2 &= P\{\mathcal{H}_{1,\ell}|\mathcal{S}_{0,\ell}\} \\ &= \frac{P\{\mathcal{H}_{1,\ell}\}P\{\mathcal{S}_{0,\ell}|\mathcal{H}_{1,\ell}\}}{P\{\mathcal{H}_{1,\ell}\}P\{\mathcal{S}_{0,\ell}|\mathcal{H}_{1,\ell}\} + P\{\mathcal{H}_{0,\ell}\}P\{\mathcal{S}_{0,\ell}|\mathcal{H}_{0,\ell}\}} \\ &= \frac{Q_\ell^L Q_\ell^m}{Q_\ell^L Q_\ell^m + (1-Q_\ell^L)(1-Q_\ell^f)}, \end{aligned} \tag{2.3}$$

where $Q_\ell^L$ represents the *a priori* probability that the sub-band of the $\ell^{th}$ sub-channel is used by PUs. Hence, the total interference introduced to the $m^{th}$ PU stemmed from the access of the $i^{th}$ SU on the $\ell^{th}$ sub-channel with unit transmission power is given as

$$I_{i,\ell,m} = \sum_{j \in \mathcal{M}_{A,m}} P_j^1 I_{i,j,m}^\ell + \sum_{j \in \mathcal{M}_{U,m}} P_j^2 I_{i,j,m}^\ell. \tag{2.4}$$

Meanwhile, the rate of transmission of the $i^{th}$ SU over the sub-channel $j$ in one time slot can be expressed as

$$r_{i,j} = (1 - \theta_i - \frac{\tau_{s_i}}{T}) log_2(1 + \frac{|h_{i,j}|^2(\chi_i \theta_i T - \epsilon_{s_i})}{\Gamma(\omega N_0 + I_i)(T - \theta_i T - \tau_{s_i})}), \tag{2.5}$$

where $\theta_i$ denotes the harvesting ratio of the $i^{th}$ SU, $\chi_i$ is the energy harvesting rate of the $i^{th}$ SU, $h_{i,j}$ denotes the channel gain of the $i^{th}$ SU over sub-channel $j$, $N_0$ represents the additive white Gaussian noise, $\epsilon_{s_i}$ denotes the energy of sensing by

the $i^{th}$ SU, and $\Gamma$ is the SNR gap. $\Gamma$ is associated with the bit-error-rate (BER) of un-coded MQAM and $\Gamma = -ln(5 \times BER)/1.5$ [23]. The interference introduced to the $i^{th}$ SU caused by the PUs' signals represented by $I_i$ is considered as noise and can be computed by the proposed method in [88]. Thus, the total transmission rate of the $i^{th}$ SU can be given as

$$R_i = \sum_{j=1}^{M} f_{i,j}(1 - \theta_i - \frac{\tau_{s_i}}{T}) log_2(1 + H_{i,j} \frac{\chi_i \theta_i T - \epsilon_{s_i}}{T - \theta_i T - \tau_{s_i}}). \tag{2.6}$$

The binary variable $f_{i,j} \in \{0, 1\}$ is utilized to represent the sub-channel assignment between SU $i$ and sub-channel $j$:

$$f_{i,j} = \begin{cases} 1, & \text{if sub-channel } j \text{ is assigned to SU } i \\ 0, & \text{otherwise.} \end{cases} \tag{2.7}$$

Note that the term of $H_{i,j} = \frac{|h_{i,j}|^2}{\Gamma(\omega N_0 + I_i)}$ is used in (2.6) for simplicity.

Finally, the general problem of the uplink sum rate maximization of SUs can be formulated by taking into consideration of interference constraints while guaranteeing the rate requirements of SUs and optimizing the time slot structure. Thus, the general optimization problem (**P1**) can be given as

$$\begin{aligned}
\max_{\theta_i, f_{i,j}} \quad & \sum_{i=1}^{K} \sum_{j=1}^{M} f_{i,j}(1 - \theta_i - \tfrac{\tau_{s_i}}{T}) log_2(1 + H_{i,j} \tfrac{\chi_i \theta_i T - \epsilon_{s_i}}{T - \theta_i T - \tau_{s_i}}) \\
s.t. \quad & \mathbf{C1} \quad \chi_i \theta_i T - \epsilon_{s_i} > 0, \ \forall i \in \mathcal{K}, \\
& \mathbf{C2} \quad T - \theta_i T - \tau_{s_i} > 0, \ \forall i \in \mathcal{K}, \\
& \mathbf{C3} \quad \sum_{i \in \mathcal{K}} \sum_{j \in \mathcal{M}} f_{i,j} \tfrac{\chi_i \theta_i T - \epsilon_{s_i}}{T - \theta_i T - \tau_{s_i}} I_{i,j,m} \leq I_m^{th}, \ \forall m \in \mathcal{L} \\
& \mathbf{C4} \quad \sum_{i \in \mathcal{K}_{\mathcal{R}}} \sum_{j \in \mathcal{M}} f_{i,j} r_{i,j} \geqslant R_i^{req}, \\
& \mathbf{C5} \quad \sum_{i \in \mathcal{K}_{\mathcal{N}}} \sum_{j \in \mathcal{M}} f_{i,j} r_{i,j} \geqslant \zeta_i, \\
& \mathbf{C6} \quad \sum_{i \in \mathcal{K}} f_{i,j} = 1, \ \forall j \in \mathcal{M}, \\
& \mathbf{C7} \quad f_{i,j} \in \{0, 1\}, \ \forall i \in \mathcal{K}, \ \forall j \in \mathcal{M}, \\
& \mathbf{C8} \quad 0 < \theta_i < 1, \ \forall i \in \mathcal{K},
\end{aligned} \tag{2.8}$$

where **C1** imposes energy of sensing to be less than the total harvested energy, **C2** means that the remaining time for data transmission must be greater than the sum of harvesting time and sensing time in one time slot, **C3** specifies that the total interference to the $m^{th}$ PU must be less than a given threshold, **C4** implies that the minimum required rate of RT SUs must be satisfied, **C5** means the NRT SUs rate must be greater than a given rate constraint, **C6** and **C7** specify that each sub-channel cannot be allocated to more than one SU, and **C8** means the harvesting ratio should be a fraction of a time slot.

# CHAPTER 3

# THROUGHPUT OPTIMIZATION

## 3.1 Solution Methodology

Note that **P1** is an MINLP problem, which contains both binary variables $f_{i,j}$ and continuous variables $\theta_i$ for optimization. In fact, the objective function of the general optimization problem is not jointly convex for $\{\theta_i, f_{i,j}\}$. The MINLP optimization problems are generally difficult to solve due to the combinatorial nature of mixed-integer programming (MIP) and the difficulty in solving nonlinear programming (NLP) problems [37].

Some methods such as outer-approximation, branch-and-bound, extended cutting plane methods, and the *sorting and removing* method [21, 37] have been proposed to solve MINLP problems. However, the aforementioned methods cannot be exploited to our problem specific structures and properties. The minimax convex relaxation technique can also be considered as a possible solution for MINLP problems. Meanwhile, it cannot be applied to solve (2.8) because it is not efficient for a large number of decision variables.

**Remark 1.** *The joint channel allocation and structure optimization problem (**P1**) is an MINLP problem, which exhibits the combinatorial nature of MIP problems and the difficulty in solving NLP problems. In fact, both MIP and NLP are considered NP-complete, and thus the joint resource allocation and structure optimization problem is NP-hard and requires exponential time complexity to solve for the optimal solutions [22, 27, 37].*

Since the general optimization problem is computationally intractable, a two-stage approach is considered to reduce the complexity of the problem. This technique

has achieved success in various scenarios [73]. Specifically, we first propose a sub-channel allocation scheme based on a factor called Energy Figure of Merit ($\alpha_{EFM}$). In this sub-channel allocation scheme, the heterogeneous SUs' rate requirements are roughly satisfied. Then, after removing the integer constraints of (2.8), the general nonconvex problem can be reduced to a new convex optimization problem. Thus, the optimum fraction of the time slot that each SU can harvest energy from the environment, can be obtained by solving the new convex optimization problem.

### 3.2 Sub-channel Allocation Scheme

We focus on solving the general optimization problem **P1** by first employing the primal decomposition method where it can be decomposed into two subproblems. By having fixed the harvesting ratios ($\theta_i$) of each time slot, **P1** is simplified to the following optimization subproblem

$$
\begin{aligned}
\mathbf{P2}: \max_{f_{i,j}} \quad & \sum_{i\in\mathcal{K}}\sum_{j\in\mathcal{M}} f_{i,j} r_{i,j} \\
s.t. \quad & \mathbf{C1} \quad \sum_{i\in\mathcal{K}}\sum_{j\in\mathcal{M}} f_{i,j} p_{i,j} I_{i,j,m} \leqslant I_m^{th},\ \forall m \in \mathcal{L}, \\
& \mathbf{C2} \quad \sum_{i\in\mathcal{K}_{\mathcal{R}}}\sum_{j\in\mathcal{M}} f_{i,j} r_{i,j} \geqslant R_i^{req}, \\
& \mathbf{C3} \quad \sum_{i\in\mathcal{K}_{\mathcal{N}}}\sum_{j\in\mathcal{M}} f_{i,j} r_{i,j} \geqslant \xi_i, \\
& \mathbf{C4} \quad \sum_{i\in\mathcal{K}} f_{i,j} = 1,\ \forall j \in \mathcal{M}, \\
& \mathbf{C5} \quad f_{i,j} \in \{0,1\},\ \forall i \in \mathcal{K},\ \forall j \in \mathcal{M},
\end{aligned}
\tag{3.1}
$$

where $p_{i,j}$ denotes the transmission power allocated by the $i^{th}$ SU to the $j^{th}$ available sub-channel.

Denote the total transmission power for each SU $\forall i \in \mathcal{K}$ as $\frac{\chi_i \theta_i T - \epsilon_{s_i}}{T - \theta_i T - \tau_{s_i}}$. It can be observed from the derivative of the transmission power with respect to $\theta_i$ that the transmission power is strictly increasing in $\theta_i \in (0,1)$, $\forall i \in \mathcal{K}$. Hence, the maximum transmission power occurs at the upper bound of the harvesting ratio

($\theta_i \simeq 1$). Meanwhile, initial harvesting ratios (initial transmission power) would not likely yield the maximum transmission power, and thus the interference limit $\sum_{i\in\mathcal{K}}\sum_{j\in\mathcal{M}} f_{i,j}p_{i,j}I_{i,j,m} \leqslant I_m^{th}$ is satisfied and can be ignored in the sub-channel allocation process. To solve **P2**, one of the most important considerations in the channel allocation process is to scrutinize the rate requirements of both RT and NRT cognitive users. Hence, the rate requirements in **C2** and **C3** play a key role in the sub-channel allocation process.

The following sub-channel allocation algorithm (Algorithm 1) requires $\theta_i$ to be initialized. Since $\theta_i > \frac{\epsilon_{s_i}}{\chi_i T}$ and $\theta_i < \frac{T-\tau_{s_i}}{T}$, $\forall i \in \mathcal{K}$, the initial $\theta_i$, $\forall i \in \mathcal{K}$ can be expressed as

$$\theta_i^{initial} = \frac{\epsilon_{s_i}}{2\chi_i T} + \frac{1}{2}\left(1 - \frac{\tau_{s_i}}{T}\right), \tag{3.2}$$

i.e., the average of the upper and lower bounds.

**Algorithm 1 E**nergy **F**igure of **M**erit (EFM) based sub-channel allocation

**Initialization:**

Initial rates of SUs: $\mathcal{R} = \{R_1, ..., R_i\} = 0$

EFM factor for each SU: $\alpha_{EFM}^{i} = \frac{\chi_i}{\epsilon_{s_i}}, \forall i \in \mathcal{K}$

$\mathcal{M}_t = \mathcal{M}, \mathcal{D}_i = \emptyset, \forall i \in \mathcal{K}$

$\theta_i^{(0)}, \forall i \in \mathcal{K}$, with the initial values in (3.2)

**Sub-channel Allocation for RT SUs:**

While $\mathcal{M}_t \neq \emptyset$ and $\min(R_i - R_i^{req}) < 0$

Find $i^*$ that satisfies $\alpha_{EFM}^{i^*} \geq \alpha_{EFM}^{i}$ for $\forall i \in \mathcal{K}_{\mathcal{R}}$;

Finding the best sub-channel for $i^*$:

Find $j^* : j^* = \arg\max_{j \in \mathcal{M}_t} r_{i^*,j^*}$;

$\mathcal{M}_t = \mathcal{M}_t / j^*$ and $\mathcal{D}_{i^*} = \mathcal{D}_{i^*} \cup j^*$;

$R_{i^*} = R_{i^*} + (1 - \theta_{i^*}^{(0)} - \frac{\tau_{s_{i^*}}}{T}) log_2(1 + H_{i^*,j^*} \frac{\chi_{i^*} \theta_{i^*}^{(0)} T - \epsilon_{s_{i^*}}}{T - \theta_{i^*}^{(0)} T - \tau_{s_{i^*}}})$;

End while

**Define** $\mathcal{K}_R^{Al} = \{i \in \mathcal{K}_R, \mathcal{D}_i \neq \emptyset\}$

**Sub-channel Allocation for NRT SUs:**

While $\mathcal{M}_t \neq \emptyset$

Find $i^*$ that satisfies $\alpha_{EFM}^{i^*} \geq \alpha_{EFM}^{i}$ for $\forall i \in \mathcal{K}_{\mathcal{N}}$;

Finding the best sub-channel for $i^*$:

Find $j^* : j^* = \arg\max_{j \in \mathcal{M}_t} r_{i^*,j^*}$;

$\mathcal{M}_t = \mathcal{M}_t / j^*$ and $\mathcal{D}_{i^*} = \mathcal{D}_{i^*} \cup j^*$;

$R_{i^*} = R_{i^*} + r_{i^*,j^*}$;

End while

**Define** $\mathcal{K}_N^{Al} = \{i \in \mathcal{K}_N, \mathcal{D}_i \neq \emptyset\}$

In the sub-channel allocation process, RT SUs have higher priority for sub-channel allocations as compared to NRT SUs. Thus, the sub-channel allocation would

be done for RT SUs until the minimum rate requirements of RT SUs are satisfied. During each cycle, RT SU whose EFM factor ($\alpha^i_{EFM} = \frac{\chi_i}{\epsilon_{s_i}}$) is greater than the others has the priority to get a sub-channel among the available ones. In fact, the higher $\alpha_{EFM}$ stems from a greater amount of energy extracted from the environment and less amount of energy consumed by the spectrum sensing process. Thus, those SUs having higher $\alpha_{EFM}$ normally need less numbers of sub-channels to meet the required rate. Furthermore, the chosen SU preferably receives a sub-channel that has the highest corresponding achievable rate.

After RT SUs have been assigned sub-channels, the remaining ones are allocated to NRT SUs to meet their rate constraints. Like the RT sub-channel allocation process, the sub-channel assignments for NRT SUs follow the EFM-based user preference. The sub-channel allocation scheme continues until all sub-channels are assigned to SUs. Note that at the end of each round of sub-channel allocation for RT and NRT SUs, we define a new set for those SUs which have been assigned sub-channels. $\mathcal{K}_R^{Al}$ and $\mathcal{K}_N^{Al}$ are sets of RT and NRT SUs that have received sub-channels, respectively, and $\mathcal{K}^{Al} = \mathcal{K}_R^{Al} \cup \mathcal{K}_N^{Al}$ is the set of all SUs with allocated sub-channels. In this work, each SU is assumed to transmit all its harvested power over all its allocated sub-channels. The power allocation procedure for the assigned sub-channels to SUs is beyond the scope of this work.

### 3.3 Structure Optimization

After sub-channel allocation, the integer constraints of Equation (2.8) are removed because binary variables $f_{i,j}$ take on 0 or 1 indicating whether sub-channels are allocated or not. Thus, the new optimization problem, which aims at maximizing the sum-rate of SUs by finding optimum fractions of harvesting for all SUs, can be

expressed as

$$
\begin{aligned}
\mathbf{P3}: \max_{\theta_i} \; & \sum_{i \in \mathcal{K}^{Al}} \sum_{j \in \mathcal{D}_i} (1 - \theta_i - \tfrac{\tau_{s_i}}{T}) log_2(1 + H_{i,j} \tfrac{\chi_i \theta_i T - \epsilon_{s_i}}{T - \theta_i T - \tau_{s_i}}) \\
s.t. \quad & \mathbf{C1} \quad \chi_i \theta_i T - \epsilon_{s_i} > 0, \; \forall i \in \mathcal{K}^{Al}, \\
& \mathbf{C2} \quad T - \theta_i T - \tau_{s_i} > 0, \; \forall i \in \mathcal{K}^{Al}, \\
& \mathbf{C3} \quad \sum_{i \in \mathcal{K}^{Al}} \sum_{j \in \mathcal{D}_i} \tfrac{X_i \theta_i T - \epsilon_{s_i}}{T - \theta_i T - \tau_{s_i}} I_{i,j,m} \leq I_m^{th}, \; \forall m \in \mathcal{L}, \\
& \mathbf{C4} \quad \sum_{j \in \mathcal{D}_i} r_{i,j} \geq R_i^{req}, \; \forall i \in \mathcal{K}_R^{Al}, \\
& \mathbf{C5} \quad \sum_{j \in \mathcal{D}_i} r_{i,j} \geq \gamma_i, \; \forall i \in \mathcal{K}_N^{Al}, \\
& \mathbf{C6} \quad 0 < \theta_i < 1, \; \forall i \in \mathcal{K}^{Al}.
\end{aligned}
\tag{3.3}
$$

If **P3** describes a convex optimization problem, it can be solved by standard convex optimization methods such as the barrier method or iterative gradient technique with duality. Hence, the optimum fractions of the time slot for energy harvesting of SUs can be obtained. Therefore, since it is important to analyze convexity of **P3**, convexity of the objective function is established by the following Lemma.

**Lemma 1.** *The objective function in **P3** for $\forall i \in \mathcal{K}$, $0 < \theta_i < 1$, is a concave function.*

*Proof.* The Lemma is proved in Section A.1. □

Having proven the convexity of **P3**, the optimal harvesting ratios can be obtained; however, the constraints should be examined. In general, if constraint functions in an MINLP optimization problem are convex, the optimization problem is called a convex MINLP [10].

**Lemma 2.** *The joint resource allocation and time slot optimization problem **P1** is a convex MINLP.*

*Proof.* The Lemma is proved in Section A.2. □

Having proven **P1** being convex MINLP, one can propose a heuristic algorithm (like Feasibility Pump[1] (FP)) to obtain the optimal solution. The FP algorithm decomposes a mathematical programming problem into two parts: integer feasibility and constraint feasibility. For the convex MINLP scenario, the solution can be achieved by solving an LP or a convex NLP, which can be done in polynomial time [10].

To obtain the optimal solution of **P3**, the associated Lagrangian can be expressed as

$$\begin{aligned}
&L(\theta_1, \theta_2, ..., \theta_K, \lambda_i, \mu_i, \nu_m, \rho_i^R, \rho_i^N) = \\
&- \sum_{i \in \mathcal{K}^{Al}} \sum_{j \in \mathcal{D}_i} \left(1 - \theta_i - \frac{\tau_{s_i}}{T}\right) log_2 \left(1 + H_{i,j} \frac{\chi_i \theta_i T - \varepsilon_{s_i}}{T - \theta_i T - \tau_{s_i}}\right) \\
&+ \lambda_i (\varepsilon_{s_i} - \chi_i \theta_i T) + \mu_i (\theta_i T + \tau_{s_i} - T) \\
&+ \nu_m \left( \sum_{i \in \mathcal{K}^{Al}} \frac{\chi_i \theta_i T - \varepsilon_{s_i}}{T - \theta_i T - \tau_{s_i}} I_{i,m} - I_m^{th} \right) \\
&+ \rho_i^R \left( \begin{array}{l} R_i^{req} - \\ \sum_{j \in \mathcal{D}_i} \left(1 - \theta_i - \frac{\tau_{s_i}}{T}\right) log_2 \left(1 + H_{i,j} \frac{\chi_i \theta_i T - \varepsilon_{s_i}}{T - \theta_i T - \tau_{s_i}}\right) \end{array} \right) \\
&+ \rho_i^N \left( \begin{array}{l} \gamma_i - \\ \sum_{j \in \mathcal{D}_i} \left(1 - \theta_i - \frac{\tau_{s_i}}{T}\right) log_2 \left(1 + H_{i,j} \frac{\chi_i \theta_i T - \varepsilon_{s_i}}{T - \theta_i T - \tau_{s_i}}\right) \end{array} \right)
\end{aligned} \tag{3.4}$$

where $\lambda_i$, $\mu_i$, $\nu_m$, $\rho_i^R$ and $\rho_i^N$ are Lagrange multipliers. The dual function of **P3** in (3.3) is

$$g(\lambda, \mu, \nu, \rho^R, \rho^N) = \sup_{\theta_1, ..., \theta_k} L(\theta_1, ..., \theta_k, \lambda, \mu, \nu, \rho^R, \rho^N). \tag{3.5}$$

Thus, the dual optimization problem for (3.3) is

$$\begin{aligned}
\textbf{P4 :} \min \quad & g(\lambda, \mu, \nu, \rho^R, \rho^N) \\
& \lambda > 0, \mu > 0, \nu > 0, \rho^R > 0, \rho^N > 0
\end{aligned} \tag{3.6}$$

[1]The Feasibility Pump (FP) is one of the most well known primal heuristic for mixed integer non-linear programming [10].

In order to solve the dual problem, an iterative scheme using the gradient projection method can be applied. Thus, the Lagrange multiplier for **C1** is given as

$$\lambda_i^{(t+1)} = \left[\lambda_i^{(t)} - \alpha^{(t)} \frac{dL}{d\lambda_i}\right]^+ = \left[\lambda_i^{(t)} - \alpha^{(t)}(\epsilon_{s_i} - \chi_i \theta_i T)\right]^+. \tag{3.7}$$

The Lagrange multiplier for **C2** can be written as

$$\mu_i^{(t+1)} = \left[\mu_i^{(t)} - \beta^{(t)} \frac{dL}{d\mu_i}\right]^+ = \left[\mu_i^{(t)} - \beta^{(t)}(\theta_i T + \tau_{s_i} - T)\right]^+. \tag{3.8}$$

Likewise, the Lagrange multiplier of **C3** is expressed as

$$\begin{aligned} \nu_m^{(t+1)} = &\left[\nu_m^{(t)} - \pi^{(t)} \frac{dL}{d\nu_m}\right]^+ = \\ &\left[\nu_m^{(t)} - \pi^{(t)} \left(\sum_{i \in \mathcal{K}^{AI}} \sum_{j \in \mathcal{D}_i} \frac{\chi_i \theta_i T - \epsilon_{s_i}}{T - \theta_i T - \tau_{s_i}} I_{i,j,m} - I_m^{th}\right)\right]^+. \end{aligned} \tag{3.9}$$

The Lagrange multipliers of transmission rates for **C4** and **C5** are

$$\begin{aligned} \rho_i^{R,(t+1)} = &\left[\rho_i^{R,(t)} - \psi^{(t)} \frac{dL}{d\rho_i^R}\right]^+ = \\ &\left[\rho_i^{R,(t)} - \psi^{(t)} \left(R_i^{req} - \sum_{j \in \mathcal{D}_i} r_{i,j}(\theta_i)\right)\right]^+, \end{aligned} \tag{3.10}$$

and

$$\begin{aligned} \rho_i^{N,(t+1)} = &\left[\rho_i^{N,(t)} - \eta^{(t)} \frac{dL}{d\rho_i^N}\right]^+ = \\ &\left[\rho_i^{N,(t)} - \eta^{(t)} \left(\gamma_i - \sum_{j \in \mathcal{D}_i} r_{i,j}(\theta_i)\right)\right]^+, \end{aligned} \tag{3.11}$$

where $t$ is the iteration index, $\alpha^{(t)}$, $\beta^{(t)}$, $\pi^{(t)}$, $\psi^{(t)}$ and $\eta^{(t)}$ are sufficiently small positive step-sizes, and $[a]^+ = \max(0, a)$.

**Proposition 1.** *Dual variables* $\lambda_i^{(t)}$, $\mu_i^{(t)}$, $\nu_m^{(t)}$, $\rho_i^{R,(t)}$, *and* $\rho_i^{N,(t)}$ *can eventually converge to the dual optimal solution* $\lambda$, $\mu$, $\nu$, $\rho$, *and* $\varphi$ *if the step sizes are chosen such that* $\alpha^t \to 0, \sum_{t=0}^{\infty} \alpha^t = \infty$, $\beta^t \to 0, \sum_{t=0}^{\infty} \beta^t = \infty$, $\pi^t \to 0, \sum_{t=0}^{\infty} \pi^t = \infty$, $\psi^t \to 0, \sum_{t=0}^{\infty} \psi^t = \infty$, *and* $\eta^t \to 0, \sum_{t=0}^{\infty} \eta^t = \infty$.

*Proof.* In order to avoid convergence to a non-stationary point, some of step sizes should be infinite. Meanwhile, with respect to the iteration index, the step sizes $\alpha^t, \beta^t, \pi^t, \psi^t$, and $\eta^t$ tend to zero. Thus, the conditions comply the convergence of dual variables to their corresponding dual optimal solutions [7, 11]. □

The primal problem in Equation (3.3) is convex with positive constraints (as verified in Lemma 1 and 2). Thus, one can conclude from Proposition 1 that the Slater's condition for strong duality of the primal problem holds (duality gap is zero). Thus, the optimal solution to (3.6) is the global maximum of the primal problem. To obtain the optimal solution of harvesting ratios for SUs, the following sub-gradient method is used.

**Algorithm 2** Structure Optimization By Iterative Gradient Method

**Initialization:**

Setting $\theta_i$

Initialize $\lambda_i^{(0)}$, $\mu_i^{(0)}$, $\rho_i^{R,(0)}$, $\rho_i^{N,(0)}$, and $\nu_m^{(0)} = 0$

**Repeat** for $t \geq 1$

Compute optimal harvesting ratios:

$\theta_i^* = \arg\max_{\theta_i}(\lambda_i^{(t)}, \mu_i^{(t)}, \rho_i^{R,(t)}, \rho_i^{N,(t)}, \nu_m^{(t)})$

Update dual variables:

$\lambda_i^{(t+1)} = [\lambda_i^{(t)} - \alpha^{(t)} \frac{dL}{d\lambda_i}]^+$, $\mu_i^{(t+1)} = [\mu_i^{(t)} - \beta^{(t)} \frac{dL}{d\mu_i}]^+$, $\rho_i^{R,(t+1)} = [\rho_i^{R,(t)} - \psi^{(t)} \frac{dL}{d\rho_i^R}]^+$, $\rho_i^{N,(t+1)} = [\rho_i^{N,(t)} - \eta^{(t)} \frac{dL}{d\rho_i^N}]^+$, and $\nu_m^{(t+1)} = [\nu_m^{(t)} - \pi^{(t)} \frac{dL}{d\nu_m}]^+$

**Until** Convergence

Apart from solving the convex optimization problem using iterative gradient method, the optimal solution can be obtained by deriving a closed-form solution. The following theorem proposes a closed-form solution for optimal harvesting ratios of SUs solved by the AP.

**Theorem 1.** *The optimal solution of the harvesting ratio in one time slot for each SU,* $\forall i \in \mathcal{K} = \{1, 2, ..., K\}$*, can be attained as:*

$$\theta_i^* = \frac{T - \tau_{s_i}}{T} - \frac{\mathcal{W}\left(\frac{H\chi_i - 1}{e}\right) H\left(\chi_i T - \chi_i \tau_{s_i} - \varepsilon_{s_i}\right)}{T\left(H\chi_i - 1\right)\left(1 + \mathcal{W}\left(\frac{H\chi_i - 1}{e}\right)\right)}, \tag{3.12}$$

*where* $\mathcal{W}(.)$ *refers to the Lambert* $\mathcal{W}$ *function [17].*

*Proof.* We begin with the assumption that the harvesting ratio allocation set of (3.3) is a nonempty, convex and compact set [44]. Hence, the objective function is strictly concave with respect to $\theta_i$. Let $\lambda_i, \mu_i \geqslant 0$, $\forall i \in \mathcal{K} = \{1, 2, ..., K\}$, $\nu_m \geqslant 0$, $\forall m \in \mathcal{L} = \{1, 2, ..., L\}$, $\rho_i^R \geqslant 0$, $\forall i \in \mathcal{K}_R = \{i_0 + 1, ..., K\}$, and $\rho_i^N \geqslant 0$, $\forall i \in \mathcal{K}_N = \{1, 2, ..., i_0\}$ denote the Lagrange multipliers of lower-bound energy and time of transmission in **C1** and **C2**, interference constraint in **C3**, lower-bound transmission rate for RT and NRT users in **C4** and **C5**, respectively.

Therefore, using the Lagrangian of the optimization problem **P2** in Equation (3.4), the objective function can be optimized by exploiting the necessary and sufficient conditions,

$$\nabla \mathcal{L}(\theta^*, \lambda, \mu, \nu, \rho^R, \rho^N) = 0. \tag{3.13}$$

The objective function is given as

$$Obj = \left(\frac{T - T\theta_i - \tau_{s_i}}{T \ln 2}\right) log_2\left(1 + H_{i,j}\frac{\chi_i \theta_i T - \varepsilon_{s_i}}{T - \theta_i T - \tau_{s_i}}\right) \tag{3.14}$$

The derivative of the objective function with respect to the vector of harvesting ratios can be expressed as

$$\begin{aligned}\frac{d}{d\theta_i}(Obj) = \frac{1}{\ln 2}\Bigg[\ln\left(1 + H\frac{\chi\theta T - \varepsilon_s}{T - \theta T - \tau_s}\right) - \\ \frac{H\chi\left(T - \theta T - \tau_s\right) + H\left(\chi\theta T - \varepsilon_s\right)}{\left(T - \theta T - \tau_s\right) + H\left(\chi\theta T - \varepsilon_s\right)}\Bigg].\end{aligned} \tag{3.15}$$

Then, considering $\frac{d(\nabla\mathcal{L})}{d\theta_i}=0$, we have

$$\begin{aligned}&\frac{1}{\ln 2}\left[\begin{array}{l}\ln\left(1+H\dfrac{\chi\theta T-\varepsilon_s}{T-\theta T-\tau_s}\right)\\ -\dfrac{H\chi\left(T-\theta T-\tau_s\right)+H\left(\chi\theta T-\varepsilon_s\right)}{\left(T-\theta T-\tau_s\right)+H\left(\chi\theta T-\varepsilon_s\right)}\end{array}\right]-\lambda_i\chi_i T\\&+\mu_i T+\nu_m I_m\frac{H\chi T\left(T-\theta T-\tau_s\right)+HT\left(\chi\theta T-\varepsilon_s\right)}{\left(T-\theta T-\tau_s\right)^2}\\&+\rho_i^R\left(\frac{d}{d\theta_i}\left(Obj\right)\right)+\rho_i^N\left(\frac{d}{d\theta_i}\left(Obj\right)\right)=0,\end{aligned}\tag{3.16}$$

and the Lagrange multipliers constraints are equal to zero as follows

$$\begin{cases}\lambda_i(\varepsilon_{s_i}-\chi_i\theta_i T)=0, & i\in\mathcal{K}\\ \mu_i(\theta_i T+\tau_{s_i}-T)=0, & i\in\mathcal{K}\\ \nu_m\left(\frac{\chi_i\theta_i T-\varepsilon_{s_i}}{T-\theta_i T-\tau_{s_i}}I_{i,m}-I_m^{th}\right)=0, & i\in\mathcal{K},\ m\in\mathcal{L}\\ \rho_i^N\left(\gamma_i-R_i^{NT}\right)=0, & i\in\mathcal{K}_N\\ \rho_i^R\left(R_i^{req}-R_i^{RT}\right)=0, & i\in\mathcal{K}_R\end{cases}\tag{3.17}$$

In order to obtain the solutions, the values of multipliers in (3.17) should be considered. The first constraint, $\varepsilon_{s_i}=\chi_i\theta_i T$, represents the special case where the total harvested energy is consumed for the spectrum sensing. The second constraint $\theta_i T=T-\tau_{s_i}$ denotes the special case where there is no remaining time for data transmission. Thus, we are not interested in special cases and one can conclude $\lambda_i=0$ and $\mu_i=0$. The rate constraints, $R_i^{RT}=R_i^{req}$ and $R_i^{NT}=\gamma_i$, represent the special cases where the transmission rates of RT and NRT users meet the lower bound values which are not generally desired. For simplicity in the last constraint, we assume that the total interference introduced by SUs is always less than the maximum interference threshold. Therefore, one can conclude that $\nu_m=0$ because the total interference is assumed to be less than the threshold ($I_m^{th}$). Hence, the optimal harvesting time can

be obtained by solving the following equation.

$$\frac{1}{\ln 2}\left[\ln\left(1+H\frac{\chi\theta T-\varepsilon_s}{T-\theta T-\tau_s}\right)\right. \\ \left.-\frac{H\chi\left(T-\theta T-\tau_s\right)+H\left(\chi\theta T-\varepsilon_s\right)}{\left(T-\theta T-\tau_s\right)+H\left(\chi\theta T-\varepsilon_s\right)}\right]=0. \tag{3.18}$$

Define intermediate variables $a$ and $b$ as $a = T-\theta T-\tau_s$ and $b = \chi\theta T-\varepsilon_s$. Thus, we can re-write (3.18) as

$$\ln\left(\frac{a+Hb}{a}\right)=\frac{H\chi a+Hb}{a+Hb}. \tag{3.19}$$

One can conclude that $b = -\chi a+c$, where $c$ is defined as $c = \chi T-\chi\tau_s-\varepsilon_s$. Therefore,

$$\ln\left(1-H\chi+\frac{Hc}{a}\right)=\frac{Hc}{a\left(1-H\chi\right)+Hc}. \tag{3.20}$$

Define a new variable $t$ as $t = 1-H\chi+\frac{Hc}{a}$. Then,

$$t\ln\left(t\right)=t+H\chi-1. \tag{3.21}$$

**Lemma 3.** *The solution of $x\ln(x) = ax+b$ ($a$ and $b$ are constants), is*

$$x=\frac{b}{\mathcal{W}\left(\frac{b}{e^a}\right)},$$

*where $\mathcal{W}(.)$ is the Lambert $\mathcal{W}$ function.*

*Proof.* The Lemma is proved in Section A.3. □

Based on Lemma 3, the solution of (3.21) can be expressed as

$$t=\frac{H\chi-1}{\mathcal{W}\left(\frac{H\chi-1}{e}\right)}. \tag{3.22}$$

Therefore, using $t = 1-H\chi+\frac{Hc}{a}$ and $a = T-\theta T-\tau_s$, the global optimal solution of Equation (3.12) is proved. □

# CHAPTER 4

# SIMULATION RESULTS

Simulations have been conducted to demonstrate the performance of our proposal. Meanwhile, the impact of various parameters like interference thresholds of PUs, transmission rate constraints, energy harvesting rate, and sensing time on the network performance have been analyzed.

## 4.1 Simulation Setup

In all the simulations, channel gains are modeled as $h_{i,j} = \mathcal{Y} d_{i,j}^{-\beta}$, where $\mathcal{Y}$ is a random value generated according to the Rayleigh distribution, $d_{i,j}^{-\beta}$ is the geographical distance between the transmitter and receiver, and $\beta$ is the path-loss exponent [56]. $d$ varies between 50 m to 200 m, and $\beta = 3$. The bandwidth of each OFDM sub-channel is 62.5 kHz, and the noise power is $10^{-13}$W (or -100 dbm) in our simulation analysis. The overall probabilities of PUs' detection, mis-detection and false alarm are uniformly distributed over [0,1], [0.01, 0.05], and [0.05, 0.1], respectively. Various experimental results are provided to deeply analyze the performance of our network and investigate effects of different system parameters.

## 4.2 One SU Scenario

In this part, an experiment has been conducted to evaluate the performance of our system versus different system parameters. Figure 4.1(a) illustrates the optimal harvesting ratio ($\theta$) versus various amounts of harvesting rate ($\chi$) and spectrum sensing time for one SU ($\epsilon_s = 1$ mJ). It is clearly shown that a larger harvesting fraction is preferred when the spectrum sensing time decreases. At the same time as energy harvesting rate of the SU declines, the harvesting ratio grows exponentially. Figure 4.1(b) demonstrates the achievable throughput versus different sensing times

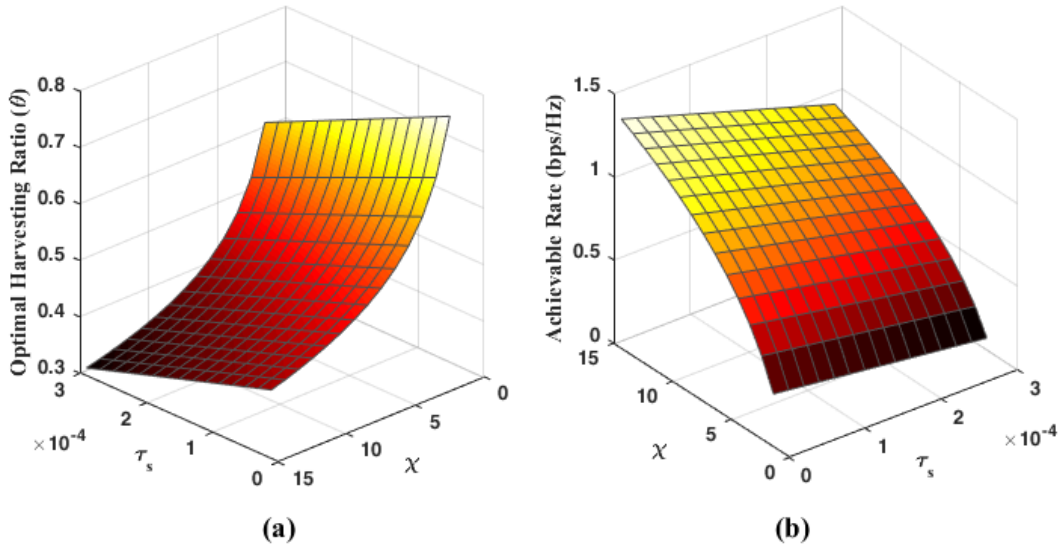


**Figure 4.1** The performance evolution of the heterogeneous CR system for one SU scenario: a) optimal harvesting ratio versus energy harvesting rate and time of sensing; b) achievable rate versus energy harvesting rate and sensing time.

and energy harvesting rates for one SU over a single sub-channel ($\epsilon_s = 1$ mJ). It can be seen that the achievable throughput experiences a sharp increase as the energy harvesting rate improves. Meanwhile, the higher achievable throughput is accomplished by decreasing the sensing time because more time is left for data transmission.

### 4.3 Sub-channel Allocation Performance

To evaluate the performance of our proposed sub-channel allocation algorithm, a series of experiments have been conducted. Figure 4.2 evaluates the sum rate of a CR network ($K = 4$ SUs) for different numbers of available sub-channels. Note that the achievable sum rate of the CR system increases as the number of available sub-channels grows. Consider four scenarios with 2 RT and 2 NRT users for two cases and 3 RT and 1 NRT users for the others. SU-1 and SU-2 are RT users whose energy harvesting rates are $\chi_1 = 30$ mJ/s and $\chi_2 = 40$ mJ/s, respectively. SU-3 and SU-4 have the energy harvesting rates of $\chi_3 = 60$ mJ/s and $\chi_4 = 120$ mJ/s,

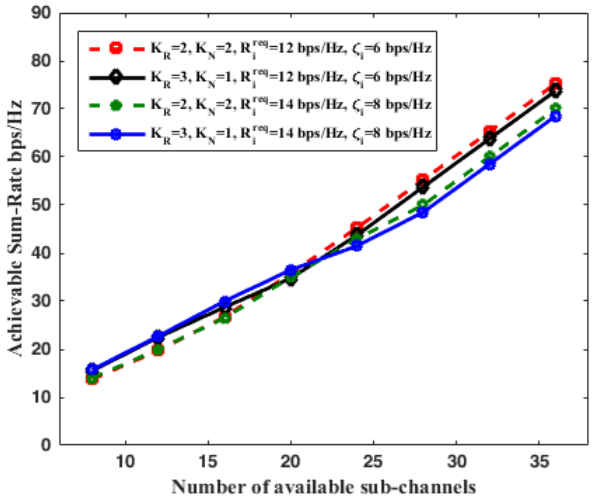


**Figure 4.2** The achievable sum-rate as a function of the number of available sub-channels.

respectively. However, SU-4 is always an NRT user while SU-3 can be RT or NRT in different cases. As shown in Figure 4.2, the achievable sum rate not only is related to the number of sub-channels and number of RT and NRT users, but also depends on the required rates of RT SUs and rate constraints of NRT users. When $R^{req}$ is higher, RT users which have lower harvesting rates need more sub-channels to meet their required rates. More specifically, as shown in Figure 4.2, as the required rate increases from $R^{req} = 12$ bps/Hz to $R^{req} = 14$ bps/Hz and the rate constraint grows from $\zeta = 6$ bps/Hz to $\zeta = 8$ bps/Hz, the achievable sum rate slightly decreases for higher number of available sub-channels.

As a second illustrative example, simulation results of a CR network with 8 RT SUs are illustrated in Table 3. In this part, we assume that the channel gains are identical for all SUs. It is shown that by increasing the value of $\alpha_{EFM}$ for different SUs, their single achievable rates improve. Thus, the RT SUs with higher $\alpha_{EFM}$ require less sub-channels to achieve the required rate. Figure 4.3 illustrates the comparison between our EFM-based sub-channel allocation in Section 3 and the sub-channel allocation scheme in [73]. Figure 4.3 explicitly shows that the number of RT users

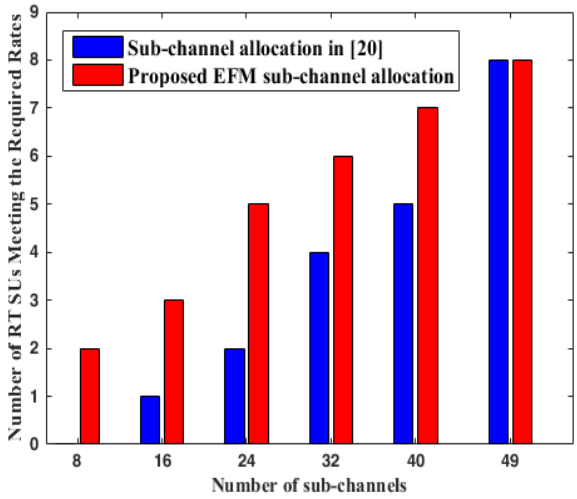


**Figure 4.3** Number of RT SUs successfully meeting their required rates versus number of available OFDM sub-channels.

which meet their required rates are significantly higher, especially for a small number of available sub-channels. In other words, since in the EFM-based method, the RT SUs with higher $\alpha_{EFM}$ have higher priority for sub-channel allocation, the SUs with less required sub-channels receive sub-channels first. Whereas, the method in [73] does not consider this prioritized criterion regarding RT SUs sub-channel allocation.

### 4.4 Structure Optimization for Fixed Sub-channel Allocations

After having completed sub-channel allocation process, the SUs receive their sub-channels and the general optimization problem is reduced to a convex NLP. In this part, the channel gains are modeled as described in the simulation setup. Figure 4.4, compares the optimal harvesting ratios depicted by orange circles with our numerical results proposed in Theorem 1. There are 20 SUs which their energy harvesting rates uniformly set to $\chi = 5$ J/s. Each SU receives a fixed number ($f$) of sub-channels and the interference thresholds of PUs are $5 \times 10^{-13}$W. It is obvious that our proposed numerical results are capable of obtaining more than 95% of the optimal harvesting

**Table 4.1** Simulation Parameters for an Experiment of 8 SUs.

| SU | $\alpha_{EFM}$ | $\chi$ | $\theta_{opt}$ | $r$ | $R^{req}$ | Req. Sub-Chan. |
|---|---|---|---|---|---|---|
| 1 | 3060 | 20 | 0.554 | 1.00 | 10 bps/Hz | 10 sub-channels |
| 2 | 5850 | 20 | 0.455 | 1.25 | 10 bps/Hz | 8 sub-channels |
| 3 | 7230 | 30 | 0.412 | 1.50 | 10 bps/Hz | 7 sub-channels |
| 4 | 10130 | 40 | 0.363 | 1.75 | 10 bps/Hz | 6 sub-channels |
| 5 | 12500 | 60 | 0.336 | 2.00 | 10 bps/Hz | 5 sub-channels |
| 6 | 15560 | 85 | 0.309 | 2.25 | 10 bps/Hz | 5 sub-channels |
| 7 | 19050 | 120 | 0.285 | 2.50 | 10 bps/Hz | 4 sub-channels |
| 8 | 31000 | 160 | 0.258 | 2.75 | 10 bps/Hz | 4 sub-channels |

ratios for all SUs, which means the performance gap between our proposal and the optimal solution is negligible.

Figure 4.5 shows the sum capacity as a function of the number of SUs, which varies from 4 to 10. The energy harvesting rate is set to $\chi = 5$ J/s. Note that each SU receives a fixed number of $f$ sub-channels. We can observe from Figure 4.5 that the sum rate of all SUs increases when the number of SUs grows from 4 to 10. Two scenarios, each SU getting $f = 2$ and $f = 6$ sub-channels, respectively, are considered. Since **P3** is a convex optimization problem, optimal solutions can be obtained by interior point methods. Note that the near optimal theoretical results are within 3.5% away from the optimal solutions for all cases.

## 4.5 Sum Rate versus Rate Constraints

We depict the sum rate of SUs versus different values of rate constraint of RT SUs in Figure 4.6, in which $\mathcal{K}_R = 4$ RT SUs and the available sub-channels are 16 with different channel gain for each SU. The channel gains are detailed in Subsection 4.1. Each sub-channel has a bandwidth of 62.5 KHz and the harvesting rate is assumed

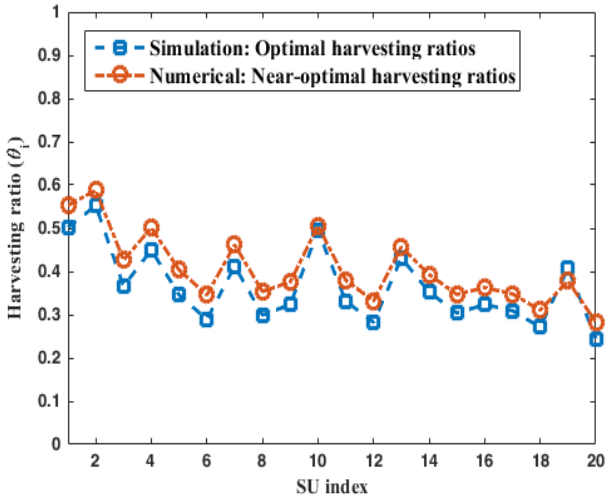


**Figure 4.4** The harvesting ratios for 20 SUs. The energy harvesting rates for SUs are set to $\chi = 5$ J/s.

to be $\chi = 5$ J/s for all SUs. The required rates of RT users vary from $R_i^{req} = 1$ to 11 bps/Hz. The time slot duration is considered $T = 1$ ms and the sensing time is $\tau_s = 10$ $\mu$s for all SUs. As shown in Figure 4.6, the highest sum rate is achieved for the lowest rate constraint ($R_i^{req} \leq 4$ bps/Hz) due to the fact that the optimizer has more freedom to allocate sub-channels to SUs. By increasing the rate constraint from 4 bps/Hz, the sum rate witnesses a slight decrease. Beyond the rate constraint of 7 bps/Hz which is shown by a red line in the figure, the sum rate experiences a sharp decrease. This stems from the fact that the optimizer has less freedom to allocate sub-channels to SUs and thus the optimal sum rate is greatly reduced.

## 4.6 System Performance versus Interference Threshold

The sum rate of all SUs versus interference thresholds of PUs are illustrated in Figure 4.7. Four SUs occupy 16 available OFDM sub-channels. The channel gains provided in Subsection 4.1 are adopted and each SU has a different channel gain. We assume that all PUs have identical interference threshold, which varies between -90 dbm to -110 dbm. We assume that the rate constraints are $R_i^{req}$= 5 bps/Hz for each SU. As can be seen from Figure 4.7, the sum rate increases with the growth of the interference

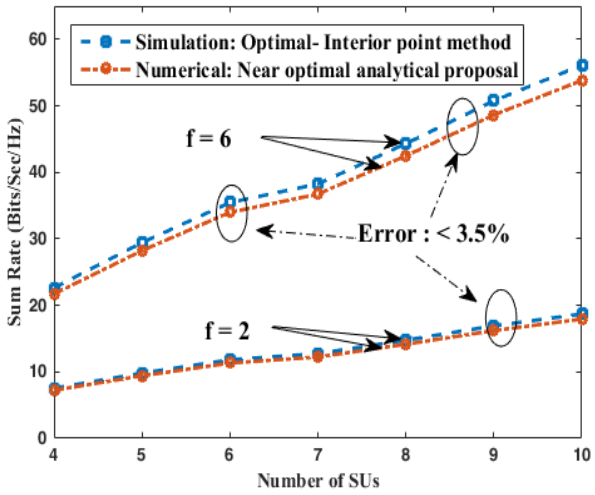


**Figure 4.5** The total sum rate versus number of SUs for a fixed number of allocated sub-channels. Energy harvesting rate is set at $\chi = 5$ J/s.

threshold. For lower interference thresholds, the SUs' transmission powers are limited and cannot be increased to its maximum amount, thus resulting in lower sum rate performance. Nonetheless, the sum rate cannot be increased beyond a certain point as the transmission power, which depends on the harvesting ratio, has reached its maximum. Therefore, the sum rate does not increase after the black ellipsoids shown in the figure for different harvesting ratios.

We also verify the effect of various PUs' interference thresholds for the achievable harvesting ratios of SUs. Figure 4.8 illustrates the harvesting ratios versus different PUs' interference thresholds for three cases, where the average harvesting rates are $\chi = 1$, 3 and 9 J/s, respectively. When the interference threshold is relatively small, SU's power and the sub-channels are interference limited. Thus, the harvesting ratios decrease because the lower interference thresholds require SUs to transmit their data with limited transmission power. Therefore, the harvesting ratios are smaller for lower interference thresholds. However, when the interference threshold increases from $10^{-15}$ W to $3 \times 10^{-13}$ W, the harvesting ratio grows exponentially in order to extract more energy for data transmission. While the harvesting ratio increases

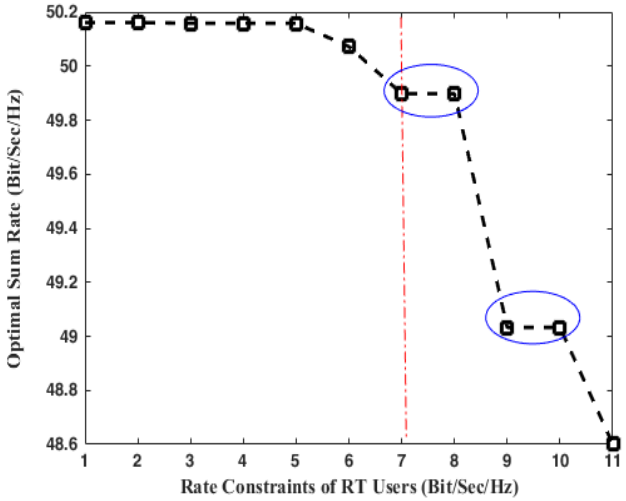


**Figure 4.6** The sum rate versus RT rate constraints ($R^{req}$). $\mathcal{K}_R = 4$ SUs and 16 available sub-channels.

sharply from $I_m^{th} = 10^{-15}$ W to $I_m^{th} = 3 \times 10^{-13}$ W, it remains almost constant for higher PUs' interference thresholds. This phenomenon stems from the trade off between having more harvesting time for energy harvesting, and less time for data transmission. In other words, for higher interference thresholds, the harvesting ratio cannot converge to $\theta = 1$ because the higher value of $\theta$ implies less time for data transmission.

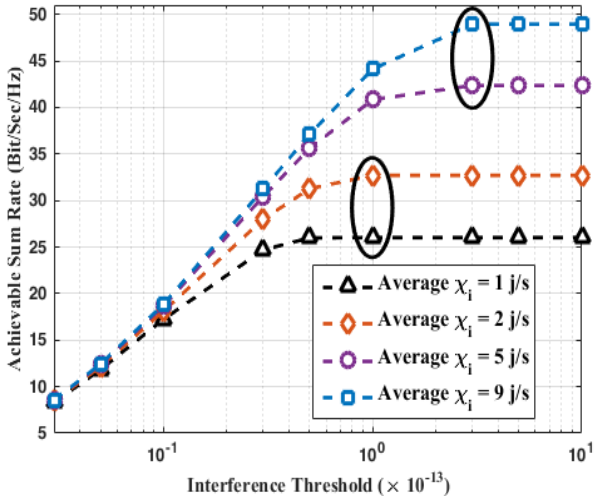


**Figure 4.7** The sum rate versus different PUs' interference thresholds (in Watt). $\mathcal{K}_R = 4$ SUs and 16 available sub-channels.

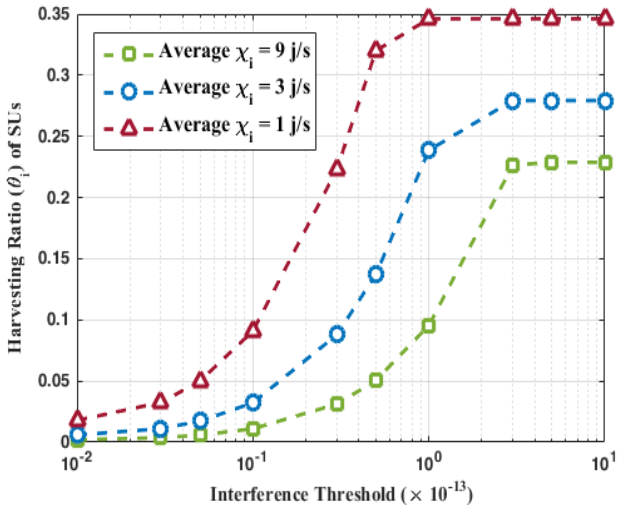


**Figure 4.8** The harvesting ratios versus interference threshold (in Watt). The average harvesting rates ($\chi_i$) are 1, 3, and 9 J/s.

# CHAPTER 5

# ENERGY EFFICIENT RESOURCE ALLOCATION IN EH-ENABLED CR NETWORKS FOR IOT

## 5.1 Introduction

Owing to myriad fields for IoT applications including smart houses, connected cars, smart cities, wearables, smart retails, and connected health, the number of connected devices has increased tremendously and anticipated to be more than 50 billions by 2020 [38, 50, 87]. Although traditional energy-constrained wireless networks are powered by fixed energy sources like batteries, it may be expensive and inconvenient to replace and recharge batteries as the number of IoT devices increases. Therefore, one of the dominant barriers to implementing IoT is supplying adequate energy to operate the network in a self-sufficient manner [32]. Wireless Energy Harvesting (WEH), a promising solutions, can potentially eliminate the need of recharging or replacing the batteries. Unlike other types of green energy sources (e.g., wind, solar, and vibrations), WEH does not depend on nature, and is thus a reliable source of energy for IoT devices [6]. WEH is classified into three categories: energy harvesting from unknown source, anticipated source and intended wireless energy transmission, respectively. While the former two are not efficient because the amount of ambient wireless energy in the environment is generally low and inconsistent, the latter, which can utilize the power transmitters, is much more efficient.

The rapid growth of higher data rate devices and wireless applications is likely to demand for more operating frequency bands. The dynamic spectrum access capabilities of Cognitive Radio (CR) can be leveraged to alleviate spectrum scarcity by utilizing the spectrum holes, i.e., underutilized spectrum bands [4]. In order to transmit data without interfering licensed users, spectrum sensing, which is the

process of detecting the spectrum holes, plays a crucial role. Owing to the effects of fading and shadowing, the performance of single spectrum sensing is generally unreliable. In this regard, Cooperative Spectrum Sensing (CSS) is applied to improve the performance of sensing by combining the observations of spatially located users. Current communication technologies cannot provision the future growth of numerous IoT devices. Therefore, transforming the IoT network into a cognitive based IoT network is essential to utilizing the available spectrum opportunistically [43].

### 5.1.1 Related Works

The energy efficiency (EE) of IoT networks has emerged as a major research issue [5, 41, 67, 86]. In particular, an energy efficient architecture was proposed in [41] for IoT networks where the sensors' sleep intervals are predicted based on their remaining energy. Sharma *et al.* [67] presented an energy efficient approach for device discovery in 5G-based IoT using multiple Unmanned Aerial Vehicles (UAVs). Zhang *et al.* [86] proposed an integrated structure to enhance the EE of IoT networks. They optimized the EE of the whole system by considering the wireless and wired parts at the same time. Alnakhli *et al.* [5] proposed a mechanism to jointly maximize the spectrum and energy efficiency for device-to-device communications enabled wireless networks.

IoT and CR networks are evolving technologies and the CR utilization in IoT is becoming an important issue. However, few works have discussed the CR capabilities (like cooperative spectrum sensing) for IoT networks. State of the arts on cognitive machine-to-machine communications from a protocol stack perspective has been reviewed in [1]. Majumdar *et al.* [53] also proposed a packet size optimization mechanism for cognitive radio based IoT networks where they considered the tradeoff in terms of EE and overhead delay for a given data packet length. Throughput maximization was proposed in [62] for energy harvesting enabled CR networks. Moreover, Hu *et al.* [30] proposed a cognitive code division multiple access scenario

by combining the concept of CR with dynamic spectrum bands and CDMA for IoT networks.

Wireless energy harvesting and transfer technologies can be leveraged for IoT networks. Li *et al.* [47] proposed a framework where network coding is applied to an IoT network to reduce IoT energy consumption. Kawabata *et al.* [42] considered a relay selection problem for energy harvesting and proposed a new scheme for energy harvesting relay selection which is based on the residual energy at each relay's battery. Song *et al.* [69] studied a tradeoff between Quality of Service provisioning and the energy efficiency for IoT networks. Moreover, Liu *et al.* [51] proposed a wireless energy harvesting protocol for an underlay cognitive relay in which the secondary users are assumed to harvest energy from the primary network. Ha *et al.* [24] proposed a harvest-then-transmit based enhanced MAC protocol to solve the problem of the tradeoff between the RF energy transfer and data communication for wireless powered sensor networks by maximizing the energy harvesting rate. Kang *et al.* [40] investigated a wireless communication network with a full-duplex hybrid energy and information access point by maximizing the sum-throughput and minimizing the total time. Che *et al.* [15] considered dual-function access points, which are able to support the energy/information transmission to/from wireless nodes.

### 5.1.2 Contributions

None of the existing works considered a trade-off between the EE and spectral efficiency (SE) by taking into consideration of the limits of spectrum resources, as well as finding the optimal fractions of time slots for energy harvesting and data transmissions in an EH-enabled CR-based network. Therefore, this study aims to address the aforementioned issue by proposing a system model that not only leverages WEH and CSS, but is also designed to optimize the EE and SE tradeoff of the network by optimizing the length of energy harvesting in each time slot while ensuring data

rate requirements of the devices and the fairness in sub-channel allocation among the users. The main contributions of this Chapter are summarized as follows.

- We propose a CR based system model for IoT using wireless energy harvesting and cooperative spectrum sensing to tackle two vital challenges of IoT networks, i.e., supplying adequate energy to operate the network in a self-sufficient manner, and providing enough radio spectrum to accommodate the massive growth of devices. To this end, we consider a time switching model in which the devices participate in the CSS process, report their results to an Access Point (AP), harvest energy that is intentionally transmitted by the AP, and finally transmit their data using the harvested energy. Since users operate in a time switching fashion, there is a tradeoff between the length of the energy harvesting process and data transmission part. Therefore, we focus on optimizing the EE and SE tradeoff of the network by optimizing the length of energy harvesting process in each time slot.

- We formulate a mixed integer nonlinear programming (MINLP) problem to maximize the tradeoff between the EE and SE while taking into consideration of practical limitations such as data rate fairness, energy causality constraints, interference constraints, and imperfect spectrum sensing. The problem is proven to be NP-hard.

- We thus propose a low complexity heuristic algorithm, referred to as joINt Sub-channel allocaTion And eNergy harvesting opTimization (INSTANT), to solve the sub-channel allocation and energy harvesting optimization problem. The proposed algorithm is shown to be capable of achieving near optimal solution with high accuracy while having polynomial complexity.

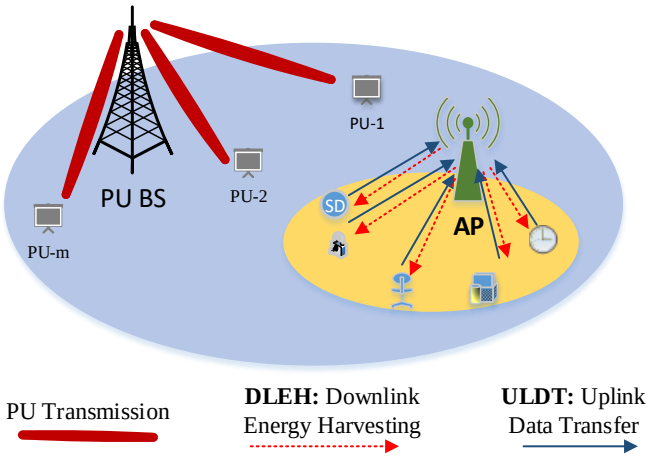


**Figure 5.1** The system model.

## 5.2 System Model

Consider two cellular systems, one with $M$ primary users (PUs) denoted by $\mathcal{M} = \{1, 2, ..., M\}$ and the other with $K$ self-powered devices represented by $\mathcal{K} = \{1, 2, ..., K\}$ forming a time-slotted CR-based IoT network (Figure (5.1)). The devices opportunistically utilize the licensed radio spectrum of the PUs via an AP. The AP is equipped with one Fusion Center (FC) to centrally process the users' sensing results and one energy transmitter to broadcast energy signals to its associated devices. Each device does local spectrum sensing by a low complexity Energy Detector (ED) concerning the presence of PUs. Users' spectrum sensing results are assumed independent [49] and each user is permitted to sense any number of sub-channels. The local spectrum sensing results are sent to the FC. Then, the FC applies CSS (to reduce the sensing errors) to achieve final decisions regarding availability of licensed sub-channels. Denote $\mathcal{N} = \{1, 2, ..., N\}$ as the subset of available sub-channels identified by the CR based IoT network for data transmission.

In this work, energy and information APs are integrated into a co-located energy-information AP, which provides both energy and data access to the users within the range of the AP [40]. The devices are also considered to be self-powered,

equipped with wireless energy harvester devices to exclusively harvest energy from wireless energy signals intentionally transmitted by the AP. In fact, the AP broadcasts a deterministic energy signal to power nearby users over the downlink channel and then receives data from these users transmitted via the uplink channel. Users store their energy in their temporary energy storage devices (e.g., capacitors). The energy harvesting process and energy consuming process cannot be done simultaneously in such devices. Owing to the *energy half-duplex constraint*, while the user transmits data via the uplink channel, its energy harvester pauses [82]. Basically, each time slot with duration $T$ is partitioned into a control slot $T_c$ and a data slot $T_d$ (Figure (5.2)). The length of the control slot is called the sensing overhead and is constant for all devices [49]. The fixed control slot period is devoted for CSS and reporting the optimization results from the AP in each slot. We assume that at the beginning of the $t^{th}$ time slot, device $k \in \mathcal{K}$ has residual energy $E_{k,t}^{res}$ that is enough for spectrum sensing during the control slot. Meanwhile, the data time slot is divided into two non-overlapping parts, namely, Downlink Energy Harvesting (DLEH) and Uplink Data Transmission (ULDT). In fact, all users have the same data time slot duration from the AP's point of view. However, during each time slot, users have different DLEH and ULDT time periods because users have various data rate requirements as well as different hardware characteristics to harvest the transmitted energy from the AP. We define the harvesting ratio for the $k^{th}$ device as $\mu_k$, $\forall k \in \mathcal{K}$, which determines the fraction of data slot devoted to energy harvesting. Nevertheless, in the slotted operating mode, with more time spent on DLEH, less time remains for ULDT, thus degrading the achievable throughput. Hence, there exists a tradeoff between DLEH and ULDT durations. Meanwhile, the users are assumed to have perfect knowledge of Channel State Information (CSI) between their transmitters and the AP receiver. For the ease of reading, frequently used notations and terminologies are summarized in Table 5.1.

**Table 5.1** List of Symbol Notations and Description

| **Symbols** | **Descriptions** |
|---|---|
| $\mathcal{M}$ ($\mathcal{K}$) | The set of primary users (the set of self powered users) |
| $\mathcal{N}$ | The set of available sub-channels identified by CR based IoT system |
| $T_c$ ($T_d$) | The duration of control time slot (the duration of data time slot) |
| $\mathbb{E}[.]$ | The expectation of the number of bits in users' buffers |
| $\tau_{s_k}$ | The sensing time of the $k^{th}$ user |
| $\mu_k$ | The harvesting ratio of the $k^{th}$ user in each time slot |
| $\rho_k$ | The harvesting rate of the $k^{th}$ user |
| $\zeta_k$ | The energy conversion efficiency of the $k^{th}$ user |
| $d_k$ | The geographical distance between the AP and the $k^{th}$ user |
| $E_k^{sen}$ | The energy consumed by the $k^{th}$ user for spectrum sensing |
| $E_k^{res}$ | The residual energy of the $k^{th}$ user |
| $E_k^{har}$ | The energy harvested by the $k^{th}$ user |
| $E_k^{idle}$ | The consumed energy of being idle for the $k^{th}$ user |
| $E_k^{tr}$ | The transmission energy of the $k^{th}$ user |
| $E_k^{con}$ | The total energy consumption of the $k^{th}$ user |
| $\eta_k$ | The weight of spectral efficiency in (5.11) |
| $\Delta(.)$ | The base data rate function |
| $X_k$ | The number of bits in the $k^{th}$ user's buffer |
| $h_{k,n}$ | The channel gain between the $k^{th}$ user and the AP over the $n^{th}$ channel |
| $I_{k,m}$ | The total interference introduced to the $m^{th}$ PU by the $k^{th}$ user |
| $g_{k,n}$ | The indicator function for allocating the $n^{th}$ channel to the $k^{th}$ user |
| $r_{k,n}$ | The transmission rate of the $k^{th}$ user over the $n^{th}$ channel |
| $R_k$ | The total transmission rate of the $k^{th}$ user |

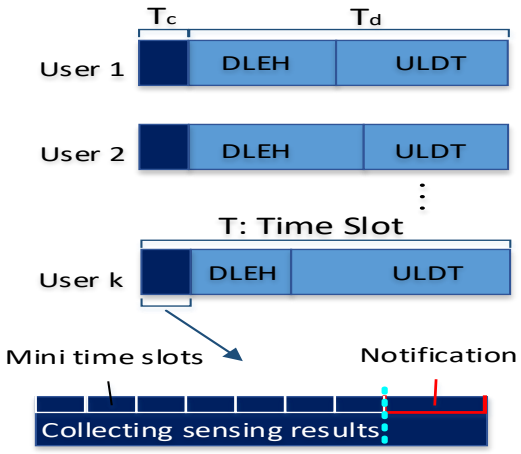


**Figure 5.2** The time slot model.

## 5.3 Problem Formulation

### 5.3.1 Energy Consumption

The amount of harvested wireless energy received by the $k^{th}$ user is

$$E_k^{har} = \zeta_k d_k^{-\beta} \left|\bar{h}_k\right|^2 P_{AP} \mu_k T_d, \ \forall k \in \mathcal{K}, \tag{5.1}$$

where $0 < \zeta \leqslant 1$ is the energy conversion efficiency, which depends on the physical circuit of the energy harvesting device, $d_k$ is the geographical distance between the AP and the $k^{th}$ user, $\beta$ is the path-loss exponent, $\bar{h}_k$ is the channel condition between users and the energy transmitter, $P_{AP}$ is the transmission power of the energy transmitter, and $\mu_k T_d$ is the amount of time in the time slot devoted for energy harvesting. For the sake of convenience, we define the energy harvesting rate of the $k^{th}$ user as $\rho_k \triangleq \zeta_k d_k^{-\beta} |h_k|^2 P_{AP}, \ \forall k \in \mathcal{K}$. In other words, users based on their locations, channel conditions, and their harvesting capabilities have different energy harvesting rates from the transmitted energy of the AP.

Since the users are assumed to have enough residual energy at the beginning of each time slot to operate spectrum sensing, the following inequality must hold

$$E_{k,t}^{res} - E_{k,t}^{sen} + E_{k,t}^{har} - E_{k,t}^{tr} \geqslant E_{k,t+1}^{sen}, \tag{5.2}$$

where $E_{k,t}^{sen}$ denotes energy expenditure of the $k^{th}$ user to sense the spectrum in time slot $t$. $E_{k,t}^{tr}$ is the amount of energy consumed by the $k^{th}$ user to transmit data in the $t^{th}$ time slot. However, the energy of sensing does not change from time slot to time slot for each user, $E_{k,t}^{sen} = E_{k,t+1}^{sen}$. Thus, the energy causality constraint for the network of $K$ users is given by

$$E_{k,t}^{res} + E_{k,t}^{har} \geqslant E_{k,t}^{tr} + 2E_{k}^{sen}, \forall k \in \mathcal{K}. \tag{5.3}$$

Accounting for the harvested and the consumed energies, the residual energy of the $k^{th}$ user $\forall k \in \mathcal{K}$ at the beginning of the next time slot is updated as follows

$$E_{k,t+1}^{res} = E_{k,t}^{res} + E_{k,t}^{har} - E_{k,t}^{tr} - E_{k}^{sen}. \tag{5.4}$$

To calculate the total energy consumption of one user in one time slot, one should consider the energy of transmission, sensing energy and the consumed energy for being idle. Based on the energy causality constraint in (5.3), the maximum transmission energy of the $k^{th}$ user in time slot $t$ is given by

$$E_{k,t}^{tr} = E_{k,t}^{res} + E_{k,t}^{har} - 2E_{k,t}^{sen}. \tag{5.5}$$

Denote $E_{k,t}^{idle}$ as the energy of the idle mode for the $k^{th}$ user in time slot $t$. Therefore, the energy consumption of the $k^{th}$ user in the $t^{th}$ time slot depends on the energy of transmission, harvested energy, spectrum sensing energy consumption and energy for remaining idle, i.e.,

$$E_{k,t}^{con} = \underbrace{E_{k,t}^{res} + \rho_k \mu_k T_d - 2E_{k,t}^{sen}}_{E_{k,t}^{tr}} + E_{k,t}^{sen} + \underbrace{P_{k,t}^{idle}(T_c - \tau_{s_k})}_{E_{k,t}^{idle}}, \tag{5.6}$$

where $\tau_{s_k}$ is the sensing time of the $k^{th}$ user. Thus, the total energy consumption of $K$ users in each time slot as a function of the harvesting ratio can be written as

$$E_{total}^{con}(\mu_k) = \sum_{k \in \mathcal{K}} \left( \rho_k^{av} \mu_k T_d + E_k^{res} - E_k^{sen} + E_k^{idle} \right). \tag{5.7}$$

### 5.3.2 Achievable Throughput

To measure the Shannon capacity for each user in the system, we define $t_k^{tr}(\mu_k) \triangleq (1-\mu_k)T_d$ and $E_k^{tr}(\mu_k) \triangleq E_k^{res} + \rho_k \mu_k T_d - 2E_k^{sen}$ as the transmission time and the transmission energy of the $k^{th}$ user as a function of the harvesting ratio $\mu_k$. Thus, the transmission rate of the $k^{th}$ user over the $n^{th}$ sub-channel can be written as

$$r_{k,n}(\mu_k) = \frac{t^{tr}(\mu_k)}{T} log_2 \left(1 + \frac{|h_{k,n}|^2 E_k^{tr}(\mu_k)}{\Gamma(BN_0 + I_k) t_k^{tr}(\mu_k)}\right), \tag{5.8}$$

where $h_{k,n}$ denotes the channel gain of the $k^{th}$ user over the $n^{th}$ sub-channel, $B$ is the bandwidth of each OFDM sub-channel, $N_0$ represents the additive white Gaussian noise, $I_k$ is the measured interference introduced to the $k^{th}$ user caused by the PUs' signals, and $\Gamma$ denotes the SNR gap associated with the bit-error-rate (BER) of un-coded MQAM.

Let $g_{k,n}$ be the binary indicator whether to allocate the $n^{th}$ sub-channel to the $k^{th}$ user. For simplicity, we define $H_{k,n} \triangleq \frac{|h_{k,n}|^2}{\Gamma(BN_0+I_k)}$. Therefore, the total transmission rate of the $k^{th}$ user over all available sub-channels, $N$, is given by

$$R_k(\mu_k, g_{k,n}) = \sum_{n=1}^{N} g_{k,n} \frac{t_k^{tr}(\mu_k)}{T} log_2 \left(1 + H_{k,n} \frac{E_k^{tr}(\mu_k)}{t_k^{tr}(\mu_k)}\right). \tag{5.9}$$

## 5.4 Energy Efficiency Maximization

In this section, we formulate the problem to maximize the energy efficiency of the users while taking into consideration of their buffer occupancy. The energy efficiency is defined as the ratio of the total transmission rate to the total energy consumption, and is measured in unit of bits/sec/Joule. Recalling the total throughput in (5.9) and the total energy consumption in (5.7), the energy efficiency of the $k^{th}$ user is

$$E_{eff_k}(\mu_k, g_{k,n}) = \frac{R_k(\mu_k, g_{k,n})}{\rho_k \mu_k T_d + E_k^{res} - E_k^{sen} + E_k^{idle}}. \tag{5.10}$$

Meanwhile, it is possible to allocate spectral resources to the users which do not have enough data in their buffers to transfer, thus resulting in a waste of spectrum

resources. Let random variable $X_k$ represent the number of bits in the buffer of the $k^{th}$ user, and $X_k,\ \forall k \in \mathcal{K}$, are assumed independent and have a common general distribution with the average of $\mathbb{E}[X_k] \triangleq \overline{X_k}$. In order to efficiently utilize the spectrum, users should not receive spectral resources more than their data in the corresponding buffers. To this end, we incorporate the probability $P(X_k \geqslant R_k(\mu_k, g_{k,n})t_k^{tr}(\mu_k)),\ \forall k \in \mathcal{K}$, into the objective function to ensure efficient utilization of the spectrum (spectral efficiency). Let $S_{eff_k} \triangleq \eta_k P(X_k \geq R_k(\mu_k, g_{k,n})t_k^{tr}(\mu_k))$, where $\eta_k$ is the weight of the spectral efficiency in the objective function. However, maximum EE and SE cannot be obtained simultaneously; in fact, there is a trade-off between EE and SE. Therefore, we propose an optimization framework that optimizes the tradeoff between EE and SE in the CR-based IoT network with downlink energy harvesting, formulated as

$$
\begin{aligned}
\textbf{P1:}\ & \max_{\mu_k, g_{k,n}} && \sum_{k\in\mathcal{K}} \left(E_{eff_k}(\mu_k, g_{k,n}) + S_{eff_k}(\mu_k, g_{k,n})\right) \\
C1\ & && R_k(\mu_k, g_{k,n}) \geq \Delta(\mathbb{E}[X_k]),\ \forall k \in \mathcal{K} \\
C2\ & && E_k^{res} + E_k^{har} \geq E_k^{tr} + 2E_k^{sen},\ \forall k \in \mathcal{K} \\
C3\ & && \textstyle\sum_{k\in\mathcal{K}} \rho_k \mu_k \leq P_{AP},\ \forall k \in \mathcal{K} \\
C4\ & && \textstyle\sum_{k\in\mathcal{K}} \sum_{n\in\mathcal{N}} g_{k,n}\bar{p}_{k,n} I_{k,n} \leqslant I_m^{th},\ \forall m \in \mathcal{M} \\
C5\ & && \textstyle\sum_{k\in\mathcal{K}} g_{k,n} = 1,\ \forall n \in \mathcal{N} \\
C6\ & && g_{k,n} \in \{0,1\},\ \forall k \in \mathcal{K},\ \forall n \in \mathcal{N} \\
C7\ & && E_k^{tr} \geq 0,\ \forall k \in \mathcal{K} \\
C8\ & && 0 < \mu_k < 1,\ \forall k \in \mathcal{K}
\end{aligned}
\tag{5.11}
$$

C1 ensures minimum transmission rates, i.e., $\Delta(\mathbb{E}[X_k])$, for all the users where $\Delta(.)$ is an increasing function in $\mathbb{E}[X_k]$. In fact, the minimum data rate requirement of each user is defined as an increasing function of the average number of bits in its buffer. C2 means that the energy causality constraint should be held. C3 imposes the total harvested energy of users to be less than the maximum transmitted

energy of the AP. C5 and C6 imply that each sub-channel is allocated to no more than one device. C7 specifies that the transmission energy of each user should not have a negative value. C8 imposes the harvesting ratio to be a fraction of one time slot. Meanwhile, C4 specifies that the total interference to the $m^{th}$ PU must be less than a given threshold where $P_k^{tr}(\mu_k)$, the transmission power of the $k^{th}$ user, can be written as $\frac{E_k^{res}+\rho_k\mu_k T_d-2E_k^{sen}}{(1-\mu_k)T_d}$, and $\bar{p}_{k,n} = \frac{P_k^{tr}(\mu_k)}{|\mathcal{N}|}, \forall n \in \mathcal{N}, \forall k \in \mathcal{K}$. Moreover, spectrum sensing errors (e.g., mis-detection of the spectrum) can also occur and lead to co-channel interference. The total interference introduced to the $m^{th}$ PU by the $k^{th}$ user's transmission over the allocated sub-channels is given by $I_{k,m} = \sum_{n\in\mathcal{N}_u} P_{1,n} I_{n,m}^k + \sum_{n\in\mathcal{N}_a} P_{2,n} I_{n,m}^k$ [63], where $\mathcal{N}_u$ is the set of unavailable sensed sub-channels, $\mathcal{N}_a$ represents the set of available sensed sub-channels, $P_{1,n}$ denotes the probability that the CR based IoT network correctly identifies the $n^{th}$ unavailable sub-channel, and $P_{2,n}$ is the probability that the network makes a wrong decision regarding availability of the $n^{th}$ occupied sub-channel.

**Lemma 4.** *The EE maximization of the CR-based IoT network in (5.11) is an NP-hard problem.*

*Proof.* The Lemma is proved in Section B.1. □

## 5.5 Algorithm Design

### 5.5.1 Solution Methodology

In fact, multiple approaches can be used to find the optimal solutions for the proposed optimization problem, which is a non-convex MINLP problem, and thus low complexity heuristic approaches are required to solve this problem. One approach is to employ a tightened lower bound for the maximization problem and then solve it by the outer approximation algorithm. To achieve a tight lower concave bound of the original maximization problem [58], the inequality in $\alpha \log z_0 + \beta \leqslant \log(1+z_0)$ can be used, where the approximation constants are $\alpha = \frac{z_0}{1+z_0}$ and $\beta = \log(1+z_0) - \alpha log z_0$.

Thus, $\alpha \log z_0 + \beta$ can be used as a rate function to make a lower bound for the objective function. However, it is well-known that solving MINLP problems by this approach requires a high computational complexity which may not satisfy user delay requirements in practical scenarios. Another technique that has achieved success in various scenarios of MINLP problems [63] is to exploit the primal decomposition, which decomposes the original optimization problem into two subproblems, thereby reducing the complexity of the problem. Thus, **P1** can be reduced to **P2** by fixing the values of the harvesting ratios $\mu_k,\ \forall k \in \mathcal{K}$.

$$
\begin{aligned}
\textbf{P2:}\ \max_{g_{k,n}}\quad & \sum_{n\in\mathcal{N}}\sum_{k\in\mathcal{K}} g_{k,n}.\hat{p}_{k,n} + \eta_k P(X_k \geqslant R_k(g_{k,n})t_k^{tr}) \\
s.t.\quad & C1: \textstyle\sum_{n\in\mathcal{N}} g_{k,n} r_{k,n} \geqslant \Delta(\mathbb{E}[X_k]),\ \forall k \in \mathcal{K}, \\
& C2: \textstyle\sum_{k\in\mathcal{K}}\sum_{n\in\mathcal{N}} g_{k,n}\bar{p}_{k,n} I_{k,n} \leqslant I_m^{th}, \\
& C3: \textstyle\sum_{k\in\mathcal{K}} g_{k,n} = 1,\ \forall n \in \mathcal{N}, \\
& C4: g_{k,n} \in \{0,1\}, \forall k \in \mathcal{K},\ \forall n \in \mathcal{N}.
\end{aligned}
\tag{5.12}
$$

Hence, a two-stage heuristic approach can be used, where the sub-channel allocation process is performed to find the optimal solution of **P2**. Note that after the sub-channel allocation phase, the integer constraints of **P1** are removed because binary variables are set to 0 or 1 to indicate whether sub-channels are allocated or not.

### 5.5.2 INSTANT

As discussed, finding the optimal solution to **P1** is intractable. Therefore, to solve this problem, we propose a heuristic algorithm as summarized in Algorithm 3 which consists of two separated phases to optimizing the channel allocation and the harvesting ratio, respectively.

We first perform a sub-channel allocation process to solve **P2**. However, one should notice that the analytical expression of $S_{eff_k}$ in the objective function should

**Algorithm 3** Jo**IN**t **S**ub-channel Alloca**T**ion **A**nd E**N**ergy Harvesting Op**T**imization: **INSTANT**

$\mu_k = \frac{\mu_k^{min}+1}{2} = \ \forall k \in \mathcal{K}$
$g_{k,n} = 0 \ \forall k \in \mathcal{K}$ and $n \in \mathcal{N}$
**Channel Allocation Phase**
$\mathcal{N}_0 \leftarrow \emptyset$
$\mathcal{K}' \leftarrow \mathcal{K}$
**for all** $n \in \mathcal{N}$ **do**
  $\hat{k} = \underset{k \in \mathcal{K}'}{argmax} \ R_k$
  $g_{\hat{k},n} = 1$ and $\mathcal{N}_0 \leftarrow \mathcal{N}_0 \cup n$
  **if** $R_{\hat{k}} \geq \Delta(\mathbb{E}[X_k])$ **then**
    $\mathcal{K}' \leftarrow \mathcal{K}' \setminus \hat{k}$
  **end if**
**end for**
$\mathcal{N} \leftarrow \mathcal{N} \setminus \mathcal{N}_0$
$\hat{o} = 0$
**for all** $n \in \mathcal{N}$ **do**
  **for all** $k \in \mathcal{K}$ **do**
    **if** $o_k^n \geq \hat{o}$ **then**
      $\hat{k} \leftarrow k$
      $\hat{o} \leftarrow o_k^n$
    **end if**
  **end for**
  $g_{\hat{k},n} = 1$
**end for**
**Harvesting Ratio Optimization Phase**
sort users in $\mathcal{K}''$ such that $\rho_1 \leq \rho_2 \leq ... \leq \rho_K$
**for all** $k \in \mathcal{K}''$ **do**
  $\hat{\mu}_k \leftarrow \underset{\mu_k^{min} \leq \mu_k \leq 1}{argmax} \ (E_{eff_k} + S_{eff_k})$
  **if** $\hat{R}_k \geq \Delta(\mathbb{E}[X_k])$ and $\hat{E}_k \leq P_{AP}.T_d$ and $\hat{I}_k \leq I_m^{th}$ **then**
    $\mu_k = \hat{\mu}_k$
  **end if**
**end for**

be derived. Therefore, for any probability distribution functions of $X_k$, $\forall k \in \mathcal{K}$, $f_{X_k}(r)$, $S_{eff_k}$ can be derived as $S_{eff_k} = \eta_k \int_{R_k t_k^{tr}(\mu_k)}^{\infty} f_{X_k}(r)dr$. Hence, to solve **P2**, the distribution function of $X_k$ has to be known. For example, if $X_k$ is uniformly distributed between $a$ and $b$, $S_{eff_k} = \int_{R_k t_k^{tr}(\mu_k)}^{\infty} f_{X_k}(r)dr = \frac{b - R_k(\mu_k, g_{k,n}) t_k^{tr}(\mu_k)}{b-a}$. As another example, $X_n$ follows an exponential distribution with parameter $\lambda$, and $S_{eff_k}$ is given by $\int_{R_k t_k^{tr}(\mu_k)}^{\infty} f_{X_k}(r)dr = e^{-\lambda R_k(\mu_k, g_{k,n}) t_k^{tr}(\mu_k)}$. In the proposed heuristic algorithm, we assume that the distribution function of $X_k$ is given. Moreover, without loss of generality, we focus on the case in which function $\Delta(.)$ is given and linear. As shown in Algorithm 3, we initially set $\mu_k = \frac{\mu_k^{min}+1}{2}$ for all $k \in \mathcal{K}$, where $\mu_k^{min} = \frac{2E_k^{sen} - E_k^{res}}{\rho_k T_d}$ is computed from constraint $E_k^{tr} \geq 0$. Accordingly, having variables $\mu_k$ fixed to $\frac{\mu_k^{min}+1}{2}$, we follow our heuristic channel allocation phase. Denote $R_k$ as the data rate of user $k$ and $\mathcal{N}_0$ as the set of the channels to be allocated to satisfy the minimum data rate requirement, i.e., $R_k \geq \Delta(\mathbb{E}[X_k])$. Let $\mathcal{K}'$ be the set of users who cannot attain their minimum data rates yet. We first allocate channels based on the channel conditions to satisfy constraint $R_k \geq \Delta(\mathbb{E}[X_k])$ for all the users (lines 6-12). In fact, among the users with unsatisfied minimum data rate, a channel is allocated to the user that has the maximum rate on that channel. Then, for the remaining channels, we search over all the users to find a favorite user to allocate each channel (lines 15-23). The favorite user $\hat{k}$ for channel $n$ is the one that achieves the maximum increase in the objective function of (5.11). In fact, the favorite user is identified by comparing $o_k^n$ which is defined as the objective function of (5.11) computed for the current channel allocation as well as the allocation of sub-channel $n$ to user $k$. After the channel allocation phase, we follow the harvesting ratio optimization phase to optimize the harvesting ratios of users based on their allocated channels (lines 25-31). Denote $\hat{R}_k$ as the data rate of user $k$ if we change $\mu_k$ to $\hat{\mu}_k$. We also have $\hat{E}_k = T_d(\sum_{l \in \mathcal{K}, l \neq k} \rho_l \mu_l + \rho_k \hat{\mu}_k)$ and $\hat{I}_k = \sum_{l \in \mathcal{K}, l \neq k} P_l^{tr}(\mu_l) I_{l,m} + P_k^{tr}(\hat{\mu}_k) I_{k,m}$. As shown in the algorithm, we fist sort the users in an increasing order according to their energy

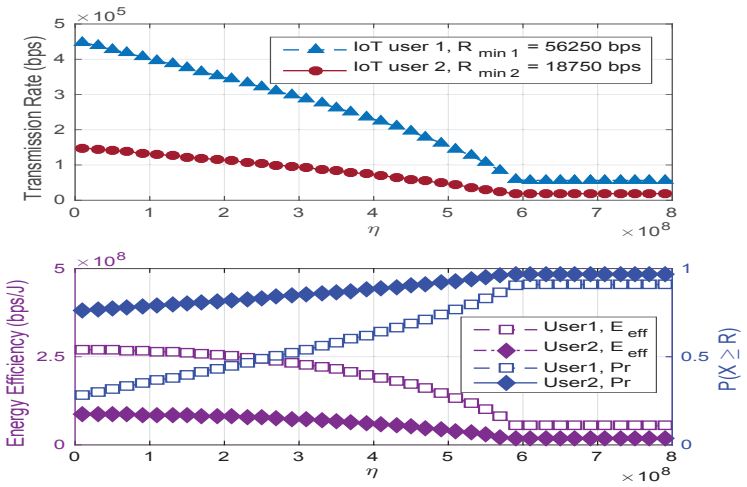


**Figure 5.3** The transmission rates of users, $P(X_k \geq R_k)$ term of SE, and EE versus deign parameter ($\eta$). Data in buffer has a uniform distribution.

harvesting rates. Then, for each user, we locally optimize the harvesting ratio while taking into consideration of the current $\hat{R}_k$, $\hat{E}_k$, and $\hat{I}_k$.

**Complexity Analysis:** The optimal solution for the joint sub-channel allocation and energy harvesting optimization in the network necessitates an exhaustive search in order to find the optimal sub-channel allocation for the $K$ devices. The complexity of this exhaustive search grows exponentially as $\mathcal{O}(K^N)$. Note that the complexity of INSTANT corresponds to $\mathcal{O}(K * N)$, which is much lower than that of the exhaustive search method.

## 5.6 Simulation Results

In this section, we evaluate the performance of the proposed optimization framework for the CR-based IoT network. The OPTI toolbox [19] is adopted to solve (5.11) by using the NOMAD [46] solver, which is a global MINLP solver and uses the mesh adaptive direct search algorithm. The channel gains are modeled as $h_{k,n} = Zd_{k,n}^{-\beta}$, where $Z$ is randomly generated according to the Rayleigh distribution, $d$, the geographical distance between the transmitter and receiver, is selected uniformly between 0 m to 50 m, and $\beta$, the path-loss exponent, is set to 3. Moreover, the

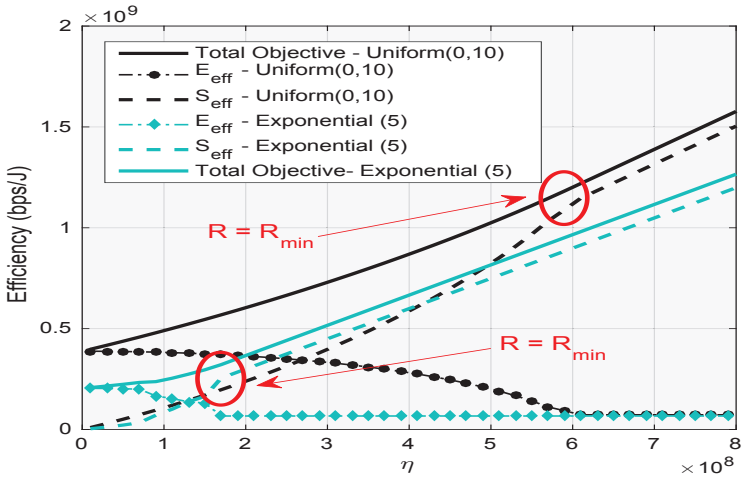


**Figure 5.4** The optimal objective function, EE and SE versus $\eta$ for both exponential and uniform distributions of data in buffers.

bandwidth of each sub-channel is 62.5 kHz, the interference threshold of the licensed user is $5 \times 10^{-13}W$, and the noise power is $10^{-13}W$ (or $-100$ dbm) in our simulation analysis.

Figure 5.3 illustrates a tradeoff between EE and SE of the network. We consider two users along with four available sub-channels. The energy of sensing, residual energy and energy of idle for both users are $E^{sen} = 2mJ$, $E^{res} = 3mJ$ and $E^{idle} = 1\mu J$, respectively. Data in their buffers follow a uniform distribution. The first subplot clearly shows that the transmission rates for both users decrease to their minimum rate constraints as $\eta$ reaches $6 \times 10^8$. In fact, the higher $\eta$ results in the higher weight of SE, and thus lowers the EE and transmission rates. The second subplot of Figure 5.3 explicitly shows the tradeoff between EE and SE. The x-axis is the parameter $\eta$ which is selected to be identical for both users. The left y-axis represents the energy efficiency, i.e., the first term of the objective function in (5.11). The purple curves reflect the EE of users, where increasing $\eta$ reduces the EE to their minimum levels. The energy efficiency reduction arises from the fact that the higher $\eta$ puts the more weight on the SE term. The higher $P(X_k \geq R_k)$ implies the higher SE, where users do not receive rates more than their available bits in their buffers.

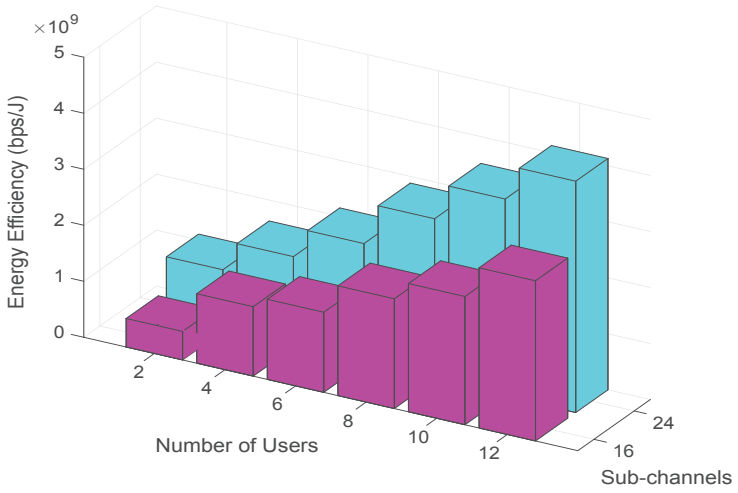


**Figure 5.5** The energy efficiency versus the number of users and sub-channels.

Figure 5.4 shows the efficiency of the network, where the number of randomly generated bits in users' buffers follow exponential and uniform distributions. The solid lines correspond to the total objective function in (5.11), which experiences a sharp increase by incrementing $\eta$ (identical for both users). When the weight of SE grows, the SE increases exponentially until the transmission rates of users reach their minimum thresholds. Beyond this point which is shown by red circle, the objective function increases with $\eta$.

Figure 5.5 shows the effect of the number of users and available sub-channels on the energy efficiency with the total number of available sub-channels being $N = 16$ and $N = 24$, respectively. For a fixed number of users, the energy efficiency of the network grows by increasing the number of available sub-channels allocated to users. Meanwhile, the x vector represents the number of users that varies from $K = 2$ to $K = 12$. In fact, the higher number of users results in the higher amount of data for transmission and also more freedom for the optimizer to choose users with better channel gains. Thus, increasing the number of users leads to improving the energy efficiency for both $N = 16$ and $N = 24$ scenarios.

Figure 5.6 illustrates the energy efficiency versus the minimum rate constraint and $\eta$. EE improves by increasing the minimum data rate because the transmission

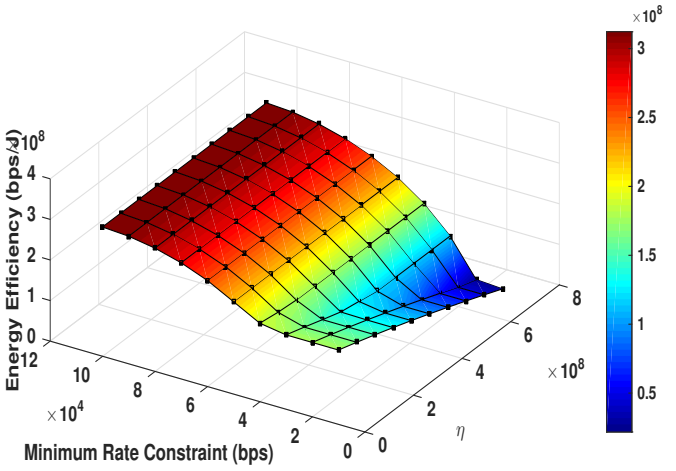


**Figure 5.6** The energy efficiency versus minimum data rate constraint of users (identical for both users) and tradeoff parameter ($\eta$).

rate of the users must increase to satisfy $C1$ in (5.11). In the low minimum data rate region, as $\eta$ grows, the SE term of the objective obtains a higher weight as compared to the EE term, and thus the energy efficiency experiences a decline. However, EE remains nearly constant for higher minimum rate constraints and does not react to the increment in values of $\eta$ because the probability $P(X_k \geq \Delta(\mathbb{E}[X_k]).t_k^{tr}(\mu_k))$ tends to zero in the high minimum data rate region. Thus, the SE term has no impact on the optimization problem regardless of the value of $\eta$, and EE remains steady.

Figure 5.7, Figure 5.8, and Table 5.1 are presented to evaluate the effectiveness and accuracy of the proposed INSTANT algorithm. In particular, we compare the performance of INSTANT and the optimal approach in Figure 5.7 for a small network with $K = 4$ users and $N = 8$ available sub-channels. The objective function of (5.11) increases as $\eta$ grows for both INSTANT and optimal approaches. The error percentage shown on the right y-axis also presents the performance gap between INSTANT and the optimal solution for different cases. For the lower values of $\eta$, INSTANT achieves the optimal result with only less than 5% error.

The comparison of the computational time between the optimal approach and INSTANT for different scenarios is shown in Table 5.1. While INSTANT provides the

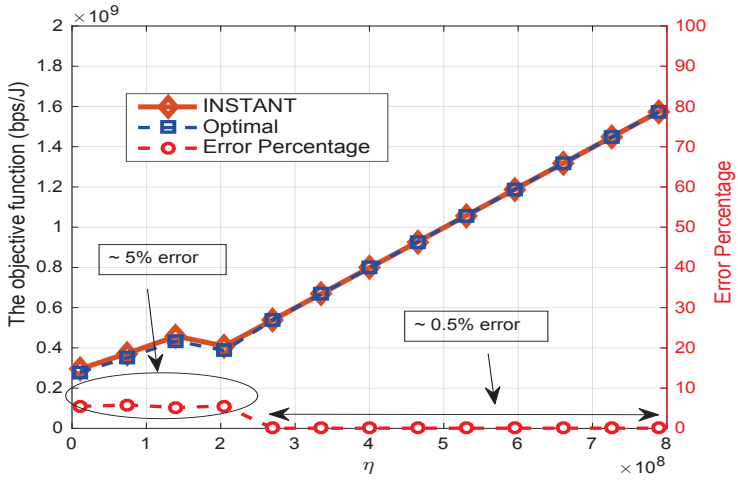


**Figure 5.7** The objective function and error percentage versus $\eta$. The comparison between INSTANT and the optimal solution. $K = 4$ and $N = 8$.

sub-optimal solution within less than 1 sec, the computational time of the optimal method grows very fast because its complexity is exponential while that of INSTANT is polynomial. Moreover, Figure 5.8 compares the energy efficiency achieved by INSTANT and the optimal method for different scenarios; they are rather close. In particular, EEs achieved by INSTANT are 97.95%, 97.72%, 97.61%, 97.21%, 96.51%, and 96.16% of the corresponding optimal EEs, for $\{K = 2,\ N = 8\}$, $\{K = 2,\ N = 24\}$, $\{K = 4,\ N = 8\}$, $\{K = 4,\ N = 16\}$, $\{K = 6,\ N = 16\}$, and $\{K = 8,\ N = 16\}$, respectively. Additionally, Figure 5.8 compares the energy efficiency of our proposal with the fixed data rate requirements (FDR) algorithm. FDR assumes that users have the fixed data rate requirements, while the data rate requirement in our approach is a function of the number of bits in users' buffers; our approach does not waste any spectral resources. FDR has been widely used in recent works [52]. As shown in this figure, our proposal performs better as compared to FDR because some of the available sub-channels are wasted by FDR. In fact, FDR allocates sub-channels based on users' required data rates, and for high data rate requirements, the optimizer has less freedom to maximize the objective function, thereby resulting in the performance degradation.

**Table 5.2** The Computational Time Complexity Comparisons.

| | **INSTANT Algorithm** | **Optimal** |
|---|---|---|
| **K=2, N=8** | 0.096 sec | 0.954 sec |
| **K=2, N=24** | 0.127 sec | 7.804 sec |
| **K=4, N=8** | 0.191 sec | 336.847 sec |
| **K=4, N=16** | 0.304 sec | 990.135 sec |
| **K=6, N=16** | 0.445 sec | 7030.431 sec |
| **K=8, N=16** | 0.612 sec | 52728.882 sec |

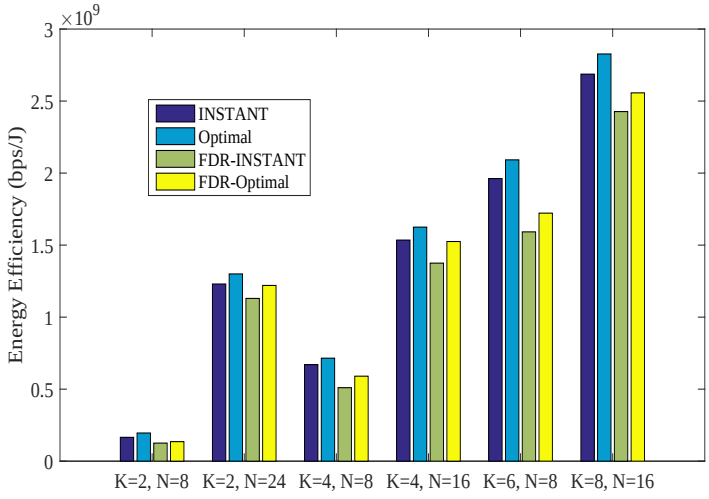


**Figure 5.8** Energy efficiency comparisons between INSTANT and the optimal approach for different scenarios.

# CHAPTER 6

# NOMA AIDED NB-IOT FOR MACHINE TYPE COMMUNICATION WITH USER CLUSTERING

## 6.1 Introduction

Internet of Things (IoT) is a world wide network of interconnected entities and is anticipated to grow in coming years with the projection of connecting as many as billions of devices with an average of 6-7 devices per person by 2020 [16, 50]. There are three typical usage scenarios for fifth generation (5G) mobile network services, including enhanced mobile broadband (eMBB), massive machine type communications (mMTC) and ultra-reliable and low-latency communications (URLLC) [61]. Different from eMBB, mMTC and URLLC mainly target services of IoT and are considered as two types of Machine Type Communications (MTC) characterized by the International Telecommunications Union (ITU). mMTC and URLLC devices as two important enablers of IoT have different characteristics. mMTC requires connectivity of a massive number of active low-power devices in co-existence in one cell, and these devices transmit small packets with relaxed latency requirements in the order of seconds or hours [13]. Unlike mMTC, ultra reliable data transmissions is essential for URLLC devices along with low latency requirements as they are used for critical applications [61].

To support MTC for next generation mobile networks, a new technology called Narrow-band Internet of Things (NB-IoT) has recently been standardized by the Third Generation Partnership Project (3GPP) in its Release 13 [71]. In particular, NB-IoT provides energy efficient communications for low power MTC devices on a narrow bandwidth of 180 kHz for both downlink and uplink [75]. In order to provide better granularity and higher utilization, the unit of resource scheduling in

the NB-IoT uplink is sub-carrier instead of Physical Resource Block (PRB). In fact, the NB-IoT uplink has sub-carrier spacing of 3.75 kHz, i.e., the minimum transmission bandwidth for a device, whereas the downlink retains the Long Term Evolution (LTE) downlink transmission structure with 15 kHz sub-carrier spacing [12]. NB-IoT can provide data rates of nearly 250 kbps in downlink and 20 kbps in uplink transmissions with the possibility to aggregate multiple sub-carriers to reach the downlink speed [68, 78]. The target of NB-IoT is to prolong the battery lifetime to reach 10 years and provide massive connectivity of devices [75]. However, the main challenge of providing connectivity to a massive number of MTC devices in 5G networks cannot be addressed by existing NB-IoT technologies.

Currently, NB-IoT exploits an orthogonal multiple access (OMA) scheme over a bandwidth of 180 kHz where each sub-carrier cannot be occupied by more than one user. Thus, the OMA scheme in NB-IoT fails to cope with the massive increase in the number of connected MTC devices. Hence, to support connectivity to a massive number of MTC devices with the limited number of sub-carriers in one PRB, a promising solution is to adopt power-domain Non-Orthogonal Multiple Access (NOMA) scheme [20, 60]. In contrast with OMA methods, NOMA supports massive connectivity by allocating multiple MTC devices to share each sub-carrier. In other words, multiple MTC devices can transmit over the same frequency resources, thus resulting in a significant increase in the network connectivity. In the power domain NOMA scenario, a different power level strategy is considered to decode the differentiated messages sequentially at the receiver side [89]. In fact, the Successive Interference Cancellation (SIC) [60] scheme is exploited at the receiver side to extract the transmitted messages. Thus, NOMA can help NB-IoT systems to meet their demands of massive connectivities, and high spectral-energy efficiency.

### 6.1.1 Contributions

While there are several research activities that investigate NOMA techniques for 5G networks, none, to our best knowledge, has leveraged the advantages of NOMA in the context of NB-IoT with user clustering of different users with various quality of service (QoS) requirements. To this end, we aim to address the aforementioned issue by proposing a general system model focusing on two emerging technologies of NOMA and NB-IoT. In fact, we propose a novel NOMA based NB-IoT model to maximize the total throughput of an NB-IoT network by increasing the number of connected devices through optimal clustering of MTC devices and optimizing the resource allocation. In particular, MTC devices are grouped into different NOMA clusters and share the same frequency resources among the cluster members. Considering the intra-cell interferences, transmission power and QoS requirements, the MTC devices are ranked in each NOMA cluster. The goal is to maximize the total uplink transmission rate of MTC devices by optimizing NOMA clustering and resource allocation of MTC devices. The main contributions of this chapter include:

- We propose a NOMA clustering method for MTC devices in an NB-IoT system. In particular, MTC devices are classified into different NOMA clusters and the same frequency resources are shared among the cluster members. Considering the intra-cell interferences, transmission power and QoS requirements, the MTC devices are ranked in each NOMA cluster. Therefore, spectral resources are allocated to the NOMA clusters based on the requirements of NOMA cluster members.

- We formulate a NOMA based optimization problem to maximize the total sum rate of uplink transmission in an NB-IoT system by optimizing the resource allocation of MTC devices and NOMA clustering while satisfying the transmission power and quality of service requirements. We further prove the NP-hardness of the proposed optimization problem.

- We propose an efficient heuristic algorithm to solve the optimization problem by jointly optimizing NOMA clustering and resource allocation of MTC devices. Furthermore, we prove that the reduced optimization problem of power control is a convex optimization task by introducing variable transformations.

- We evaluate the performance of our proposal and the heuristic algorithm via simulations to demonstrate the benefits of NOMA in increasing the total throughput of MTC devices in an NB-IoT system.

### 6.1.2 Related Works

In this section, related works including NB-IoT, NOMA, and resource allocation are discussed. In the past few years, several works investigated the major challenges of NB-IoT and researchers came up with different algorithms and models. Recently, Yang *et al.* [81] investigated the small-cell assisted traffic offloading for NB-IoT systems and formulated a joint traffic scheduling and power allocation problem to minimize the total power consumption. Oh and Shin [57] proposed an efficient small data transmission scheme for NB-IoT in which devices that are in an idle state can transmit a small data packet without the radio resource control connection. Malik *et al.* [54] investigated radio resource management in NB-IoT systems by proposing an interference aware resource allocation for the rate maximization problem.

Al-Imari *et al.* [3] proposed a NOMA scheme for uplink data transmission that allows multiple users to share the same sub-carrier without any coding/spreading redundancy. Mostafa *et al.* [55] studied the connectivity maximization for the application of NOMA in NB-IoT, where only two users can share the same sub-carrier. Kiani and Ansari [45] proposed an edge computing aware NOMA technique in which MEC users' uplink energy consumption is minimized via an optimization framework. Wu *et al.* [77] investigated the spectral efficiency maximization problem for wireless powered NOMA IoT networks. Shahini *et al.* [65] proposed the energy efficiency

maximization problem for cognitive radio (CR) based IoT networks by taking into consideration of user buffer occupancy and data rate fairness. Qian *et al.* [59] proposed an optimal SIC ordering to minimize the maximum task execution latency across devices for MEC-aware NOMA NB-IoT network. Zhai *et al.* [85] proposed a joint user scheduling and power allocation for NOMA based wireless networks with massive IoT devices. Xu and Darwazeh [80] proposed a compressed signal waveform solution, termed fast-orthogonal frequency division multiplexing (Fast-OFDM), to potentially double the number of connected devices.

Several works have investigated NOMA for 5G networks, but none has looked into employing NOMA clustering for NB-IoT users with various QoS requirements. Therefore, we propose a novel NOMA based NB-IoT model to maximize the total throughput of the network by optimizing both NOMA clustering and the resource allocation of MTC devices in an NB-IoT system.

## 6.2 System Model

We consider a single-cell scenario with one eNB where it supports MTC based on NB-IoT standard [71]. We assume there is no inter-cell interference from other neighboring cells. Denote $\mathcal{U} = \{1, ..., U\}$ and $\mathcal{M} = \{1, ..., M\}$ as the sets of mMTC and URLLC devices, respectively. Active URLLC and mMTC devices share a bandwidth of one physical resource block (PRB) for uplink data transmission in one transmission time interval (TTI). The available bandwidth of one PRB is assumed to be divided into a set of sub-channel frequencies $\mathcal{S} = \{1, ..., S\}$ and the bandwidth of each sub-channel is $W$. In fact, the system bandwidth can be equally divided into either 48 or 12 sub-carriers in NB-IoT systems. In particular, the sub-carrier spacing of 3.75 kHz can only be supported for uplink transmissions [78]. Therefore, we consider one PRB with 48 sub-carriers of 3.75 kHz for the uplink data transmissions.

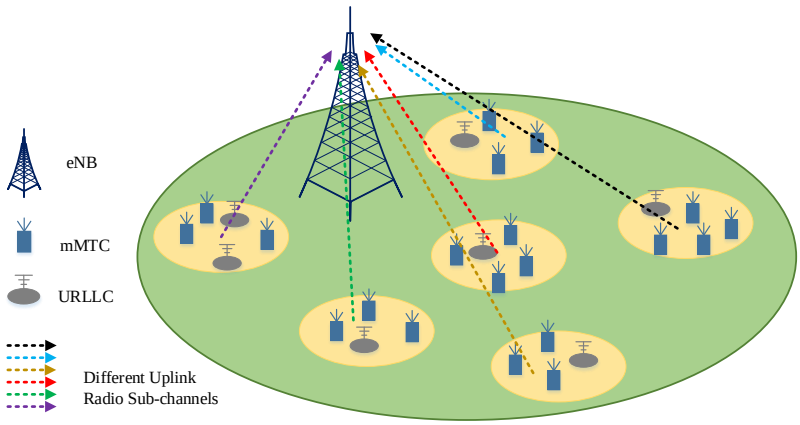


**Figure 6.1** The NOMA clusters include mMTC and URLLC devices, where the allocated sub-channels to each NOMA cluster are shared by the MTC devices.

### 6.2.1 NOMA Clustering

We propose a power-domain NOMA scheme by clustering mMTC and URLLC devices in a NB-IoT network as shown in Figure 6.1. According to the NOMA scheme, the mMTC and URLLC devices share each sub-carrier (sub-channel), and transmit data in a non-orthogonal manner, i.e., more than one user can share the same sub-channel. Therefore, the devices are divided into different groups, called the NOMA clusters. Denote $\mathcal{C} = \{1, ..., C\}$ as the set of NOMA clusters, and $\gamma^{s,c}$ as the binary variable to assign sub-channel $s \in \mathcal{S}$ to NOMA cluster $c \in \mathcal{C}$. Hence, $\gamma^{s,c} = 1$ if sub-channel $s$ is allocated to the $c^{th}$ NOMA cluster, and $\gamma^{s,c} = 0$ otherwise. The URLLC and mMTC devices transmit their messages on the same sub-channel with transmission powers of $p_u$ and $p_m$, respectively. A combined message from URLLC and mMTC devices with additive noise $N_0$ is received at the eNB. In order to successfully decode messages from the combined received message, the eNB employs successive interference cancellation (SIC). Thus, the users need to be ordered in each cluster for the SIC method.

Define the set of the order (ranks) in each cluster as $\mathcal{K} = \{1, ..., k_{\max}\}$, where $k_{\max}$ specifies the maximum number of users that are allowed to be in one cluster and consequently share the allocated sub-channels. Note that we assume $C \times k_{\max}$ should be greater than the total number of the devices. According to the principles

of SIC [20], the $k^{th}$ user's message in each cluster is decoded before the other users with higher orders. Therefore, the users with higher ranks ($\{k+1, k+2, ...\}$) in each cluster introduce interference to the $k^{th}$ user. In other words, the user with the highest rank in each cluster does not experience interference from other users and the first user receives interference from other users with higher ranks ($k = 2, ..., k_{\max}$). Note that URLLC devices have higher data rate requirements as compared to mMTC devices. Thus, the transmission power of URLLC devices are higher than the mMTCs' transmission power. Therefore, in each cluster, the URLLC devices are required to have higher ranks as compared to mMTC devices. In fact, the SIC decoder at the eNB starts decoding with URLLCs, and consequently the mMTC devices are not affected by high interference caused by URLLCs.

### 6.2.2 Quality of Service Constraints

Denote $p_m^s$ as the transmission power of the $m^{th}$ mMTC over the $s^{th}$ sub-channel and $\alpha_m^{c,k}$ as the binary variable to assign the $m^{th}$ mMTC to the $k^{th}$ order of the cluster $c$. In fact, $\alpha_m^{c,k} = 1$ if there is an assignment, and $\alpha_m^{c,k} = 0$ otherwise. Thus, the achievable data rate of the $m^{th}$ mMTC device, $R_m$, in terms of the aggregate rate over the allocated sub-carriers can be expressed as

$$R_m = \sum_{c\in\mathcal{C}} \sum_{k\in\mathcal{K}} \alpha_m^{c,k} \sum_{s\in\mathcal{S}} \gamma^{s,c} W \log_2 \left( 1 + \frac{|h_m^s|^2 p_m^s}{N_0 W + \sum\limits_{d\in\mathcal{M}\setminus m} \sum\limits_{h=k+1}^{k_{\max}} \alpha_d^{c,h} |h_d^s|^2 p_d^s} \right), \tag{6.1}$$

where $N_0$ is the noise power spectral density and $h_m^s$ denotes the channel gain between the $m^{th}$ mMTC device and the eNB on sub-channel $s$. Since the NOMA clustering procedure requires mMTC devices to have higher ranks as compared to URLLCs, the

**Table 6.1** List of Symbol Notations and Description

| **Symbols** | **Descriptions** |
|---|---|
| $\mathcal{U}$ ($\mathcal{M}$) | The set of URLLC users (the set of mMTC users) |
| $\mathcal{S}$ | The set of sub-channels in an NB-IoT system |
| $\mathcal{C}$ ($\mathcal{K}$) | The set of NOMA clusters (the set of orders in each NOMA cluster) |
| $k_{max}$ | The maximum number of users in one NOMA cluster |
| $\gamma^{s,c}$ | The binary indicator whether to allocate the $s^{th}$ sub-channel to the $c^{th}$ cluster |
| $p_u^s$ | The transmission power of the $u^{th}$ URLLC device over the $s^{th}$ channel |
| $p_m^s$ | The transmission power of the $m^{th}$ mMTC device over the $s^{th}$ channel |
| $N_0$ | The Additive White Gaussian Noise |
| $\alpha_m^{c,k}$ | The binary indicator whether to assign the $m^{th}$ mMTC to the $k^{th}$ order of cluster $c$ |
| $\beta_u^{c,k}$ | The binary indicator whether to assign the $u^{th}$ URLLC to the $k^{th}$ order of cluster $c$ |
| $R_m$ | The total transmission rate of the $m^{th}$ mMTC device |
| $R_u$ | The total transmission rate of the $u^{th}$ URLLC device |
| $W^{RB}$ | The total bandwidth of one resource block in the NB-IoT |
| $W$ | The bandwidth of one tone in one RB |
| $h_m^s$ | The channel gain of the $m^{th}$ mMTC device over the $s^{th}$ sub-channel |
| $h_u^s$ | The channel gain of the $u^{th}$ URLLC device over the $s^{th}$ sub-channel |
| $R_m^{th}$ | The minimum transmission rate of the $m^{th}$ mMTC device |
| $R_u^{th}$ | The minimum transmission rate of the $u^{th}$ URLLC device |
| $P_m^{max}$ | The maximum power budget of the $m^{th}$ mMTC device |
| $P_u^{max}$ | The maximum power budget of the $u^{th}$ URLLC device |

URLLC devices do not interfere mMTCs. Thus, the $m^{th}$ mMTC only experiences interference from the other mMTCs of the same cluster with higher ranks.

Note that each mMTC device requires a threshold for its data rate that is greater than the minimal data rate of $R_m^{th}$, i.e.,

$$R_m \geqslant R_m^{th}, \quad \forall m \in \mathcal{M}. \tag{6.2}$$

The total transmission power of the $m^{th}$ mMTC device is limited to its maximum power budget $P_m^{max}$, i.e.,

$$\sum_{s \in \mathcal{S}} p_m^s \leqslant P_m^{\max}, \quad \forall m \in \mathcal{M}. \tag{6.3}$$

Similarly, the achievable data rate of the $u^{th}$ URLLC device can be given by the Shannon-Hartley theorem. Note that the ranks of URLLCs are always greater than those of mMTCs in each NOMA cluster. Thus, they receive interference from all the mMTC cluster members as well as those URLLC cluster members with higher ranks. Denote $\beta_u^{c,k}$ as the binary variable whether to assign the $u^{th}$ URLLC to the $k^{th}$ order of the cluster $c$. In other words, $\beta_u^{c,k} = 1$ if such assignment is made, and $\beta_u^{c,k} = 0$ otherwise. Hence, the achievable data rate of the $u^{th}$ URLLC device over the allocated sub-carriers can be given in Equation (6.4), where $h_u^s$ is the channel gain between the $u^{th}$ URLLC device and the eNB on sub-channel $s$, and $p_u^s$ represents the transmission power of the $u^{th}$ URLLC over the $s^{th}$ sub-channel. Owing to performing critical tasks by URLLC devices, their power consumption is not of significant importance. Therefore, the transmission powers of URLLC devices are set to their maximum limit,

i.e.,

$$R_u = \sum_{c\in\mathcal{C}}\sum_{k\in\mathcal{K}}\beta_u^{c,k}\sum_{s\in\mathcal{S}}\gamma^{s,c}W \log_2\left(1+\frac{|h_u^s|^2 p_u^s}{N_0W+\sum_{d\in\mathcal{U}\setminus u}\sum_{h=k+1}^{k_{\max}}\beta_d^{c,h}|h_d^s|^2p_d^s+\sum_{m\in\mathcal{M}}\sum_{h=k+1}^{k_{\max}}\alpha_m^{c,h}|h_m^s|^2p_m^s}\right), \tag{6.4}$$

$$\sum_{s\in\mathcal{S}} p_u^s = P_u^{\max}, \quad \forall u\in\mathcal{U}. \tag{6.5}$$

Meanwhile, the data rate of the $u^{th}$ URLLC device should be greater than a given minimal rate $R_u^{th}$,

$$R_u \geqslant R_u^{th}, \quad \forall u\in\mathcal{U}. \tag{6.6}$$

### 6.3 The Optimization Framework

In this section, the optimization problem of NOMA clustering for NB-IoT is formulated as a sum rate maximization of URLLC and mMTC devices. Apart from the QoS constraints in (6.2), (6.3), (6.5), and (6.6), we should enforce extra constraints for the NOMA clustering process. In particular, each URLLC and mMTC device should be assigned to only one cluster with one specific rank, i.e.,

$$\sum_{c\in\mathcal{C}}\sum_{k\in\mathcal{K}}\alpha_m^{c,k}=1, \quad \forall m\in\mathcal{M}, \tag{6.7}$$

$$\sum_{c\in\mathcal{C}}\sum_{k\in\mathcal{K}}\beta_u^{c,k}=1, \quad \forall u\in\mathcal{U}. \tag{6.8}$$

Moreover, each rank of one cluster should be assigned either to one URLLC or one mMTC, i.e.,

$$\sum_{m\in\mathcal{M}} \alpha_m^{c,k} + \sum_{u\in\mathcal{U}} \beta_u^{c,k} = 1, \quad \forall c \in \mathcal{C}, \quad \forall k \in \mathcal{K}. \tag{6.9}$$

Since the concept of NOMA is to share spectral resources between multiple users, the NOMA clustering is subject to a constraint that enforces existence of more than one user in each cluster, i.e.,

$$\sum_{m\in\mathcal{M}} \sum_{k\in\mathcal{K}} \alpha_m^{c,k} + \sum_{u\in\mathcal{U}} \sum_{k\in\mathcal{K}} \beta_u^{c,k} \geqslant 2, \quad \forall c \in \mathcal{C}. \tag{6.10}$$

The URLLC devices have priority to have first ranks of clusters due to their higher data rate and transmission power requirements. In other words, the high power of URLLCs do not affect the low power mMTC devices during the SIC process, if they are assigned to the first ranks of clusters. Therefore, for the $k^{th}$ rank of each cluster that is $2 \leqslant k \leqslant k_{\max}$, the mMTC devices should always have higher ranks as compared to the URLLC devices, i.e.,

$$\beta_u^{c,k} \geqslant \alpha_m^{c,k-1}, \quad \forall m \in \mathcal{M}, \quad \forall u \in \mathcal{U}, \quad \forall c \in \mathcal{C}, \tag{6.11}$$

and we ensure the rank priority in each cluster, by starting rank assignments from the first rank of each cluster, i.e.,

$$\alpha_m^{c,k} \leqslant \alpha_m^{c,k-1}, \ \forall m \in \mathcal{M}, \ \forall c \in \mathcal{C}, \ 2 \leqslant k \leqslant k_{\max}, \tag{6.12}$$

$$\beta_u^{c,k} \leqslant \beta_u^{c,k-1}, \ \forall u \in \mathcal{U}, \ \forall c \in \mathcal{C}, \ 2 \leqslant k \leqslant k_{\max}. \tag{6.13}$$

Finally, the NOMA clustering optimization problem for NB-IoT as a sum rate maximization of URLLC and mMTC devices can be expressed as

$$\textbf{P1:} \quad \max_{p_m^s, p_u^s, \alpha_m^{c,k}, \beta_u^{c,k}, \gamma^{s,c}} \sum_{m \in \mathcal{M}} R_m + \sum_{u \in \mathcal{U}} R_u$$

*s.t.*

$$\begin{aligned}
&C1: R_m \geqslant R_m^{th}, \quad \forall m \in \mathcal{M}, \\
&C2: \sum_{s \in \mathcal{S}} p_m^s \leqslant P_m^{\max}, \quad \forall m \in \mathcal{M}, \\
&C3: R_u \geqslant R_u^{th}, \quad \forall u \in \mathcal{U}, \\
&C4: \sum_{s \in \mathcal{S}} p_u^s = P_u^{\max}, \quad \forall u \in \mathcal{U}, \\
&C5: \beta_u^{c,k} \geqslant \alpha_m^{c,k-1}, \quad \forall m \in \mathcal{M}, \quad \forall u \in \mathcal{U}, \quad \forall c \in \mathcal{C}, \quad 2 \leqslant k \leqslant k_{\max}, \\
&C6: \alpha_m^{c,k} \leqslant \alpha_m^{c,k-1}, \ \forall m \in \mathcal{M}, \ \forall c \in \mathcal{C}, \ 2 \leqslant k \leqslant k_{\max} \\
&C7: \beta_u^{c,k} \leqslant \beta_u^{c,k-1}, \ \forall u \in \mathcal{U}, \ \forall c \in \mathcal{C}, \ 2 \leqslant k \leqslant k_{\max} \\
&C8: \sum_{c \in \mathcal{C}} \sum_{k \in \mathcal{K}} \alpha_m^{c,k} = 1, \quad \forall m \in \mathcal{M}, \\
&C9: \sum_{c \in \mathcal{C}} \sum_{k \in \mathcal{K}} \beta_u^{c,k} = 1, \quad \forall u \in \mathcal{U}, \\
&C10: \sum_{m \in \mathcal{M}} \alpha_m^{c,k} + \sum_{u \in \mathcal{U}} \beta_u^{c,k} = 1, \quad \forall c \in \mathcal{C}, \quad \forall k \in \mathcal{K}, \\
&C11: \sum_{m \in \mathcal{M}} \sum_{k \in \mathcal{K}} \alpha_m^{c,k} + \sum_{u \in \mathcal{U}} \sum_{k \in \mathcal{K}} \beta_u^{c,k} \geqslant 2, \quad \forall c \in \mathcal{C}, \\
&C12: \sum_{c \in \mathcal{C}} \gamma^{s,c} = 1, \quad \forall s \in \mathcal{S}, \\
&C13: \sum_{s \in \mathcal{S}} \sum_{c \in \mathcal{C}} \gamma^{s,c} \mathcal{W}^{s,c} \leqslant W^{RB}, \quad \forall c \in \mathcal{C}, \quad \forall s \in \mathcal{S} \\
&C14: p_m^s \geqslant 0, \quad \forall m \in \mathcal{M}, \quad \forall s \in \mathcal{S}, \\
&C15: p_u^s \geqslant 0, \quad \forall u \in \mathcal{U}, \quad \forall s \in \mathcal{S}, \\
&C16: \gamma^{s,c} \in \{0,1\}, \quad \forall c \in \mathcal{C}, \quad \forall s \in \mathcal{S}, \\
&C17: \alpha_m^{c,k} \in \{0,1\}, \quad \forall m \in \mathcal{M}, \quad \forall c \in \mathcal{C}, \quad \forall k \in \mathcal{K}, \\
&C18: \beta_u^{c,k} \in \{0,1\}, \quad \forall u \in \mathcal{U}, \quad \forall c \in \mathcal{C}, \quad \forall k \in \mathcal{K},
\end{aligned} \tag{6.14}$$

where C1 imposes the data rates of mMTC devices to be greater than the minimum data rate requirement; C2 limits the total transmission power of the $m^{th}$ mMTC to the maximum power budget, $P_m^{max}$; C3 implies that the minimum data rate constraint for each URLLC device must be satisfied; C4 is the power budget constraint for each URLLC device; C5 is to ensure that the ranks of mMTC devices are higher than URLLCs for each NOMA cluster; C6 and C7 imply that mMTC and URLLC devices can be assigned to the $k^{th}$ rank of the $c^{th}$ cluster if all the previous ranks are already allocated to other users; C8 and C9 are designed to guarantee that each device (mMTC and URLLC) is allocated to only one cluster and one specific order within the cluster; C10 specifies that each rank of a cluster cannot be allocated to both mMTC and URLLC devices; C11 is to guarantee each NOMA cluster to have more than one member; C12 implies that each sub-carrier cannot be allocated to more than one cluster; C13 ensures that the total bandwidth allocated to all NOMA clusters is not more than the bandwidth of one RB (bandwidth of one RB in NB-IoT is 180 kHz); C14 and C15 are to limit the transmission powers of mMTCs and URLLCs to positive values; and C16, C17 and C18 ensure that the variables $\gamma^{s,c}$, $\alpha_m^{c,k}$, and $\beta_u^{c,k}$ are restricted to binary values, respectively.

**Lemma 5.** *The general optimization problem of NOMA clustering problem for NB-IoT in (6.14) is an NP-hard problem.*

*Proof.* The Lemma is proved in Section B.2. □

The formulated optimization problem is a non convex mixed integer nonlinear programming (MINLP) problem which is combinatorial, and exploiting exhaustive search presents exponential time complexity. Therefore, we solve the optimization problem by proposing a heuristic algorithm.

## 6.4 Proposed Algorithm

In this section, we propose an efficient heuristic algorithm to find sub-optimal solutions of the non convex MINLP problem in (6.14). The proposed algorithm optimizes the NOMA clustering of mMTC and URLLC devices and allocates spectral resources to the NOMA clusters. The pseudo code for solving the optimization problem is summarized in Algorithm 1. The first phase of the algorithm is the URLLC clustering, where the URLLC devices are sorted based on their average channel gains, $\tilde{h}_u = \sum_{s \in \mathcal{S}} h_u^s / S$. As discussed in Subsection 6.2.1, the URLLC devices have higher data rate and transmission power requirements. Therefore, to mitigate the adverse impacts of interference caused by the URLLCs' high transmission powers, the ranks of URLLC devices in each cluster should be less than the mMTC ones. In the URLLC clustering process, URLLC devices with higher $\tilde{h}_u$ are assigned to the lowest ranks of NOMA clusters, i.e., $k = 1$. If the number of URLLC devices, $U$, is greater than the number of NOMA clusters, $C$, the remaining devices are assigned to the next ranks of clusters. Similar to the URLLC clustering approach, the mMTC clustering procedure is based on the average channel gain of mMTC devices, $\tilde{h}_m = \sum_{s \in \mathcal{S}} h_m^s / S$. The mMTC devices with higher $\tilde{h}_m$ are allocated to the next available rank of clusters. Then, the remaining mMTC devices are allocated to the higher ranks of NOMA clusters. By this NOMA clustering approach, Constraints 5-11 in (6.14) are taken into consideration. After the NOMA clustering process, the resource allocation for URLLC and mMTC devices are detailed in Algorithm 1. The initial values for the transmission rates and powers of URLLC and mMTC devices are $R_u = 0$, $p_u^s = P_u^{max}$, and $R_m = 0$, $p_m^s = P_m^{max}$, respectively. The resource allocation phase continues until all the sub-channels are allocated to NOMA clusters and the data rate requirements of mMTC and URLLC devices are satisfied.

**Algorithm 4** NOMA Clustering and Resource Allocation for MTC

**Initializing:** $C$, $R_m^{th}$, $R_u^{th}$, $P_m^{max}$, $P_u^{max}$.

**URLLC Clustering**

Sorting URLLCs: $\tilde{h}_1 \geqslant \tilde{h}_2 \geqslant ... \geqslant \tilde{h}_U$

***for all*** $u \in \mathcal{U}$ ***do***

***if*** $U \leq C$ ***do***

Assign URLLC devices $\{1, 2, ..., U\}$ to the first rank ($k = 1$) of $\{1, 2, ..., C\}$ clusters

***else***: Assign URLLC $\{1, 2, ..., C\}$ to the first rank of all $C$ clusters, and $\{C+1, C+2, ..., U\}$ to the higher ranks

***end if***

***end for***

**mMTC Clustering**

Sorting mMTCs: $\tilde{h}_1 \geqslant \tilde{h}_2 \geqslant ... \geqslant \tilde{h}_M$

***for all*** $k \in \mathcal{K}$ ***do***

***if*** $U < C$ ***do***

Assign mMTC $\{1, ..., (C-U)\}$ to the first rank ($k = 1$) of $\{(U+1), ..., C\}$ clusters.

***else***: Assign mMTC $\{1, ..., (C-U)\}$ to the next available rank of $\{(U+1), ..., C\}$.

***end if***

***end for***

**Resource Allocation for Clusters**

Set $R_u = 0$, $R_m = 0$, $p_m^s = P_m^{max}$, $p_u^s = P_u^{max}$, $\hat{S} \leftarrow \emptyset$, $S_a^c \leftarrow \emptyset$, $C_{ns} \leftarrow \mathcal{C}$

***While*** $\mathcal{S} \neq \emptyset$ & $R_u < R_u^{th}$ & $R_m < R_m^{th}$

Find $c^*$, $\forall c \in \mathcal{C}$, for each $s \in \mathcal{S}$:

$c^* = \arg\max_{c \in C_{ns}} \left(\sum_{u \in \mathcal{U}} R_u + \sum_{m \in \mathcal{M}} R_m\right)$;

Allocate the sub-carrier $s$ to cluster $c^*$:

Set $\gamma^{s,c^*} = 1$, and update $S_a^{c^*} \leftarrow S_a^{c^*} \cup \{s\}$, $\hat{S} \leftarrow \hat{S} \cup \{s\}$

Update $R_u = R_u + R_{u,s}$, $R_m = R_m + R_{m,s}$

Update the powers: URLLC and mMTC of $c^*$ individually perform SUWF over all allocated sub-carriers:

$p_m^s = \frac{p_m^s}{|S_a^{c^*}|+1}$, $p_u^s = \frac{p_u^s}{|S_a^{c^*}|+1}$, $\forall s \in \mathcal{S}$

***if*** $R_u \geqslant R_u^{th}$ and $R_m \geqslant R_m^{th}$; $\forall m, u$ from cluster $c^*$ ***do***

$C_{ns} \leftarrow C_{ns} \backslash \{c^*\}$

***end if***

$\mathcal{S} \leftarrow \mathcal{S} \backslash \hat{S}$

***if*** $R_u \geqslant R_u^{th}$ and $R_m \geqslant R_m^{th}$, $\forall m \in \mathcal{M}$, $\forall u \in \mathcal{U}$ ***do***

***for all*** $s \in \mathcal{S}$ ***do***

$c^* = \arg\max_{c \in C} \left(\sum_{u \in \mathcal{U}} R_u + \sum_{m \in \mathcal{M}} R_m\right)$

Set $\gamma^{s,c^*} = 1$, $S_a^{c^*} \leftarrow S_a^{c^*} \cup \{s\}$

***end for***

Update $p_m^s = \frac{p_m^s}{|S_a^{c^*}|+1}$, $p_u^s = \frac{p_u^s}{|S_a^{c^*}|+1}$

***end if***

***End while***

Denote $S_a^c \leftarrow \emptyset$ as the set of allocated sub-channels to the $c^{th}$ cluster, and $C_{ns} \leftarrow \mathcal{C}$ as the set of clusters of devices with unsatisfied rates. For each sub-carrier, the best cluster ($c^*$) is the one that maximizes the total throughput, i.e., $c^* = \underset{c \in C_{ns}}{\arg\max} \left( \sum_{u \in \mathcal{U}} R_u + \sum_{m \in \mathcal{M}} R_m \right)$. Then, the data rates of the mMTC and URLLC devices and their transmission powers are updated accordingly. Note that each MTC device performs Single User Water Filling (SUWF) [3] technique over all allocated sub-channels. During the resource allocation process, clusters with satisfied data rates are excluded from the set of $C_{ns}$. The algorithm iteratively allocates the sub-channels one by one until all the mMTC and URLLC devices' rate requirements are met.

### 6.4.1 Power Allocation

Given the URLLC and mMTC user allocation to NOMA clusters and spectrum allocation to the clusters, the binary variables of $\alpha_m^{c,k}$, $\beta_u^{c,k}$ and $\gamma^{s,c}$ in **P1** take on 0 or 1. Therefore, all integer constraints are removed and the new optimization problem, which tries to find optimal values of URLLC and mMTC transmission powers, can be expressed as

$$\begin{aligned} \textbf{P3:} \quad & \max_{p_m^s, p_u^s} \sum_{m \in \mathcal{M}} R_m + \sum_{u \in \mathcal{U}} R_u \\ & s.t. \\ & C1,\ C2,\ C3,\ C4,\ C14, \text{ and } C15 \text{ in } \textbf{P1} \end{aligned} \tag{6.15}$$

The reduced optimization problem, given its original formulation in **P3**, is apparently non-convex due to the interference users introduced to each other. To address this, we first define a new set of both URLLC and mMTC users, $\mathcal{J} = \{1, 2, ..., U, U+1, ..., U+M\}$ for one cluster (the result is also valid for more clusters). Let $\lambda_j \triangleq \frac{|h_j|^2}{N_0 W}$, where $h_j$ is the channel coefficient from the $j^{th}$ user to the eNB.

Without loss of generality, we order users by their normalized channel gains as $\lambda_1 \leqslant \lambda_2 \leqslant ... \leqslant \lambda_{U+M}$. Note that users exploit SIC at their receivers such that $P_1 \geqslant P_2 \geqslant ... \geqslant P_U \geqslant P_{U+1} \geqslant ... \geqslant P_{U+M}$, where $P_j \triangleq \sum_{s\in\mathcal{S}} p_j^s$. Therefore, **P3** can be rewritten as

$$\begin{aligned}
&\textbf{P4:} \quad \max_{P_j} \sum_{j\in\mathcal{J}} R_j \\
&s.t. \\
&C1: R_j \geqslant R_j^{th}, \quad \forall j \in \mathcal{J}, \\
&C2: \sum_{j\in\mathcal{J}} P_j \leqslant P^{\max}, \quad \forall j \in \mathcal{J}, \\
&C3: P_1 \geqslant P_2 \geqslant ... \geqslant P_U \geqslant P_{U+1} \geqslant ... \geqslant P_{U+M},
\end{aligned} \tag{6.16}$$

where $R_j \triangleq W^{RB}\log_2(1+\frac{\lambda_j P_j}{1+\lambda_j \sum_{l=j+1}^{U+M} P_l})$. To make **P4** convex, we use the variable transformations of $Z_j = \sum_{l=j}^{U+M} P_l$, $\forall j \in \mathcal{J}$, or $P_j = Z_j - Z_{j+1}$, $\forall j \in \{1,2,...,U+M-1\}$ and $P_{U+M} = Z_{U+M}$. Therefore, we can rewrite $R_j$, $\forall j \in \{1,2,...,U+M-1\}$ as

$$\begin{aligned}
R_j &= \log_2\left(1+\frac{\lambda_j P_j}{1+\lambda_j \sum_{l=j+1}^{U+M} P_l}\right) = \log_2\left(\frac{1+\lambda_j \sum_{l=j}^{U+M} P_l}{1+\lambda_j \sum_{l=j+1}^{U+M} P_l}\right) \\
&= \log_2\left(\frac{1+\lambda_j Z_j}{1+\lambda_j Z_{j+1}}\right) = \log_2\left(1+\lambda_j Z_j\right) - \log_2\left(1+\lambda_j Z_{j+1}\right),
\end{aligned} \tag{6.17}$$

while for $j = U+M$, $R_{U+M} = \log_2(1+\lambda_{U+M} Z_{U+M})$. Thus, the objective function in **P3** ($\sum_{j=1}^{U+M} R_j$) can be written as

$$\begin{aligned}
&\sum\nolimits_{j=1}^{U+M-1} W^{RB}\left[\log_2\left(1+\lambda_j Z_j\right) - \log_2\left(1+\lambda_j Z_{j+1}\right)\right] \\
&\quad + W^{RB}\log_2\left(1+\lambda_{U+M} Z_{U+M}\right) = \sum\nolimits_{j=1}^{U+M} \Phi_j(Z_j),
\end{aligned} \tag{6.18}$$

where $\Phi_1(Z_1) \triangleq W^{RB}\log_2(1+\lambda_1 Z_1)$, and for all $j \in \{2,3,...,U+M\}$,

$$\Phi_j(Z_j) \triangleq W^{RB}\left[\log_2\left(1+\lambda_j Z_j\right) - \log_2\left(1+\lambda_{j-1} Z_j\right)\right]. \tag{6.19}$$

The rate constraint, C1 in **P4**, can be linearized by using $Z_{j+1} \leqslant \delta_j Z_j - \rho_j$ for all $j \in \{1, 2, ..., U+M-1\}$, and $Z_{U+M} \geqslant \theta_{U+M}$, where $\delta_j \triangleq 2^{-R_j^{th}}$, $\rho_j \triangleq \frac{(1-\delta_j)}{\lambda_j}$, and $\theta_j \triangleq \frac{(2^{R_j^{th}}-1)}{\lambda_j}$. The transmission power in C2 of **P4** can be equivalent to $Z_1 = \sum_{j=1}^{U+M} P_j = P^{\max}$. The power order constraint, C3 in **P4**, $P_1 \geqslant P_2 \geqslant ... \geqslant P_{U+M} \geqslant 0$ is equivalent to $Z_1 - Z_2 \geqslant Z_2 - Z_3 \geqslant ... \geqslant Z_{U+M} \geqslant 0$. Therefore, the power allocation problem in **P4** can be transformed to the following optimization problem

$$\begin{aligned}
&\textbf{P5:} \quad \max_{\mathbf{Z}} \sum_{j\in\mathcal{J}} \Phi_j(Z_j) \\
&s.t. \\
&C1: Z_{j+1} \leqslant \delta_j Z_j - \rho_j, \\
&C2: Z_1 = P^{\max}, \\
&C3: Z_1 - Z_2 \geqslant Z_2 - Z_3 \geqslant ... \geqslant Z_{U+M} \geqslant \theta_j,
\end{aligned} \tag{6.20}$$

where $\mathbf{Z} \triangleq (Z_j)_{j=1}^{U+M}$. Note that the transformation between $P$ and $Z$ is linear, and therefore the convexity of **P3** is equivalent to the convexity of **P5**.

**Theorem 2.** *Given $\lambda_1 \leqslant \lambda_2 \leqslant ... \leqslant \lambda_{U+M}$, the power allocation problem in **P3** (or equivalently **P5**) is a convex optimization problem, for all $j \in \{2, 3, ..., U+M\}$.*

*Proof.* The Theorem is proved in Section C.1. □

## 6.5 Simulation Results

In this section, we evaluate the system performance of the proposed NOMA based NB-IoT scheme with sub-carrier and power allocation, and the NOMA clustering via Monte Carlo simulation. We consider one cell with 0.5 km radius where the locations of the mMTC and URLLC devices are randomly generated and uniformly

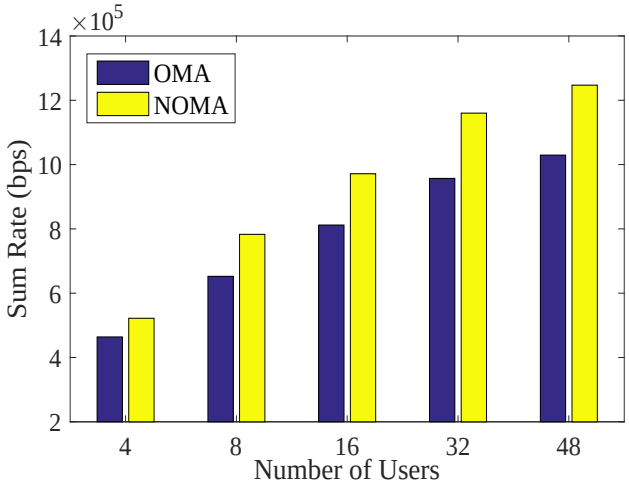


**Figure 6.2** The total throughput of a NOMA based NB-IoT system with respect to the number of users (mMTC and URLLC devices).

distributed within the cell. We consider one PRB with 48 sub-carrier spacing of 3.75 kHz for the MTC uplink transmissions in one time slot. We model the channel gains of the mMTC devices as $h_m^s = \mathcal{Y} d_{m,s}^{-\beta}$ (similarly $h_u^s$ for URLLCs), where $\mathcal{Y}$ is a random value generated based on the Rayleigh distribution, $d_{m,s}^{-\beta}$ represents the distance between the transmitter and receiver, and $\beta$ is the path-loss exponent. We set $\beta = 3$ and $d$ is varied between 0.1 m to 500 m. We also consider Additive White Gaussian Noise (AWGN) with power spectral density of -173 dBm/Hz. The maximum transmission power budgets of all URLLC and mMTC devices, $P_u^{max}$ and $P_m^{max}$ $(\forall u \in \mathcal{U}, \forall m \in \mathcal{M})$, are set to 23 dbm. The data rate thresholds of the mMTC devices follow uniform distribution, i.e., $R_m^{th}$ =Uniform $(0.1, 2)$ kbps. The bandwidth of each sub-carrier in one PRB with 48 sub-carriers is set to $w = 3.75$kHz. The Orthogonal Frequency Division Multiple Access (OFDMA) scheme as an OMA scenario and the fast OFDM [80] approach are used for benchmark comparison.

Figure 6.2 compares the sum rate of the NOMA and the OMA schemes for an NB-IoT system with respect to the total number of mMTC and URLLC devices. As we can see in this figure, the performance gain in the total throughput for the

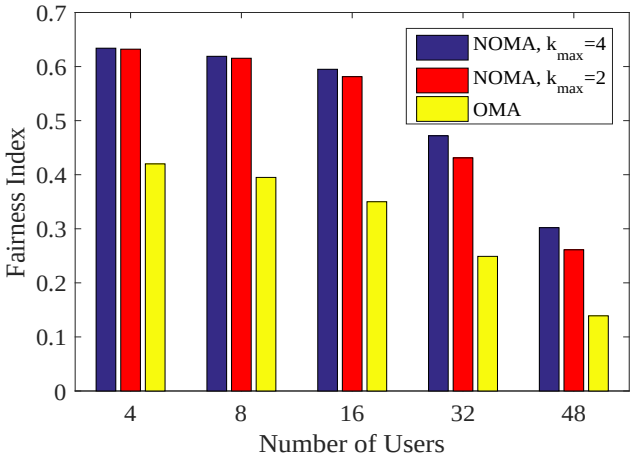


**Figure 6.3** The fairness comparison between OMA and NOMA schemes.

proposed NOMA based NB-IoT scheme over the OMA scenario is approximately 28% for a sufficiently large number of users. Owing to the multi-user diversity gain, the sum rate increases according to the number of users. Note that the ratio of the mMTC devices to the URLLC ones is set to 3, and the data rate thresholds of the URLLC devices are uniformly distributed between 0.1 kbps and 20 kbps.

To compare the fairness of the proposed NOMA scheme and the OMA scenario, the Jain's fairness index [3] is adopted for data rates of mMTC and URLLC devices, i.e., Fairness Index= $\frac{\left(\sum_{u=1}^{U} R_u + \sum_{m=1}^{M} R_m\right)^2}{(U+M)\left(\sum_{u=1}^{U} R_u^2 + \sum_{m=1}^{M} R_m^2\right)}$. In fact, Jain's fairness index is bounded between 0 and 1, and the maximum value is obtained if all the devices achieve exactly the same throughput. Figure 6.3 shows the Jain's fairness index for both NOMA and OMA schemes. As shown in the figure, the NOMA scheme for both $k_{max} = 2$ and $k_{max} = 4$ scenarios are fairer as compared to the OMA scheme. This is due to the fact that the OMA scheme does not allocate one sub-channel to more than one user, thus depriving some users from spectral resources.

Figure 6.4 compares the performance of the proposed NOMA based NB-IoT with the OMA and the fast OFDM approaches with respect to the number of the MTC devices with satisfied rate requirements. As shown in the figure, the OMA

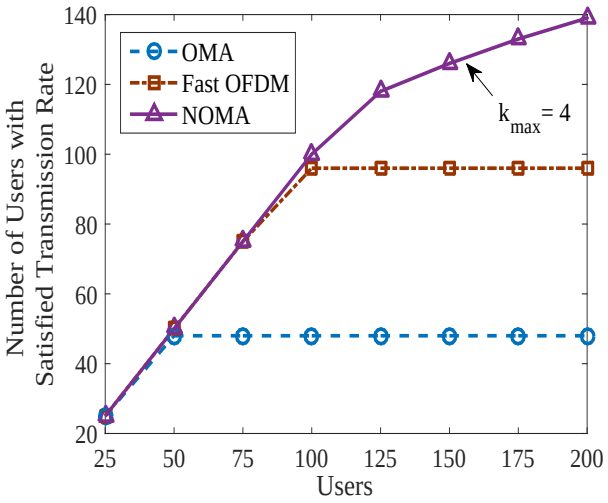


**Figure 6.4** The comparison between NOMA, OMA and fast OFDM in terms of the number of users with satisfied rate requirements.

scheme cannot support more than 48 users as it allocates each sub-carrier of an NB-IoT system to only one user. The NOMA scheme outperforms both the fast OFDM and the OFDMA (as an OMA technique), and facilitates a higher number of successfully connected MTC devices.

# CHAPTER 7

# CONCLUSION

In this dissertation, first, we have studied the joint resource allocation and structure optimization in multiuser OFDM-based HCRN. We have formulated the general problem of maximizing the sum rate of SUs in green powered OFDM based HCRN under consideration of some practical limitations such as various traffic demands of SUs, interference constraints and imperfect spectrum sensing. We have considered some practical limitations such as various traffic demands of SUs, interference constraint and imperfect spectrum sensing. Then, the general problem of joint resource allocation and structure optimization is formulated as an MINLP task. Since the general problem is NP-hard and intractable, we have tackled the problem in two steps. First, we have proposed a sub-channel allocation scheme based on a factor called Energy Figure of Merit to approximately satisfy SUs' rate requirements and remove the integer constraints. Second, we have proved that the general optimization problem is reduced to a nonlinear convex optimization task. Since the reduced optimization problem cannot achieve exact closed-form solutions, we have thus proposed near optimal closed-form solutions by applying Lambert-W function. We have also exploited the iterative gradient method based on Lagrangian dual decomposition to achieve near optimal solutions. The optimum fractions of the time slot that each SU can harvest energy from the environment are finally obtained.

Second, we have proposed a novel system model for CR based IoT by wireless energy harvesting and cooperative spectrum sensing to tackle two vital challenges of an IoT network, i.e., supplying adequate energy to operate the network in a self-sufficient manner, and providing enough radio spectrum for massive increase of devices. More importantly, we have formulated an MINLP problem to maximize the

tradeoff between EE and SE while taking into consideration of practical limitations. Moreover, we have proposed a low complexity heuristic algorithm, called INSTANT, to solve the sub-channel allocation and energy harvesting optimization problem. We have shown that INSTANT is able to obtain near optimal solution with high accuracy while having polynomial complexity.

Third, we have proposed a power domain NOMA scheme with user clustering in an NB-IoT system. In particular, the MTC devices are assigned to different ranks within the NOMA clusters where they transmit over the same frequency resources. Then, we have formulated an optimization problem to maximize the total throughput of the network by optimizing the resource allocation of MTC devices and NOMA clustering while satisfying the transmission power and quality of service (QoS) requirements. We have further designed an efficient heuristic algorithm to solve the proposed optimization problem by jointly optimizing NOMA clustering and resource allocation of MTC devices. Finally, we have presented simulation results to validate the efficiency of our proposal.

# APPENDIX A

# PROOF OF LEMMAS

## A.1 Proof of Lemma 1

Consider the rate formula in our problem:

$$\left(1-\theta_i-\frac{\tau_{s_i}}{T}\right) log_2\left(1+H_{i,j}\frac{\chi_i\theta_i T-\epsilon_{s_i}}{T-\theta_i T-\tau_{s_i}}\right). \tag{A.1}$$

Since the objective function is a sum of rates, if we prove that the rate formula is convex, then the whole objective function becomes a convex problem. Thus,

$$\begin{aligned}&\left(1-\theta_i-\frac{\tau_{s_i}}{T}\right) log_2\left(1+H_{i,j}\frac{\chi_i\theta_i T-\varepsilon_{s_i}}{T-\theta_i T-\tau_{s_i}}\right)= \\ &\underbrace{\left(1-\theta_i-\frac{\tau_{s_i}}{T}\right)\log_2(T-\theta_i T-\tau_{s_i}+H_{i,j}\chi_i\theta_i T-H_{i,j}\epsilon_{s_i})}_{\mathbf{A}} \\ &\underbrace{-\left(1-\theta_i-\frac{\tau_{s_i}}{T}\right)\log_2(T-\theta_i T-\tau_{s_i})}_{\mathbf{B}}.\end{aligned} \tag{A.2}$$

Consider the second part (B):

$$\begin{aligned}\mathbf{B}&=-\left(1-\theta_i-\frac{\tau_{s_i}}{T}\right)\log_2(T-\theta_i T-\tau_{s_i}) \\ &=-\frac{1}{T}(T-\theta_i T-\tau_{s_i})\log_2(T-\theta_i T-\tau_{s_i}) \\ &=-\frac{1}{T}Z\log_2(Z),\end{aligned} \tag{A.3}$$

where Z is equal to **C2** in **P1** and it is always greater than zero ($Z>0$). Thus, the second part is similar to the famous form of concave functions ($-Xlog(X)$). Thus, this part is proved to be concave.

Now, consider the first part (A):

$$\mathbf{A}=\left(1-\theta_i-\frac{\tau_{s_i}}{T}\right)\log_2(T-\theta_i T-\tau_{s_i}+H_{i,j}\chi_i\theta_i T-H_{i,j}\epsilon_{s_i}) \tag{A.4}$$

Then, we take the second derivative (Hessian) with respect to $\theta_i$:

$$\left[\frac{(\tau_{s_i} - T + 2H_{i,j}\epsilon_{s_i} + \theta_i T) \times T(H_{i,j}\chi_i - 1)}{(\tau_{s_i} - T + H_{i,j}\epsilon_{s_i} + \theta_i T - H_{i,j}\chi_i\theta_i T)^2} + \frac{(-H_{i,j}\chi_i T + H_{i,j}\chi_i\tau_{s_i} - H_{i,j}\chi_i\theta_i T) \times T(H_{i,j}\chi_i - 1)}{(\tau_{s_i} - T + H_{i,j}\epsilon_{s_i} + \theta_i T - H_{i,j}\chi_i\theta_i T)^2}\right]. \tag{A.5}$$

We need to prove that the second derivative is less than zero. The denominator is always positive:

$$(\tau_{s_i} - T + H_{i,j}\epsilon_{s_i} + \theta_i T - H_{i,j}\chi_i\theta_i T)^2 > 0 \tag{A.6}$$

Thus, we consider the nominator

$$\tau_{s_i} - T + 2H_{i,j}\epsilon_{s_i} + \theta_i T - H_{i,j}\chi_i T + H_{i,j}\chi_i\tau_{s_i} - H_{i,j}\chi_i\theta_i T. \tag{A.7}$$

By adding and subtracting $H_{i,j}\chi_i\theta_i T$, we have

$$(\tau_{s_i} - T + \theta_i T) + H_{i,j}(-\chi_i\theta_i T + \epsilon_{s_i}) + H_{i,j}\epsilon_{s_i} - H_{i,j}\chi_i(\theta_i + 1 - \theta_i)T + H_{i,j}\chi_i\tau_{s_i} - H_{i,j}\chi_i\theta_i T. \tag{A.8}$$

Further rearranging the terms proves that the nominator is negative.

$$\underbrace{(\tau_{s_i} - T + \theta_i T)}_{<0} + H_{i,j}\underbrace{(-\chi_i\theta_i T + \epsilon_{s_i})}_{<0} + H_{i,j}\underbrace{(-\chi_i\theta_i T + \epsilon_{s_i})}_{<0} + H_{i,j}\chi_i\underbrace{(\tau_{s_i} - T + \theta_i T)}_{<0} < 0. \tag{A.9}$$

Thus, $T(H_{i,j}\chi_i - 1) > 0$ (i.e., $H_{i,j}\chi_i > 1$) must be held such that the whole objective function becomes convex for minimization (concave for maximization). Then, the convex problem can be solved by standard convex optimization techniques.

## A.2 Proof of Lemma 2

To prove **P1** to be convex MINLP, one should consider convexity of constraints functions $\forall i \in \mathcal{K}$, $0 < \theta_i < 1$ [10]. Thus, we consider the constraints **C3**, **C4**, and **C5**. The constraint function of **C3** has the function of $\frac{\chi_i \theta_i T - \epsilon_{s_i}}{T - \theta_i T - \tau_{s_i}}$ and its derivative is

$$\frac{\chi_i T \left(T - \theta_i T - \tau_{s_i}\right) + T \left(\chi_i \theta_i T - \epsilon_{s_i}\right)}{\left(T - \theta_i T - \tau_{s_i}\right)^2}, \tag{A.10}$$

where the numerator can be simplified, and the derivative function is always positive $\frac{T\left(\chi_i\left(T-\tau_{s_i}\right)-\epsilon_{s_i}\right)}{\left(T-\theta_i T-\tau_{s_i}\right)^2} > 0$ over the $\theta_i \in (0,1)$. Then, the second derivative with respect to $\theta_i$ is

$$\frac{2T^2 \left({\theta_i}^2 T - \left(T - \tau_{s_i}\right)\right) \left(\chi_i \left(T - \tau_{s_i}\right) - {}_{s_i}\right)}{\left(T - \theta_i T - \tau_{s_i}\right)^4}, \tag{A.11}$$

where the denominator is always positive; however, the term of $\left({\theta_i}^2 T - \left(T - \tau_{s_i}\right)\right)$ in the numerator is always negative since $T - \tau_{s_i}$ is greater than ${\theta_i}^2 T$. Thus, the second derivative is negative and the constraint **C3** is a concave function for the maximization problem (convex for standard minimization). Meanwhile, the convexity of constraints **C4** and **C5** can be proved similarly to the proof of Lemma 1.

## A.3 Proof of Lemma 3

To prove this Lemma, we need to write the equation ($x = \frac{b}{\mathcal{W}\left(\frac{b}{e^a}\right)}$) in the form of the *Lambert* function. Thus, the solution can be derived as follows:

$$\ln\left(x\right) = a + \frac{b}{x}. \tag{A.12}$$

Taking the exponential power from both sides results in

$$x = e^{\left(a + \frac{b}{x}\right)}. \tag{A.13}$$

Let $y = \frac{b}{x}$. Then, (A.13) can be expressed as

$$y e^y = \frac{b}{e^a}. \tag{A.14}$$

The *Lambert* $\mathcal{W}$ function can now be applied, resulting in

$$y = \mathcal{W}\left(\frac{b}{e^a}\right). \tag{A.15}$$

Finally, substituting $x = \frac{b}{y}$ into (A.15) results in Lemma 3.

# APPENDIX B

# PROOFS OF NP-HARDNESS

## B.1 Proof of Lemma 4

To prove the NP-hardness of the optimization problem, one can show that the problem is reducible to one of the proven NP-hard problems. Given spectral resources are allocated to users regardless of the amount of data in their buffers, the second term of the objective function, $S_{eff_k}$ is eliminated. Therefore, the objective function is reduced to $\sum_{k\in\mathcal{K}} \frac{R_k(\mu_k,g_{k,n})}{\rho_k^{av}\mu_k T_d+E_k^{res}-E_k^{sen}+E_k^{idle}}$. Thus, the objective function is $\sum_{n\in\mathcal{N}}\sum_{k\in\mathcal{K}} g_{k,n}.\hat{p}_{k,n}$, where the first term, $g_{k,n}$, is a binary variable and the second term can be considered as a profit in the generalized assignment problem (GAP) problem, i.e., $\hat{p}_{k,n} = \frac{\frac{t_k^{tr}(\mu_k)}{T} log_2\left(1+H_{k,n}\frac{E_k^{tr}(\mu_k)}{t_k^{tr}(\mu_k)}\right)}{\rho_k^{av}\mu_k T_d+E_k^{res}-E_k^{sen}+E_k^{idle}}$. Given the decision variables $\mu_k,\ \forall k \in \mathcal{K}$, are fixed, the constraints C2, C3, C7, and C8 are relaxed. Moreover, C1 can also be relaxed by appointing very small data rate requirements. Thus, the problem becomes the problem of packing $|\mathcal{N}|$ items (sub-channels) into $|\mathcal{K}|$ knapsacks (users). Each item (sub-channel) $n$ has a weight $\bar{p}_{k,n}I_{k,n}$ if assigned to the $k^{th}$ knapsack (user). Therefore, one can conclude that the reduced problem can be categorized as a GAP which is a known NP-hard problem, and thus **P1** is also NP-hard. More details of the proof are provided in [66].

## B.2 Proof of Lemma 5

Without loss of generality, we assume that URLLC and mMTC users are assigned to different clusters with various ranks in the clusters. Therefore, the values of $\alpha_m^{c,k}$, and $\beta_u^{c,k}$ are determined and the corresponding constraints in **P1** are relaxed. Given URLLC and mMTC users transmit their data with predetermined transmission powers of $p_u^s$ and $p_m^s$, the constraints related to these two variables are relaxed and

the NOMA clustering optimization problem for NB-IoT as a sum rate maximization of URLLC and mMTC devices is reduced to the following:

$$
\begin{aligned}
\textbf{P2:}\ & \max_{\gamma^{s,c}} \sum_{s\in\mathcal{S}}\sum_{c\in\mathcal{C}} \gamma^{s,c}\left(\sum_{m\in\mathcal{M}} R_m^{s,c} + \sum_{u\in\mathcal{U}} R_u^{s,c}\right) \\
& s.t. \\
& C1: \sum_{s\in\mathcal{S}}\sum_{c\in\mathcal{C}} \gamma^{s,c}\mathcal{W}^{s,c} \leqslant W^{RB}, \quad \forall c\in\mathcal{C}, \quad \forall s\in\mathcal{S} \\
& C2: \sum_{c\in\mathcal{C}} \gamma^{s,c} = 1, \quad \forall c\in\mathcal{C}, \quad \forall s\in\mathcal{S} \\
& C3: \gamma^{s,c} \in \{0,1\}, \quad \forall c\in\mathcal{C}, \quad \forall s\in\mathcal{S}
\end{aligned}
\tag{B.1}
$$

Hence, the reduced optimization problem, **P2**, is similar to a Multiple Choice Knapsack Problem (MCKP). In fact, the problem would be the problem of packing $|\mathcal{S}|$ items (sub-channels) into $|\mathcal{K}|$ knapsacks (clusters). Each item (sub-channel), $s$, has a weight if allocated to the $c^{th}$ knapsack (cluster). Moreover, each sub-channel has a profit which is $(\sum_{m\in\mathcal{M}} R_m^{s,c} + \sum_{u\in\mathcal{U}} R_u^{s,c})$ and the problem is to choose one item such that the profit sum is maximized without exceeding the capacity, $W^{RB}$. Therefore, **P2** is NP-hard because it is categorized as a MCKP which is a generalization of the ordinary knapsack problem. Thus, as **P2** is a special case of **P1**, the general optimization problem in (6.14) is an NP-hard problem.

# APPENDIX C

# CONVEXITY OF THE POWER ALLOCATION PROBLEM

## C.1 Proof of Theorem 2

We start to prove the theorem by investigating the objective function of **P5** ($\Phi_j(Z_j)$) due to the fact that all constraints are linear. The derivative of the objective function for all $j \in \{2, 3, ..., U + M\}$ is given by

$$\frac{\Phi_j(Z_j)}{dZ_j} = \frac{\lambda_j}{1 + \lambda_j Z_j} - \frac{\lambda_{j-1}}{1 + \lambda_{j-1} Z_j}. \tag{C.1}$$

The second derivative of $\Phi_j(Z_j)$ is given by

$$\begin{aligned} \Phi_j^{''}(Z_j) &= \frac{-(\lambda_j)^2}{(1 + \lambda_j Z_j)^2} - \frac{-(\lambda_{j-1})^2}{(1 + \lambda_{j-1} Z_j)^2} \\ &= \frac{\lambda_{j-1}^2 - \lambda_j^2 + 2\lambda_j Z_j \lambda_{j-1}^2 - 2\lambda_{j-1} Z_j \lambda_j^2}{(1 + \lambda_j Z_j)^2 (1 + \lambda_{j-1} Z_j)^2} \end{aligned} \tag{C.2}$$

Given $\lambda_1 \leqslant \lambda_2 \leqslant ... \leqslant \lambda_{U+M}$, the numerator of the second derivative is negative and the denominator is always positive. Therefore, the second derivative is negative and the objective function is concave.

# BIBLIOGRAPHY


[1] A. Aijaz and A. H. Aghvami. Cognitive machine-to-machine communications for internet-of-things: A protocol stack perspective. *IEEE Internet of Things Journal*, 2(2):103–112, April 2015.

[2] I. F. Akyildiz, B. F. Lo, and R. Balakrishnan. Cooperative spectrum sensing in cognitive radio networks: A survey. *Physical communication*, 4(1):40–62, 2011.

[3] M. Al-Imari, P. Xiao, M. A. Imran, and R. Tafazolli. Uplink non-orthogonal multiple access for 5G wireless networks. In *2014 11th International Symposium on Wireless Communications Systems (ISWCS)*, pages 781–785, 2014.

[4] A. Ali and W. Hamouda. Advances on spectrum sensing for cognitive radio networks: Theory and applications. *IEEE Communications Surveys Tutorials*, 19(2):1277–1304, 2017.

[5] M. Alnakhli, S. Anand, and R. Chandramouli. Joint spectrum and energy efficiency in device to device communication enabled wireless networks. *IEEE Transactions on Cognitive Communications and Networking*, 3(2):217–225, June 2017.

[6] N. Ansari and T. Han. *Green Mobile Networks: A Networking Perspective*. Wiley-IEEE Press, ISBN: 978-1-119-12510-5, 2017.

[7] SM. Azimi, MH. Manshaei, and F. Hendessi. Cooperative primary–secondary dynamic spectrum leasing game via decentralized bargaining. *Wireless Networks*, 22(3):755–764, 2016.

[8] A. Bagheri, A. Shahini, and A. Shahzadi. Analytical and learning-based spectrum sensing over channels with both fading and shadowing. In *International Conference on Connected Vehicles and Expo (ICCVE)*, pages 699–706, Dec 2013.

[9] G. Bansal, J. Hossain, and V. K. Bhargava. Adaptive power loading for OFDM-based cognitive radio systems. In *IEEE International Conference on Communications*, pages 5137–5142, June 2007.

[10] T. Berthold. *Heuristic algorithms in global MINLP solvers*. Verlag Dr. Hut, 2014.

[11] D. Bertsekas. *Nonlinear programming*. Nashua, NH: Athena Scientific, 1999.

[12] Y. D. Beyene, R. Jantti, O. Tirkkonen, K. Ruttik, S. Iraji, A. Larmo, T. Tirronen, and A. J. Torsner. NB-IoT technology overview and experience from Cloud-RAN implementation. *IEEE Wireless Communications*, 24(3):26–32, June 2017.

[13] C. Bockelmann, N. Pratas, H. Nikopour, K. Au, T. Svensson, C. Stefanovic, P. Popovski, and A. Dekorsy. Massive machine-type communications in 5G: physical and MAC-layer solutions. *IEEE Communications Magazine*, 54(9):59–65, September 2016.

[14] A. Cacciapuoti, M. Caleffi, L. Paura, and R. Savoia. Decision maker approaches for cooperative spectrum sensing: participate or not participate in sensing? *IEEE Transactions on Wireless Communications*, 12(5):2445–2457, 2013.

[15] Y. L. Che, L. Duan, and R. Zhang. Spatial throughput maximization of wireless powered communication networks. *IEEE Journal on Selected Areas in Communications*, 33(8):1534–1548, Aug 2015.

[16] Cisco Systems Incorporation. White Paper The Internet of Things: How the Next Evolution of the Internet Is Changing Everything. 2011.

[17] R. M. Corless, G. H. Gonnet, D. E. G. Hare, D. J. Jeffrey, and D. E. Knuth. *On the LambertW function.* Advances in Computational Mathematics, 1996.

[18] Powercast Corporation. Product datasheet, P2110 915 MHz RF powerharvester receiver [online], 2010.

[19] J. Currie and D. I. Wilson. OPTI: Lowering the barrier between open source optimizers and the industrial MATLAB use. *in Proc. Foundat. Computer-Aided Process Operations*, pages 8–11, 2012.

[20] L. Dai, B. Wang, Y. Yuan, S. Han, C. l. I, and Z. Wang. Non-orthogonal multiple access for 5G: solutions, challenges, opportunities, and future research trends. *IEEE Communications Magazine*, 53(9):74–81, September 2015.

[21] Q. Du and X. Zhang. Qos-aware base-station selections for distributed mimo links in broadband wireless networks. *IEEE Journal on Selected Areas in Communications*, 29(6):1123–1138, 2011.

[22] C. Gao, S. Chu, and X. Wang. Distributed scheduling in mimo empowered cognitive radio ad hoc networks. *IEEE Transactions on Mobile Computing*, 13(7):1456–1468, 2014.

[23] A. J. Goldsmith and Soon-Ghee Chua. Variable-rate variable-power MQAM for fading channels. *IEEE Transactions on Communications*, 45(10):1218–1230, 1997.

[24] T. Ha, J. Kim, and J. Chung. He-mac: Harvest-then-transmit based modified edcf mac protocol for wireless powered sensor networks. *IEEE Transactions on Wireless Communication*, 17(1):3–16, Jan 2018.

[25] VN. Ha and LB. Le. Fair resource allocation for OFDMA femtocell networks with macrocell protection. *IEEE Transactions on Vehicular Technology*, 63(3):1388–1401, 2014.

[26] Z. Hadzi-Velkov, I. Nikoloska, G. K. Karagiannidis, and T. Q. Duong. Wireless networks with energy harvesting and power transfer: Joint power and time allocation. *IEEE Signal Processing Letters*, 23(1):50–54, 2016.

[27] Q. Han, B. Yang, G. Miao, C. Chen, X. Wang, and X. Guan. Backhaul-aware user association and resource allocation for energy-constrained hetnets. *IEEE Transactions on Vehicular Technology*, 66(1):580–593, 2017.

[28] T. Han and N. Ansari. Powering mobile networks with green energy. *IEEE Wireless Communications*, 21(1):90–96, 2014.

[29] S. Haykin. Cognitive radio: brain-empowered wireless communications. *IEEE Journal on Selected Areas in Communications*, 23(2):201–220, 2005.

[30] S. Hu, H. Guo, C. Jin, Y. Huang, B. Yu, and S. Li. Frequency-domain oversampling for cognitive CDMA systems: Enabling robust and massive multiple access for internet of things. *IEEE Access*, 4:4583–4589, 2016.

[31] S. Huang, X. Liu, and Z. Ding. Opportunistic spectrum access in cognitive radio networks. In *INFOCOM 2008. The 27th Conference on Computer Communications. IEEE*, page 14271435, April 2008.

[32] X. Huang and N. Ansari. Energy sharing within EH-enabled wireless communication networks. *IEEE Wireless Communications*, 22(3):144–149, 2015.

[33] X. Huang and N. Ansari. Joint spectrum and power allocation for multi-node cooperative wireless systems. *IEEE Transactions on Mobile Computing*, 14(10):2034–2044, 2015.

[34] X. Huang and N. Ansari. Optimal cooperative power allocation for energy-harvesting-enabled relay networks. *IEEE Transactions on Vehicular Technology*, 65(4):2424–2434, 2016.

[35] X. Huang, T. Han, and N. Ansari. On green-energy-powered cognitive radio networks. *IEEE Communications Surveys Tutorials*, 17(2):827–842, 2015.

[36] H. Jabbar, Y. S. Song, and T. T. Jeong. RF energy harvesting system and circuits for charging of mobile devices. *IEEE Transactions on Consumer Electronics*, 56(1):247–253, 2010.

[37] C. Jiang, Y. Shi, Y. T. Hou, W. Lou, and H. D. Sherali. Throughput maximization for multi-hop wireless networks with network-wide energy constraint. *IEEE Transactions on Wireless Communications*, 12(3):1255–1267, 2013.

[38] P. Kamalinejad et al. Wireless energy harvesting for the internet of things. *IEEE Communication Magazine*, 53(6):102–108, 2015.

[39] P. Kamalinejad, C. Mahapatra, Z. Sheng, S. Mirabbasi, V. C. M. Leung, and Y. L. Guan. Wireless energy harvesting for the internet of things. *IEEE Communications Magazine*, 53(6):102–108, 2015.

[40] X. Kang, C. K. Ho, and S. Sun. Full-duplex wireless-powered communication network with energy causality. *IEEE Transactions on Wireless Communications*, 14(10):5539–5551, Oct 2015.

[41] N. Kaur and S. K. Sood. An energy-efficient architecture for the internet of things (IoT ). *IEEE Systems Journal*, 11(2):796–805, June 2017.

[42] H. Kawabata, K. Ishibashi, S. Vuppala, and G. T. F. de Abreu. Robust relay selection for large-scale energy-harvesting IoT networks. *IEEE Internet of Things Journal*, 4(2):384–392, April 2017.

[43] A.A. Khan, M.H. Rehmani, and A. Rachedi. When cognitive radio meets the internet of things? In *2016 Intl. Wireless Comm. & Mobile Comput. Conf. (IWCMC)*, pages 469–474, Sep. 2016.

[44] A. Kiani and N. Ansari. Toward hierarchical mobile edge computing: An auction-based profit maximization approach. *IEEE Internet of Things Journal*, 4(6):2082–2091, Dec 2017.

[45] A. Kiani and N. Ansari. Edge computing aware NOMA for 5G networks. *IEEE Internet of Things Journal*, 5(2):1299–1306, April 2018.

[46] S. LeDigabel. Algorithm 909: NOMAD: Nonlinear optimization with the MADS algorithm. *ACM Trans. Math. Software*, 37(4), Feb. 2011.

[47] J. Li, Y. Liu, Z. Zhang, J. Ren, and N. Zhao. Towards green IoT networking: Performance optimization of network coding based communication and reliable storage. *IEEE Access*, 5:8780–8791, 2017.

[48] S. Li, Z. Zheng, E. Ekici, and N. Shroff. Maximizing system throughput by cooperative sensing in cognitive radio networks. *IEEE/ACM Transactions on Networking*, 22(4):1245–1256, 2014.

[49] S. Li, Z. Zheng, E. Ekici, and N. Shroff. Maximizing system throughput by cooperative sensing in cognitive radio networks. *IEEE/ACM Transactions on Networking*, 22(4):1245–1256, Aug. 2014.

[50] X. Liu and N. Ansari. Green relay assisted D2D communications with dual batteries in heterogeneous cellular networks for IoT. *IEEE Internet Things Journal*, 4:1707–1715, 2017.

[51] Y. Liu, S. A. Mousavifar, Y. Deng, C. Leung, and M. Elkashlan. Wireless energy harvesting in a cognitive relay network. *IEEE Transactions on Wireless Communications*, 15(4):2498–2508, April 2016.

[52] Y. Luo et al. Resource allocation for energy harvesting-powered d2d communication underlaying cellular networks. *IEEE Transactions on Vehicular Technology*, 66(11):10486–10498, Nov 2017.

[53] C. Majumdar, D. Lee, A. A. Patel, S. N. Merchant, and U. B. Desai. Packet size optimization for cognitive radio sensor networks aided internet of things. *IEEE Access*, 5:6325–6344, 2017.

[54] H. Malik, H. Pervaiz, M. Mahtab Alam, Y. Le Moullec, A. Kuusik, and M. Ali Imran. Radio resource management scheme in NB-IoT systems. *IEEE Access*, 6:15051–15064, 2018.

[55] A. E. Mostafa, Y. Zhou, and V. W. S. Wong. Connectivity maximization for narrowband iot systems with noma. In *2017 IEEE International Conference on Communications (ICC)*, pages 1–6, May 2017.

[56] D. T. Ngo, S. Khakurel, and T. Le-Ngoc. Joint Subchannel Assignment and Power Allocation for OFDMA Femtocell Networks. *IEEE Transactions on Wireless Communications*, 13(1):342–355, 2014.

[57] S. Oh and J. Shin. An efficient small data transmission scheme in the 3GPP NB-IoT system. *IEEE Communications Letters*, 21(3):660–663, March 2017.

[58] J. Papandriopoulos and J. S. Evans. Scale: A low-complexity distributed protocol for spectrum balancing in multiuser dsl networks. *IEEE Transactions on Information Theory*, 55(8):3711–3724, Aug 2009.

[59] L. P. Qian, A. Feng, Y. Huang, Y. Wu, B. Ji, and Z. Shi. Optimal SIC ordering and computation resource allocation in MEC-aware NOMA NB-IoT networks. *IEEE Internet of Things Journal*, pages 1–1, 2018.

[60] Y. Saito, Y. Kishiyama, A. Benjebbour, T. Nakamura, A. Li, and K. Higuchi. Non-orthogonal multiple access (NOMA) for cellular future radio access. In *2013 IEEE 77th Vehicular Technology Conference (VTC Spring)*, pages 1–5, June 2013.

[61] M. Shafi, A. F. Molisch, P. J. Smith, T. Haustein, P. Zhu, P. De Silva, F. Tufvesson, A. Benjebbour, and G. Wunder. 5G: A tutorial overview of standards, trials, challenges, deployment, and practice. *IEEE Journal on Selected Areas in Communications*, 35(6):1201–1221, June 2017.

[62] A. Shahini and N. Ansari. Sub-channel allocation in green powered heterogeneous cognitive radio networks. In *2016 IEEE 37th Sarnoff Symposium*, pages 13–18, Sep 2016.

[63] A. Shahini and N. Ansari. Joint spectrum allocation and energy harvesting optimization in green powered heterogeneous cognitive radio networks. *Computer Communication*, 127:36 – 49, 2018.

[64] A. Shahini, A. Bagheri, and A. Shahzadi. A unified approach to performance analysis of energy detection with diversity receivers over nakagami-m fading channels. In *International Conference on Connected Vehicles and Expo (ICCVE)*, pages 707–712, Dec 2013.

[65] A. Shahini, A. Kiani, and N. Ansari. Energy efficient resource allocation in EH-enabled CR networks for IoT. *IEEE Internet of Things Journal*, pages 1–1, 2018.

[66] A. Shahini, A. Kiani, and N. Ansari. Energy efficient resource allocation in EH-enabled CR networks for IoT. *arXiv preprint arXiv:1807.02558*, Jul. 2018.

[67] V. Sharma, F. Song, I. You, and M. Atiquzzaman. Energy efficient device discovery for reliable communication in 5G-based IoT and BSNs using unmanned aerial vehicles. *Journal of Network and Computer Applications*, 97(Supplement C):79 – 95, 2017.

[68] M. Shirvanimoghaddam, M. Condoluci, M. Dohler, and S. J. Johnson. On the fundamental limits of random non-orthogonal multiple access in cellular massive IoT. *IEEE Journal on Selected Areas in Communications*, 35(10):2238–2252, Oct 2017.

[69] L. Song, K. K. Chai, Y. Chen, J. Schormans, J. Loo, and A. Vinel. Qos-aware energy-efficient cooperative scheme for cluster-based IoT systems. *IEEE Systems Journal*, PP(99):1–9, 2017.

[70] S. Tabatabaee, A. Bagheri, A. Shahini, and A. Shahzadi. An analytical model for primary user emulation attacks in ieee 802.22 networks. In *2013 International Conference on Connected Vehicles and Expo (ICCVE)*, pages 693–698, Dec 2013.

[71] 3GPP TS 36.213 V14.0.0. Evolved universal terrestrial radio access (E-UTRA): Physical layer procedures (release 13). September 2016.

[72] L. R. Varshney. Transporting information and energy simultaneously. In *IEEE International Symposium on Information Theory (ISIT)*, pages 1612–1616, July 2008.

[73] S. Wang, Z. H. Zhou, M. Ge, and C. Wang. Resource allocation for heterogeneous cognitive radio networks with imperfect spectrum sensing. *IEEE Journal on Selected Areas in Communications*, 31(3):464–475, 2013.

[74] SH. Wang, F. Huang, M. Yuan, and S. Du. Resource allocation for multiuser cognitive OFDM networks with proportional rate constraints. *International Journal of Communication Systems*, 25(2):254–269, 2012.

[75] Y. P. E. Wang, X. Lin, A. Adhikary, A. Grovlen, Y. Sui, Y. Blankenship, J. Bergman, and H. S. Razaghi. A primer on 3GPP Narrowband Internet of Things. *IEEE Communications Magazine*, 55(3):117–123, March 2017.

[76] T. A. Weiss and F. K. Jondral. Spectrum pooling: an innovative strategy for the enhancement of spectrum efficiency. *IEEE Communications Magazine*, 42(3):8–14, 2004.

[77] Q. Wu, W. Chen, D. W. K. Ng, and R. Schober. Spectral and energy-efficient wireless powered iot networks: NOMA or TDMA? *IEEE Transactions on Vehicular Technology*, 67(7):6663–6667, July 2018.

[78] N. Xia, H. H. Chen, and C. S. Yang. Radio resource management in machine-to-machine communications; a survey. *IEEE Communications Surveys Tutorials*, 20(1):791–828, Firstquarter 2018.

[79] R. Xie, F. R. Yu, and H. Ji. Energy-efficient spectrum sharing and power allocation in cognitive radio femtocell networks. In *INFOCOM, Proceedings IEEE*, pages 1665–1673, March 2012.

[80] T. Xu and I. Darwazeh. Non-orthogonal narrowband internet of things: A design for saving bandwidth and doubling the number of connected devices. *IEEE Internet of Things Journal*, 5:2120–2129, June 2018.

[81] X. Yang, X. Wang, Y. Wu, L. P. Qian, W. Lu, and H. Zhou. Small-cell assisted secure traffic offloading for narrowband internet of thing (NB-IoT) systems. *IEEE Internet of Things Journal*, 5(3):1516–1526, June 2018.

[82] S. Yin, Z. Qu, and S. Li. Achievable throughput optimization in energy harvesting cognitive radio systems. *IEEE Journal on Selected Areas in Communications*, 33(3):407–422, March 2015.

[83] S. Yin, E. Zhang, L. Yin, and S. Li. Optimal saving-sensing-transmitting structure in self-powered cognitive radio systems with wireless energy harvesting. In *IEEE International Conference on Communications (ICC)*, pages 2807–2811, June 2013.

[84] T. Yucek and H. Arslan. A survey of spectrum sensing algorithms for cognitive radio applications. *IEEE Communications Surveys Tutorials*, 11(1):116–130, 2009.

[85] D. Zhai, R. Zhang, L. Cai, B. Li, and Y. Jiang. Energy-efficient user scheduling and power allocation for NOMA-based wireless networks with massive IoT devices. *IEEE Internet of Things Journal*, 5(3):1857–1868, June 2018.

[86] D. Zhang, Z. Zhou, S. Mumtaz, J. Rodriguez, and T. Sato. One integrated energy efficiency proposal for 5G IoT communications. *IEEE Internet of Things Journal*, 3(6):1346–1354, Dec 2016.

[87] H. Zhang et al. Computing resource allocation in three-tier IoT fog networks: a joint optimization approach combining stackelberg game and matching. *IEEE Internet Things Journal*, 4:1204–1215, 2017.

[88] Y. Zhang and C. Leung. Resource allocation in an OFDM-based cognitive radio system. *IEEE Transactions on Communications*, 57(7):1928–1931, 2009.

[89] Z. Zhang, H. Sun, and R. Q. Hu. Downlink and uplink non-orthogonal multiple access in a dense wireless network. *IEEE Journal on Selected Areas in Communications*, 35(12):2771–2784, Dec 2017.